NEUTRONICS AND DOSE CALCULATION FOR PROSPECTIVE SPENT NUCLEAR FUEL CASK FOR GHANA RESEARCH REACTOR-1 FACILITY.

BY

REX GYEABOUR ABREFAH, 10235608

BSc Physics, (KWAME NKRUMAH UNIVERSITY OF SCIENCE AND TECHNOLOGY), 2005

MPhil. Nuclear Engineering,(UNIVERSITY OF GHANA), 2008

A DISSERTATION PRESENTATION TO THE DEPARTMENT OF NUCLEAR ENGINEERING, THE SCHOOL OF NUCLEAR AND ALLIED SCIENCES, THE UNVERSITY OF GHANA FOR THE PARTIAL FULFILMENT OF THE DOCTOR OF PHILOSOPHY (PhD) IN NUCLEAR ENGINEERING

JUNE, 2014

DECLARATION

I declare that apart from references of other people's work that this dissertation is the product of my own research and hard work and that it has neither been in part or whole being presented elsewhere for another degree.

SIGNED……

DATE……

REX GYEABOUR ABREFAH

(STUDENT)

SIGNED…… SIGNED…….

DATE…… DATE…….

PROF. EMERITUS E.H.K. AKAHO PROF. B.J.B. NYARKO

(SUPERVISOR) (CO-SUPERVISOR)

SIGNED……

DATE……

PROF. J. J FLETCHER

(CO-SUPERVISOR)

DEDICATION

This document is dedicated to my lovely wife for her encouragement and support throughout my study. Also, to everyone who helped me in diverse ways during my research and write up.

ACKNOWLEDGEMENTS

Firstly, I am most grateful to the Almighty God who gave me the strength to undertake this study. He has indeed brought me to an expected end and all honour, praise and glory be to His name.

I wish to express my profound gratitude to all my lecturers, especially my supervisors Prof. Emeritus E.H.K Akaho, Prof. B.J.B. Nyarko and Prof. J.J Fletcher for their expert guidance, advice and encouragement.

My special thanks also to the whole core conversion team and partners, the staff of the Argonne National Laboratory, Argonne, U.S.A, for their support in terms of logistics and guidance.

I am highly indebted to Dr. Jay Liaw of the Argonne National Laboratory, under whose advice and direction I was able to set up and run the input decks for this work.

Lastly my heartfelt appreciation goes to my family, friends and course mates who have in diverse ways helped in the fulfillment and success of this study but have not been mentioned – I thank you all.

TABLE OF CONTENTS

LIST OF TABLES

LIST OF FIGURES

LIST OF SYMBOLS

LIST OF ABBREVIATIONS

HEU- Highly Enriched Uranium

LEU- Low Enriched Uranium

WIMS- Winfrith Improved Multigroup Scheme

ANL- Argonne National Laboratory

ORIGEN-**O**ak **R**idge **I**sotope **GEN**eration

MCNP-Monte Carlo "N" Particle

REBUS- REactor BUrnup System

GHARR-1- Ghana Research Reactor -1

RR - Research Reactor

IAEA - International Atomic Energy Agency

RRSFDB - Research Reactor Spent Fuel Database

TRIGA- Training Reactor Isotopics General Atomics

HM - Heavy Metal

SNF- Spent nuclear fuel

MTHM - Metric tons heavy metal

DOE - Department of Energy

HLW - High Level Waste

ORNL- Oak Ridge National Laboratory

HFIR- High-Flux Isotope Reactor

SRS- Savanah River Site

ANS-Advanced Neutron Source

BSR - Bulk Shielding Reactor

ORR - Oak Ridge Research Reactor

MTR - Material Test Reactor

MSRE - Molten Salt Reactor Experiment

HRE - Homogenous Reactor Experiment

SNAP-Space Nuclear Auxiliary Power

HPRR -Health Physics Research Reactor

UF -Uranium hexafluoride

ALARA- As Low As Reasonably Achievable

SCALE- Standardized Computer Analyses for Licensing Evaluation

SAS2H- Shielding Analysis Sequence No. 2H

RRRSFR -Russian Research Reactor Spent Fuel Return

FRRSNF -Foreign Research Reactor Spent Nuclear Fuel

NRI -Nuclear Research Institute

HLWSF -High Level Waste Storage Facility

GTRI -Global Threat Reduction Initiative

EURATOM- The European Atomic Energy Community

ENDF- Evaluated Nuclear Data File

JENDL- Japanese evaluated nuclear data library

TLD- Thermo Luminescent Dosimeter

MNSR- Miniature Neutron Source Reactors

ARC-Argonne Reactor Code

RSICC- Radiation Safety Information Computational Center

RERTR -Reduced Enrichment Research and Test Reactor Program

ABSTRACT

Ghana Research Reactor-1 core is to be converted from Highly Enrich Uranium (HEU) fuel to Low Enriched Uranium (LEU) fuel in the near future; a storage cask will be needed to store the HEU fuel. Notwithstanding the core conversion process, it is also important for the facility to have a storage cask ready when the fuel is finally spent to temporarily store the fuel until permanent storage is provided. Winfrith Improved Multigroup Scheme-Argonne National Laboratory (WIMS-ANL), REactor BUrnup System (REBUS), **O**ak **R**idge **I**sotope **GEN**eration (ORIGEN2) and Monte Carlo "N" Particle (MCNP5) codes have been used to design the cask. WIMS-ANL was used in generating cross sections for the REBUS code which was used in the burnup calculations. The REBUS code was used to estimate the core life time. An estimated core life of approximately 750 full-power-equivalent-days was obtained for reactor operation of 2hours a day, 4 days a week and 48 weeks in a year. The ORIGEN2 code recorded U-235 burnup weight percent of 2.90% whilst the result from the REBUS3 code was 2.86%. The amount of Pu-239 at the end of the irradiation period was 145 mg which is very low relative to other low power reactors. Isotopic inventory obtained from the ORIGEN2 and REBUS3 runs were used in setting up the MCNP5 input deck for the MCNP5 calculation of the criticality and dose rate. Six cask design options were investigated. The materials for the casks designs were selected bas on their attenuation coefficient properties and their high removal cross section properties. The various materials were arranged in no specific order in multilayered casks. The reason for investigating six casks was to look at various arrangements of the cask layers that will optimize effective shielding. The spent nuclear fuel at discharge was used as the

radioactivity source during the MCNP simulation. The multilayer cask shield comprise of serpentine concrete of density 5.14 g/cm^3 and thickness 21.94cm which was used as the main gamma shield, lead (two thick layers of 1.91cm and 2.50cm respectively), boron carbide (two layers of 2cm thick each), resin (2cm thick), stainless steel (two thick layers of 2.63cm and 1.17cm respectively) and aluminium (2cm thick). Serpentine was chosen because it has higher water content than ordinary concrete thereby helping in neutron shielding. The casks were designed to be cooled by natural circulation and to have radii of approximately 60cm hence making them relatively portable. Effective multiplication factor values of Cask A, Cask B, Cask C, Cask D, Cask E and Cask F were recorded as 0.02969±0.00001, 0.06304 ± 0.00002, 0.19809 ± 0.00027, 0.15393 ± 0.00025, 0.02028 ± 0.00001 and 0.01717 ± 0.00001 respectively. This showed that all the six designs were capable of keeping the spent fuel sub critical.

CHAPTER ONE

1.0 INTRODUCTION

1.1 BACKGROUND

For over 50 years, research reactors (RRs) have made valuable contributions to the development of nuclear power, basic science, materials development, radioisotope production for medicine and industry, and education and training. As of June 2004, the International Atomic Energy Agency's Research Reactor Database contained information on 672 RRs, of which 274 are operational in 56 countries (85 in 39 developing countries), 214 are shutdown, 168 have been decommissioned and 16 are planned or under construction [1]

A decline in the number of new research reactors being brought into operation in the past four and a half decade and an increase in the number being shutdown is evident. The pattern reflects the nuclear field's evolution from a relatively new science into an established technology. It does not mean, however, that new research reactors are unnecessary. For the most part, the new RRs are innovative, multipurpose reactors designed to produce high neutron fluxes. Many will meet all the nuclear research and development needs envisioned in the countries in which they are being built, and will offer opportunities for visiting scientists from abroad. In addition, some will provide radioisotopes locally and regionally [1].

While a few of the old reactors give cause for safety concerns, the majority have been refurbished at least once so that their key components meet modern safety and technology standards. The thermal power distribution of operating RRs indicates that a large fraction of RRs, 77%, are less than 5 MW, and that, even in the worst case accident

scenario, there will not be any significant radiological consequences off site. Research reactors of less than 100kW operate with a lifetime core and so no spent fuel problems arise until these reactors are shut down permanently. But many of them operate with highly enriched uranium fuel (HEU), i.e., a ^{235}U concentration $\geq$ 20% [1].

The International Atomic Energy Agency (IAEA) circulated questionnaires for its Research Reactor Spent Fuel Database (RRSFDB), and responses indicate that there are 62,027 spent fuel assemblies in storage and another 24,338 assemblies in the standard cores. Of the 62,027 in storage, 45,108 are in industrialized countries and 16,919 are in developing countries; 21,732 are HEU and 40,295 are LEU (low enriched uranium). The majority use standard types of fuel plus aluminium cladding, although some TRIGA fuel elements have stainless steel cladding. The remaining non-standard fuel types in 59 facilities pose special problems both for their continued safe storage and for their eventual final disposal. Currently, 12,850 spent fuel assemblies of US-origin, and 21,732 of Russian-origin, are located in research reactors in other countries [2].

Research reactors present special challenges in the back end of the fuel cycle because many different designs using a large variety of fuel types have been built, often for special purposes. These include the management of experimental and exotic fuels with no reprocessing route, and significant numbers of fuel assemblies that failed in their reactors or were subsequently corroded in wet storage. Similarly the variety of designs poses special challenges for decommissioning.

Several numerical and computational methods or approaches based on nuclear reactor physics, nuclear engineering and mathematical theories exist for performing particle transport analysis [3] [4]. Over the years, both deterministic and stochastic methods have

been employed in the performance of analysis of particle transport. With the advent of advanced, powerful and sophisticated computers, innovative methods involving the extensive use of Monte Carlo-based computational codes or tools and large scale computing facilities have now been adopted in analyzing complex nuclear and radiation transport processes. In particular, previous models and codes which were hitherto limited to running on low-speed computers, have also been improved and can now be adapted to performing equally time-demanding simulations and calculations [5] [6].

With improved mathematical and numerical computational methods, analyses of particle transport have even become more involving howbeit exacting in time, space and energy.

Nuclear power is becoming an ever more significant part of the energy programmes of many countries. The spent fuel resulting from reactor operations must be safely stored and managed pending its reprocessing or disposal. The International Atomic Energy Agency recognizes the increasing need for such interim spent fuel storage and has consequently established a programme to provide guidance to its Member States on the key safety aspects of safe storage. As a result continuing development affecting nuclear power and its fuel cycle, the coming years will be challenging for the international nuclear community. Spent fuel management is one of the most vital and common problems for countries with reactors. It also invokes the concern of the public at large. Three management options currently exist: the open, once- through cycle with direct disposal of spent fuel (Ghana falls into this category); the closed cycle with the reprocessing of spent fuel and recycling of plutonium and uranium in the form of mixed oxide; and the wait and see approach where countries continue to evaluate their back end strategy while in the meantime taking ‘intermediate’ steps [7].

The total amount of spent fuel accumulated worldwide at the end of 1994 was over 155,000 tonnes heavy metal (t HM). Of this, over 60% is presently being stored in facilities awaiting either reprocessing or final disposal. The quantity of accumulated spent fuel outweighs the reprocessing capacity. The projected cumulative amount of spent fuel generated by 2010 is expected to reach 300,000t HM. Assuming that part of it is reprocessed, the amount to be stored by the year 2010 is projected to be about 200,000t HM [8].

Ghana has no plans or facilities for permanent storage yet. The option that is available to Ghana now is the scenario that the manufacturers of the core would take back the spent nuclear fuel and manage it themselves. Therefore, interim storage will be the primary spent fuel management option in many countries for the next 20 years or so. The requirement for the interim storage of the spent fuel is derived from a number of considerations associated with the management option selected. In the closed nuclear fuel cycle, further fuel storage capacity may be required to match the arisings of spent fuel with the available capacity of reprocessing plants [9]. With respect to the once-through cycle, interim storage casks is required until a final repository is constructed and in service. Clearly, for a deferred decision, the availability of adequate storage cask is a key element. There is a scientific consensus that present fuel storage technologies provide adequate protection to the population and the environment. However, there is a keen interest in seeing whether further improvements can be achieved in the area of spent fuel cask storage [9].

Clearly, the analyses of storage cask designs for the Ghana Research Reactor -1 cannot be over emphasized.

1.2 PROBLEM STATEMENT

Due to the call by the international community and the IAEA for Highly enriched uranium fuel to be converted to Low enriched uranium fuel; GHARR-1 is involved in a project to convert its HEU fuel to LEU. Ghana will sooner or later have to deal with spent fuel from the core of its research reactor (i.e. taking into consideration the predicted core lifetime of 10 years); the reactor has been operating for about twenty years already due to the fact that it operates at half power. In the event of any of the two scenarios, Ghana will have to effectively store and finally dispose of the HEU spent fuel. A suitable spent fuel cask is clearly required for the purpose of effective shielding. The design of the spent fuel storage casks will assist in the efficient storage of the spent fuel as well as its transportation.

1.3 OBJECTIVE

- To design appropriate cask for the spent HEU fuel in GHARR-1.
- To select and evaluate suitable materials and the best arrangement of multilayer for the cask.
- To select and employ a suitable computational tool to carry out the calculations in order to achieve the set goals.
- To provide details on the design of interim spent fuel storage facilities and assist in preparing technical documentation to satisfy licensing requirements.
- To obtain appropriate design parameters, estimate fuel burnup and core lifetime regimes and technical design specification.
- To simulate radiation transport and shielding behaviour of the spent fuel cask in favour of radiation protection and monitoring (occupational and public health)

1.4 JUSTIFICATION

Due to the emission of fission products and high energy gamma radiation from the spent fuel, it is imperative to shield the spent fuel from the radiation workers, the public as well as the environment. There is the need to also contain the neutrons and high energy betas emanating from the spent fuel. Neutronic and dose calculation codes can present the opportunity to undertake an extensive analysis of the neutron population and gamma dose being emitted from the spent fuel. In the eventual event that the HEU fuel becomes spent, the spent HEU core will need an appropriate storage cask; the cask should be able to ensure that the spent fuel is sub critical, it should be able to ensure that the cask has an efficient heat removal system due to the decay heat that will be generated and it should also be able to protect the workers, public and environment from radiation.

Presently, processes are ongoing to ensure that Ghana is able to add nuclear power to its energy mix. When Ghana finally decides to go nuclear, the cask could become relevant as it will serve as a starting point for any further cask development.

The mining of serpentine for its use in the cask design could also provide employment for folks in the areas where serpentine are abundant. It can also serve as a foreign exchange earner for the country because countries with MNSRs could purchase the cask for use.

Therefore an extensive work in the design of a storage cask will be prudent.

Our decision to design, model, construct and license an interim spent fuel cask is undoubtedly very important and will help address issues about security and safety of our spent nuclear fuel. Since a cask is not in place at the moment, the designed cask, when

constructed, will serve as a secure home for the spent fuel. Moreover, it will also ensure the safety of personnel, environment and public because it will have the capacity to keep the spent nuclear fuel sub critical and also keep absorbed doses on the surface of the cask low.

1.5 SCOPE OF WORK

Casks present enabling conditions that prevent the nuclear material that are contained in them from achieving criticality. It considers the various materials that may be used in fabricating the casks as well as their arrangements in the cask designs and how effective they are in gamma and neutron shielding. The various shielding materials were chosen based on their high shielding and attenuation properties. Other materials were chosen due to their high absorption or scattering cross sections. WIMS-ANL code was used as a lattice code to set up libraries of cross section for use by the burn up code REBUS3. The cross sections generated were also used by ORIGEN2 for the estimation of core burnup and production of plutonium. The MCNP5 code used the isotopic inventory generated by ORIGEN2 to set up a neutronic and dose calculation input deck (i.e. the materials constituting the spent core were obtained from the ORIGEN2 calculation). MCNP5 was used to investigate six cask designs proposed for GHARR-1 to determine which of the designs is best able to prevent criticality. It also investigates the amount of radiation (Gy/h) that emanate from the spent nuclear fuel casks. This is important because the amount of radiation released into the environment and the amount received by personnel that will handle it should be kept as low as reasonably possible.

1.6 STRUCTURE OF WORK

Chapter one looks at the background information types of reactors and their uses. It also looks at the problem that this work is trying to solve, the objectives and the justification for this work. Chapter two is the literature review and it generally looks at what research work has already been done in the field of cask design and how different and advantageous this work is. Chapter three looks at the theories used in developing the various codes that were used in this work. Chapter four considers the various codes used in this work and how exactly they were used (methodology) in reaching the results in the end. Chapter five discusses the results obtained from the core life estimation, fuel depletion, criticality and neutron distribution in cask, dose calculation etc. Chapter six makes conclusions and recommendations based on the results discussed in chapter five. The recommendations are also based on the scope of work.

CHAPTER TWO

2 LITERATURE REVIEW

In the late 1970s and early 1980s, the need for alternative storage began to grow when pools at many nuclear reactors began to fill up with stored spent fuel. Utilities began looking at options such as dry cask storage for increasing spent fuel storage capacity. The most recent inventory of the amount of spent nuclear fuel (SNF) stored in the United States indicates that approximately 2700 metric tons heavy metal (MTHM) exist. This SNF consists primarily of stored material at the US Department of Energy (DOE) Hanford, Idaho, and Savannah River sites. About 1 MTHM (or about 0.03% of the nation's total) is stored at the DOE complex in Oak Ridge, Tennessee. The Oak Ridge SNF is currently divided into 16 different listings; two of these categories contain less than 1 kg of heavy metal (HM). However small the quantity of material stored at Oak Ridge, some of the material is quite singular in character and, thus, may pose unique management concerns. Currently, indications are that it may be very expensive to qualify a single SNF type for disposal in the proposed national high level waste (HLW) geologic repository. A clear understanding of the various SNF types stored at Oak Ridge is vital to the development of a national program plan for the management of SNF. A discussion of the various types of SNF stored at Oak Ridge is presented below. Included are various issues that pertain to each fuel type. It is intended that the presented list be as complete as possible. However, given the uncertainties in the current definition of what is included in the national SNF program, there may very well be some future deletions or additions in the list of the Oak Ridge material [10].

The following information has been extracted from a variety of sources, including the Oak Ridge SNF data base, internal and external Oak Ridge National Laboratory (ORNL) reports, formal and informal presentations, and personal communications of authors. One of the most complete sources for information on SNF at all of the DOE facilities is DOE Programmatic Spent Nuclear Fuel Management and Idaho National Engineering Laboratory Environmental Restoration and Waste Management Program's Drafi Environmental Impact Statement, DOE/EIS-0203-D, June 1994. [11]

2.0 OAK RIDGE SNF INVENTORY

2.0.1 High-Flux Isotope Reactor (HFIR) fuel

The HFIR is an operational beryllium-reflected, light water-cooled and -moderated, flux-trap-type reactor. The reactor uses 540 aluminum-clad involutes fuel plates containing 93% enriched ^{235}U fuel. The reactor became operational in 1965 and is normally operated at a level of 85 MW. Current missions for the HFIR include the production of isotopes for medical and industrial applications, neutron-scattering experiments, and various material-irradiation experiments.

HFIR is the only source of transuranic isotopes, especially ^{252}Cf in the western world. [12]

The HFIR averages ten fuel cycles per year. Currently, there are 57 HFIR cores (576 kg of HM) in on-site pool storage with a total capacity of 60 cores. Reracking the existing storage facility and installing modular dry-storage units are being considered in order to expand the limited storage capacity [13].

In the past, HFIR SNF was shipped to the Savannah River Site (SRS). If shipment of SNF to another DOE site is precluded or if the reracking at the HFIR is not approved, the reactor will be required to shut down because the pool storage racks will be full by early 1995. Each HFIR fuel assembly contains approximately 9.4 kg of ^{235}U (no burnup credit) in a matrix that is not suitable for disassembly. Current estimates are that the criticality limit for the geologic repository waste package may be 700 g of fissile mass. Although several methods for the conversion of SNF to HLW have been proposed, none have been successfully demonstrated [14].

The Advanced Neutron Source (ANS) reactor is currently in the conceptual design stage as a replacement for the HFIR and may be operational as early as the year 2002 or 2003. Current estimates are that up to 18 cores will be discharged per year. The configuration of the fuel elements is expected to be similar to the present HFIR fuel design. Current missions for the HFIR include the production of isotopes for medical and industrial applications, neutron scattering experiments, and various material-irradiation [10] [13].

2.0.2 Bulk Shielding Reactor (BSR) and Oak Ridge Research Reactor (ORR)

These two reactors were shutdown in 1987 (ORR) and in 1991 (BSR). Most of this fuel was transported to the SRS, but 41 elements for the BSR and 32 elements for the ORR remain in on-site wet storage in the BSR pool. The total amount of these 73 elements is about 59 kg HM. Both the BSR and ORR used material test reactor-type (MTR-type) assemblies of an aluminum-clad plate-type design. The fuel-containing matrix is a uranium-oxide (in the BSR) or uranium-silicide (in the ORR) and aluminum mixture. The BSR fuel is 93% enriched in ^{235}U, whereas the ORR fuel is 20% enriched [10] [13].

2.0.3 Molten Salt Reactor Experiment (MSRE) fuel

The MSRE operated from June 1965 to December 1969 at a normal power level of 8 MW. The purpose of the reactor was to test the practicality of a molten-salt-reactor concept. The circulating fuel solution was a mixture of fluoride salts containing uranium fluoride as the fuel. The initial charge was ^{235}U but this was later replaced with a charge of ^{233}U. Processing capabilities were included as part of the facility for on-line fuel additions, removal of impurities, and uranium recovery. Following reactor shutdown, the fuel and flush salts were drained to three critically safe storage tanks. Currently, the inventory at the MSRE consists of about 11,550 kg of the fluoride salt mixture (4,650 kg fuel salt, 4,290 kg flush salt, and 2,610 kg coolant salt). The uranium salt is contained mainly in the fuel salt and is predominately ^{233}U (31 kg) with lesser amounts of ^{234}U**,** ^{235}U and ^{238}U**.**The remainder of the salt mixture is composed of lithium fluoride, beryllium fluoride, and zirconium fluoride. A total mass of 38 kg HM is present in the three Hastelloy storage tanks. Some migration of fissile material has been detected from the storage tanks and is currently being investigated. If left uncorrected, access to the hot-cell area, where the tanks are contained, may become difficult. The presence of the fluoride salt mixture will mandate that special care be taken in the removal and storage of this fuel. The approach that will be used has yet to be decided upon [13] [14].

2.0.4 Homogenous Reactor Experiment (HRE) fuel

The HRE was operated from 1957 through 1961 to evaluate the potential application of aqueous fueled homogenous reactors to power plant applications and in 1959 operated for 105 d (a record, at the time, for continuous reactor operation). The fuel for the HRE consisted of 145 gal of 4M sulfuric acid solution containing 4.5 kg of 85% ^{235}U enriched

uranium. In 1964, the residual fuel solution and fission products were disposed of in seven unlined auger holes in the Melton Valley region at ORNL [10].

The auger holes are 1 ft in diameter, 17 ft deep, and 10 ft apart. After disposal, the wells were backfilled with soil, and concrete caps and brass plaques were installed to mark the well locations. Preliminary indications from recently installed monitoring wells have not indicated any migration of the material.

2.0.5 Miscellaneous SNF stored in ORNL's

Solid Waste Storage Area (SWSA): A variety of SNF and other materials were placed in shielded, retrievable stainless-steel dry storage positions during the 1970s and 1980s. These facilities are now closed to further storage, and the existing material is expected to be removed once new storage is completed in the late 1990s. The storage cylinders vary from 20 to 76 cm in diameter and from 3 to 4.6 m in depth [14].

Each storage cylinder is fabricated from stainless steel, placed on a concrete pad, held in place by concrete collars or slabs, and backfilled with dirt or concrete. Facility 7823A has 8 storage positions containing less than 1 kg of HM, the 7827 facility consists of 54 storage positions with 85 kg HM, and the 7829 facility has 10 storage positions with about 10 kg HM. The SNF stored in the SWSA wells varies in the degree to which it is characterized. Some of this SNF is well defined; however, some of it is assumed to be fuel based only on the listed isotopes. Very little is known about the fuel form or condition. In addition, a separate 13- by

100-cm pipe, containing 23 kg HM of grouted uranium-thorium fuel microspheres [irradiated in the Keuring van Electrotechnische Materialen Suspension Test Reactor (KSTR), Netherlands] was disposed of in 1988 [10] [13] [14].

2.0.6 SNF stored in the Y-12 Plant 9720-5 Warehouse

The 9720-5 building at the Y- 12 Plant is a large warehouse containing vaults for the storing and safeguarding of highly enriched uranium. The SNF material at 9720-5 is in dry storage and is either very low burnup or unirradiated material. Currently, irradiated SNF located at 9720-5 includes about 5 kg HM of Space Nuclear Auxiliary Power-(SNAP-) 10A fuel, 184 kg HM from the Health Physics Research Reactor **(**HPRR**)** and 2 kg HM from the DOE Demonstration Reactor [10].

The stored SNAP-IOA material includes the entire reactor and 36 fuel rods of 93% enriched uranium Zirconium hydride in a liquid sodium-potassium (NaK) alloy.

The reactor is secured vertically in a double 55-gal stainless steel drum, which in turn is placed in a standard uranium hexafluoride (UF) shipping container. The burnup of this fuel was very low, with the inner drum and outer shipping container providing the only shielding present. The HPRR material is composed of a uraniummolybdenum alloy that can be stacked into a right circular cylinder to construct a small unmoderated and unshielded reactor. Two cores and a variety of test specimens are currently stored at the 9720-5 Warehouse in a disassembled condition in 14 individual “bird cages.” This material has very little “burnup” and is contact-handled [10].

The DOE Demonstration Reactor material is anticipated to contain about 2 kg of highly enriched uranium from a Lockheed IO-kW pool-type light-water-moderated and -cooled

reactor that was operated briefly in Brazil in 1969.The SNF and various other unknown components are currently stored in eight 3- by 5-ft packages. It is unknown which, or how many of the packages contain the SNF [10] [13] [14].

2.1 THE DUCRETE CONCEPT

The USDOE has over 675,000 MT of depleted uranium hexafluoride (UF6) from the enrichment process accumulated over the last 50 years. The UF6 once was conceived as a material for use in the breeder reactor fuel cycle. However, absent a breeder fuel cycle in the foreseeable future, the material has no known use.

In 1993, DOE Environmental Management Office of Science and Technology initiated studies to identify the potential liability associated with disposal of the depleted uranium and to investigate other possible uses. The cost of disposal of UF6 would include the cost of conversion to an oxide and the subsequent packaging and disposal of the oxide. Depending upon regulations in place and the disposal site, stabilization of the depleted uranium oxide might also be required, thus, further adding to the cost. The net result was an estimated disposal liability that ranged from $3 to $11 billion [15].

Radiation shielding engineers have used depleted uranium metal in transportation casks where weight or size limits required maximizing the shielding efficiency. However, due to its high cost (raw material and fabrication), depleted uranium metal has never been seriously considered as a shielding material for spent nuclear fuel storage systems. It was recognized that if depleted uranium could be deployed at lower cost, then its use in spent fuel and HLW storage applications might be economically feasible. Subsequently, the INEEL staff developed a new radiation shielding material where the high atomic weight

benefits of depleted uranium can be used in spent fuel and HLW storage systems without incurring all of the cost for conversion to metal.

This concept came to be called DUCRETE as in depleted uranium concrete [16] . A US patent for this advanced radiation shielding material was granted in 1998 [14].

The USDOE has over 675,000 MT of depleted uranium hexafluoride (UF6) from the enrichment process accumulated over the last 50 years. The UF6 once was conceived as a material for use in the breeder reactor fuel cycle. However, absent a breeder fuel cycle in the foreseeable future, the material has no known use.

DUCRETE concrete uses depleted uranium oxide aggregate – DUAGG -- as the large aggregate in a portland cement concrete mixture. The DUAGG ceramic is produced by liquid phase sintering a mixture consisting of 93 weight percent urania (UO_2) with silica and alumina comprising most of the remaining ingredients. The DUAGG composition was developed to make the UO_2 resistant to oxidation and to allow sintering at a comparably low temperature compared to pure UO_2. DUCRETE is then made by combining portland cement with DUAGG and other ingredients to produce very dense DUCRETE concrete [17].

Table 2.1 describes two representative samples of DUCRETE. Other mixtures using fly ash and silica fume as fine additives are also being investigated. This high density (5.87 g/cm^3 versus 2.24g/cm^3 for normal concrete) results in a superior shielding material for spent fuel and high level waste applications where the source radiation is composed of both gamma and neutron flux.

Table 2.1: Composition of DUCRETE Sample

Major Ingredient	Sample 1	Sample 2
Cement	1.00	.1.00
DUAGG	9.60	8.18
Fly Ash	0.20	--
Water	0.32	0.29
Density (g/cm^3)	5.72	5.87
Compresive Strength	29.7	30.6

Both Samples contained small quantities of thin metal steel fibers and superplastizer.

Last year, researchers from Japan visited the inventors to discuss their progress in developing depleted uranium concrete [18]. The Japanese investigators have successfully made depleted uranium concrete using depleted uranium oxide pressed UO_2 pellets as the aggregate.

Mechanical tests conducted by both investigators have established that the compressive strength properties of the depleted uranium concrete are similar to that of ordinary concrete.

When DUCRETE is used for spent fuel or high-level waste shielding, the casks or overpacks are smaller in diameter and lighter weight compared to casks made from normal concrete.

For metal storage casks, very thick walls are required to attenuate both the gamma and neutron source terms unless the metal is combined with another material such as borated polyethylene or concrete. Several studies were performed by INEEL subcontractors to evaluate the use of DUCRETE concrete in spent fuel storage cask applications [19] [20]

[21] [22]. An additional, more recent, study was prepared to address a high-level waste storage cask application at the Savannah River Site [23]. Additional evaluations of DUCRETE shielding applications are underway within the Yucca Mountain Project.

The design concept for a Yucca Mountainspent fuel overpack is shown in Figure 2.1. The concept is a right circular cylinder with both bottom and top vents for natural circulation cooling. The vents in this figure are shown schematically and would be designed to minimize shine in the actual overpack. This design concept, similar to several systems available for use at reactor spent fuel storage sites, contains the spent fuel inside of the disposal waste package

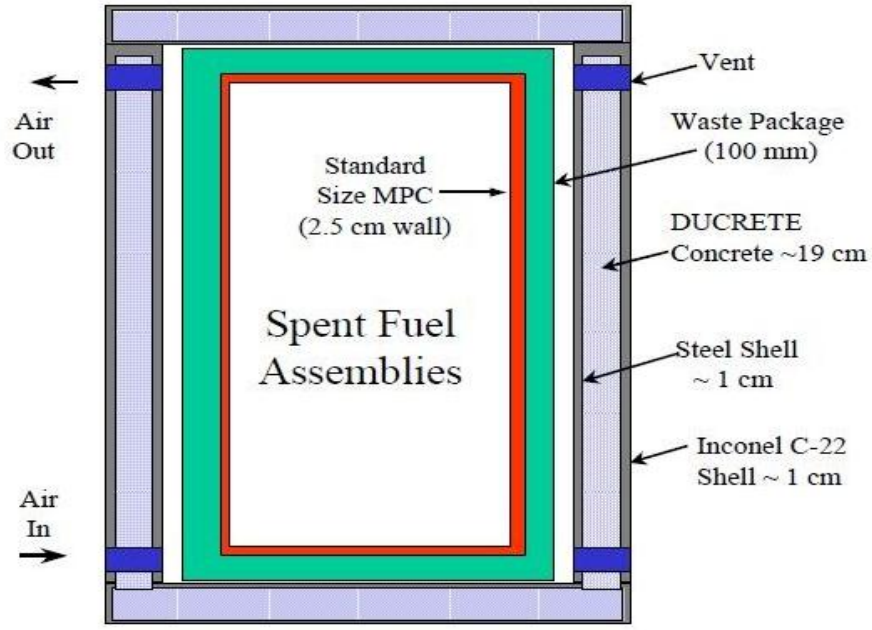

Figure 2.1: DUCRETE Spent Fuel Overpack Concept

The DUCRETE overpack has an interior steel liner and an optional exterior metal shell. The optional exterior shell material could be either carbon steel, stainless steel, or the same C-22 (Hasteloy) corrosion resistant alloy as used in the current concept of the

Yucca Mountain waste package [23]. The use of C-22 would enhance the value of the overpack as a drip shield and provide long-term protection of the waste package, although at a cost increase.

The waste package itself provides considerable radiation attenuation as it is composed of 100 mm of A-516 carbon steel and 20 mm of C-22 alloy. The DUCRETE overpack provides the additional gamma and neutron radiation attenuation necessary to allow human occupancy after the waste packages have been emplaced in a drift. After the waste package is loaded into the DUCRETE overpack, the external dose is reduced to levels safe for contact handling.

The potential benefits of a DUCRETE overpack were estimated for a DOE Workshop in 1997 [24]. The average and peak estimated dose from the unshielded waste package is about 8 and 40 R/h. The higher external dose is representative of the burnup from a waste package which meets the 18 kW limiting heat load. Clearly, such a high dose rate eliminates human occupancy in the vicinity of the waste packages. However, with the addition of a relatively thin (19 cm) DUCRETE overpack, doses external to the overpack can be reduced to about 5 and 25 mR/h for the average and peak waste package doses, respectively. The DUCRETE density used in these calculations was 5.24 g/cm3. No radiation reduction credit was taken for the two 1.27 cm steel shells in this calculation. A 19-cm wall is not necessarily optimum for dose reduction (as higher density DUCRETE has been made) but will be used as the reference concept.

The weight of the DUCRETE overpack and the total waste package system is dependent upon the overpack wall thickness. Thus, there is the balance between external dose to

workers and the total system emplacement weight. The weight optimization is beyond the scope of this thesis but is dependent upon a detailed evaluation of handling systems in the surface and in the underground facilities combined with ALARA considerations for workers.

If this DUCRETE dual purpose overpack can be used for both storage at the DOE sites and to replace the Yucca Mountain carbon steel and C-22 waste package for HLW canisters, significant cost savings can be achieved with minimal consequences to long term repository performance.

It has been estimated that 20,000 HLW canisters will be produced from the HLW from SRS, Hanford, West Valley, and INEEL [25]. With 5 canisters per waste package, this equates to about 4000 waste packages. At an estimated capital cost of $350 to $500K per waste package, replacing the waste package with a dual purpose DUCRETE dry storage system could save in excess of $1.4 to $2 billion of capital cost. Operating cost savings will be additional. If DUCRETE overpacks are used for HLW storage until Yucca Mountain becomes available. There is no significant incremental cost for the re-use of the overpack in the repository as proposed. The original cost for the DUCRETE overpack for storage is approximately equivalent to a unit cost per canister for free standing storage facility such as the Glass Waste Storage.

Building used at the Savannah River Site. Due to the small diameter of the DUCRETE overpack, the storage overpacks can be transported empty by rail between the storage site and the Yucca Mountain proposed repository. The HLW canisters will have to be transported in a licensed transportation cask meeting the requirements of 10CFR71.

In addition to cost savings, over the pre-closure period of the repository, a much safer work environment is provided assuring that any unforeseen event requiring human access can be safely accommodated within reasonable means.

2.2 THE KN-12 CONCEPT

As the number of nuclear power plants increase, the number of nuclear spent fuel discharged from the plants have gradually increased. In Korea, the storage of spent fuel will be beyond capacity, and in particular, the storage capacity of the Kori 1 unit will be at the uppermost limit within 3 or 4 years. The Korean Electric Power Cooperation considers the on-site transshipment between neighboring units to be the most useful for the spent fuel management at this time. Therefore, the Nuclear Environment Technology Institute has been developing the KN-12 spent fuel shipping cask. The shipping cask used in transporting spent fuel should be secured to protect the public and the environment from radioactive dangers. The cask is required to withstand both normal transport and hypothetical accident conditions as required by the IAEA Safety Standard Series, No ST-1 [26] and the Korean domestic regulations [27] [28]. The cask should maintain subcritical, radiation shielding, thermal and structural integrity not to release radioactive material in any condition of normal transport and hypothetical accident condition. The functional requirement of the cask is to store and transport all fuel assemblies from the Kori unit 1, 2, 3, 4, Yongwang unit 1,2 and the Ulchin 1,2. It must be approved by the Korean Competent Authority and must comply with the NETEC design criteria. The cask will be designed to transport 12 PWR spent fuel assemblies under dry internal cavity transport condition. The cask will be designed for both wet and dry cavity conditions in order to reduce the cycle time during on-site transport operation.

The KN-12 as shown in Figure 2.2 is a right circular cylinder with impact limiters at each end. A stainless steel, lead and solid shielded cask were chosen for the main parts of the body as it provided maximum shielding efficiency within the weight limit. The total weight of the cask including its contents and the impact limiters was 70 tons. The body consist of three concentric stainless steel shells; inner, intermediate and outer shells. The annular layer between the inner and the intermediate shells is filled with lead as gamma shield. The inner and intermediate shells are welded to stainless steel plates at the top and bottom of the cask. The bottom of the cask consist of two inner stainless steel circular plates

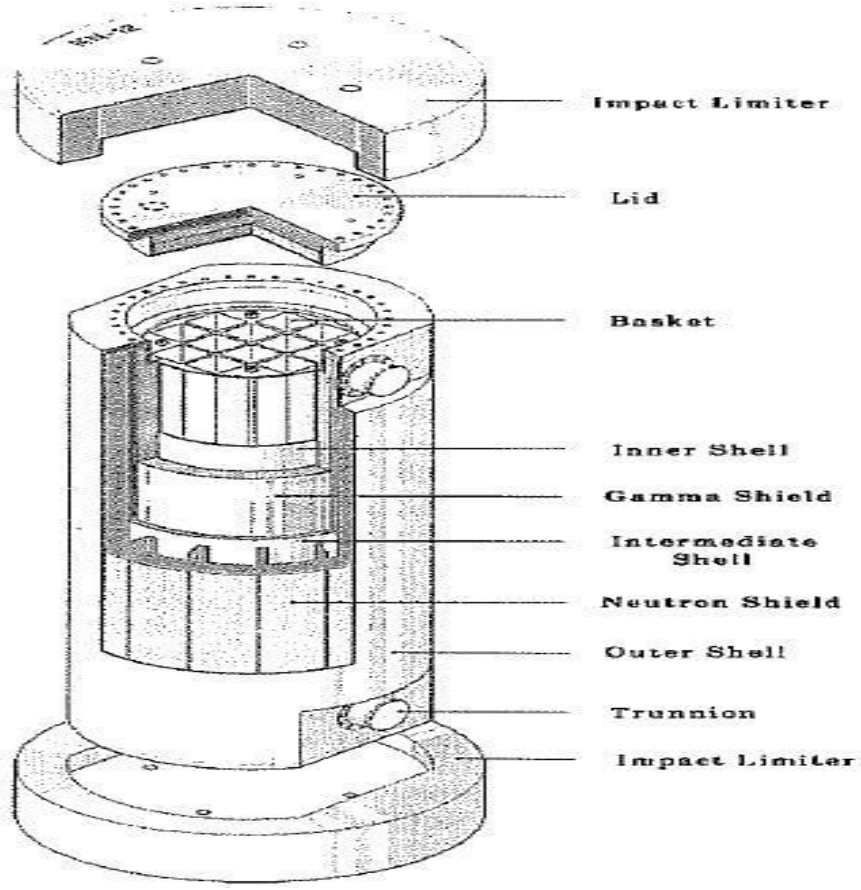

Figure 2.2: The KN-12 storage cask

The spaces between the bottom plates are filled with solid resin neutron shielding material. The cask body is surrounded by a stainless steel outer shell. The outer shell is supported by longitudinal copper heat transfer fins. The fuel assemblies are positioned in square sleeve made of stainless steel [29].

In conformance with regulations, the principal criterion for criticality safety is a maximum effective criticality factor (k_{eff}) of 0.95, evaluated with 95% probability at the 95% confidence level including the effects of manufacturing tolerances and calculational uncertainties. Confirmation of criticality safety of the fuel basket under flooded conditions, when filled with fuel of the maximum permissible reactivity for which it was designed was accomplished with SCALE 4.3 system to determine effective multiplication factor under transport and hypothetical accident conditions. Benchmark calculations were made to compare with experimental data using critical experiment to encompass the design of the cask. The 27 group library was used in all calculations including those used to evaluate the sensitivity of the cask to a range of moderator density and center-to-center spacing. Through the calculations, the effective multiplication factor was found to be below 0.95 [27] [28].

The dose rate limits specified in the regulation for normal transport conditions are 2mSv/hr (200mrem/hr) on the surface of the cask and 0.1mSv/hr (10mrem/hr) at 1m from the surface of the cask and the limit for hypothetical accident conditions are 10mSv/hr (1000mrem/hr) at 1m from the surface of the cask. The shielding analyses used the SAS2H sequence of the SCALE-4.3 to calculate radiation sources. It used the ORIGEN-S code to calculate the entire source strength and energy spectrum for radiation emitted from the basis fuel assembly. The energy spectrum for neutron and gamma radiation was

27 and 18 energy group structure respectively. The XSDRNPM-S and XSDOSE code were used to calculate the cask dose rate for normal transport and hypothetical accident conditions. The total neutron and gamma dose rate calculated for normal transport conditions are 0.2562mSv/hr (22.56mrem/hr) on the surface of the cask and 0.0842mSv/hr (8.42mrem/hr) at 1m from the surface of the cask. The accidental dose rates occurred in the event of the loss of neutron shield was 0.3385mSv/hr (33.85mrem/hr) at 1m from the surface of the cask. The maximum dose rate for both the normal transport and the hypothetical accident conditions were less than the regulatory limits [29].

The heat transfer analysis was performed with the HEATING 7.2 code to demonstrate that the cask could maintain a design basis temperature required for fuel cladding integrity under a range of thermal conditions and to demonstrate that the containment boundary system of the cask was maintained within safe operating temperature ranges. Temperature for the cask components including the fuel which were used in the input data for the fire transient analysis were calculated for normal conditions of 12.6kW decay heat load, 38^{o}C ambient temperature and solar insulation. The maximum fuel cladding temperature was 276^{o}C and maintained below 380^{o}C. The hypothetical fire accident condition was evaluated by imposing an 800^{o}C fire temperature for 30 minutes followed by post fire equilibrium which was followed for 4 hours. The temperature time history of several points and maximum cask temperature during and post fire accident were calculated. The maximum fuel cladding temperature was 276^{o}C and maintained within the safe operating ranges.

To perform a stress evaluation for the cask, the dynamic analyses under a 9m free drop and 1m puncture conditions were performed with a three dimensional analyses model using the ABAQUS finite element code. For each 9m drop, the impact force was linearly jumped and suddenly decreased such that it was absorbed by the crush of the impact limiters which is made of balsa and red wood. For the 1m puncture, the outer shell and neutron shield layer of the cask impacted onto the round bar and were largely and locally deformed but scarcely any part of the cask body was damaged. Any maximum stress intensity on each part of the cask for each condition did not exceed the allowable value prescribed in the regulations [28].

The requirement for the interim storage of the spent fuel is derived from a number of considerations associated with the management option selected. In the closed nuclear fuel cycle, further fuel storage capacity may be required to match the arisings of spent fuel with the available capacity of reprocessing plants. With respect to the once through cycle, interim storage casks is required until a final repository is constructed and in service. Clearly, for a deferred decision, the availability of adequate storage cask is a key element. There is a scientific consensus that present fuel storage technologies provide adequate protection to the population and the environment. However, there is a keen interest in seeing whether further improvements can be achieved in the area of spent fuel cask storage [30].

Some of the spent fuel management options available include the conditioning and possible repatriation of spent sealed radioactive sources, conversion of fuel from highly enriched to low enriched and the return of spent fuel to USA and the Russian Federation. These activities have great challenges and are connected with important legal and

administrative procedures. The activities are done in close and positive cooperation with the Office of Nuclear Security and the Department of Technical Cooperation and with the support of the Office of Legal Affairs of the IAEA.

Fuel take-back programmes are ongoing between countries. For instance, in December 2005, the first shipment of spent HEU fuel under the Russian Research Reactor Spent Fuel Return (RRRSFR) took place with the return of spent fuel from Uzbekistan to the Russian Federation [31].

The removal of spent nuclear fuel from the research reactor at Serbia's Vinca Institute of Nuclear Sciences has been an ongoing activity of the IAEA since 2002. Safe removal of spent fuel from the Vinca RA research reactor institute achieved a major milestone with the signing of the spent fuel repackaging and repatriation contract between the IAEA, a Russian consortium and Serbia. Under the contract, in excess of two metric tones of spent nuclear fuel from the Vinca RA reactor were repackaged and transported to the Russian Federation.

Meanwhile, the Foreign Research Reactor Spent Nuclear Fuel (FRRSNF) acceptance program of the United States was recently extended until 2016. "So far, 27 countries have participated in the program, returning a total of 6,783 spent nuclear fuel elements to the U.S., most of this being HEU fuel. But, as of October 2005, there were more than 15,000 fuel assemblies eligible to be returned under this program stored outside the U.S. The scope of the program includes an estimated 5000 kg of HEU that the United States exported to research reactors in 34 countries, as well as an estimated 15,000 kg of LEU [32].

Fuel rods holding the spent fuel may be stored in water pools for several years to allow decay of the most intensely radioactive fission products. Subsequently, they are removed to dry storage about 300 m underground in a dry, geologically stable medium. Alternatively, the spent fuel rods are reprocessed by separating the uranium and plutonium, which is followed by reprocessing to produce new fuel. Isotopes for specialty medical or industrial uses may also be separated. Long-lived fission products and actinides may be separated and returned to the reactor for transformations to stable or rapidly decaying isotopes (transmutation). Because uranium and plutonium make up 97.1% of the spent fuel while industrially usable isotopes and actinides constitute 2.6%, reprocessing utilizes valuable waste components while reducing the waste to about 1/300 of its initial volume. The result is that the annual per capital high-level waste is about the size of an asprin tablet. [33] This waste may be encapsulated in molten glass, cooled, and then buried about 300 m deep in a dry geologic medium impermeable to water before being packed in bentonite clay. The radioactive components will decay to the level of natural uranium within about 10,000 years. The currently preferred burial site is Yucca Mountain in Nevada where the water table is about 550 m deep. At a depth of 300m, the waste will not be exposed to either rainfall or upwelling groundwater. At the site, a vertical central shaft will be connected to horizontal tunnels holding the waste canisters, which are made of corrosion-resistant titanium or steel. After filling with waste, this structure will be sealed with bentonite clay. Use of the described multiple barriers should retain the high-level wastes safely for the required long periods of time [34].

2.3 Nuclear Research Institute Řež plc (NRI)

The VVR-S reactor started its operation in 1957. The original EK-10 fuel was made up of rods of a 10 % enriched uranium dioxide-magnesium alloy in aluminium cladding. The fuel assembly (FA) consisted of 16 rods in an aluminium casing [31].

In 1974, the IRT-2M fuel with 80 % enrichment was introduced. This consisted of 4 or 3 concentric square rings of uranium/aluminium alloy fuel/metal clad on either side with aluminium. In 1996, the IRT-2M fuel with 36 % enrichment and used uranium dioxide was introduced [31].

In the years 1969 – 1975, EK-10 Spent Nuclear Fuel was transferred from the reactor site to the Reloading Site. SNF was held in dry storage drums. The SNF was then transferred to the High Level Waste Storage Facility (HLWSF) between the years 1996-7 (see Figure 2.3, Figure 2.4). According to the period of storage, the character of construction materials of drums (carbon steel drum filled with concrete, carbon steel liner) and the possible interaction of the drum material with aluminium cladding, corrosion of the cladding had to be taken into consideration. It was decided to repack all EK-10 SNF into canisters [31] [35].

Figure 2.3: Temporary Storage of drums with EK-10 SNF in the HLWSF

Figure 2.4: View inside one EK-10 drum after plug removal

The new hot cell had been constructed in the HLWSF and EK-10 SNF was repacked into stainless steel canisters, hermetically sealed (welded) (see Fig. 2.3), put into a cask basket and then stored in a special storage facility located close to the hot cell. SNF repacking started in 2006 and was completed this year. Additionally, some leaked IRT-2M FAs were repacked in the hot cell. Figure 2.5 shows the canister welding process [35].

Figure 2.5: Welding of canister with EK-10 FA inside the hot cell

The most of IRT-2M fuel was moved out of the initial AFR pool in the reactor building into the HLWSF pool between the years 1996 – 2003. The ŠKODA 1xIRTM transport cask for one FA was used. This cask was also used for the transport of 2 leaky FAs from the reactor site to the HLWSF facility [35].

2.4 THE CZECH REPUBLIC`S PARTICIPATION WITHIN THE GLOBAL THREAT REDUCTION INITIATIVE (GTRI) PROGRAM

The Czech Republic was included into the GTRI program in 2004. In 2005, the contract between United States Department of Energy (US DOE) and the Nuclear Research Institute Řež plc (NRI) was signed. Preparation and implementation of the shipment of HEU SNF are very demanding and highly professional problems requiring cooperation of a number of organizations. With the significant technical and financial aid of the US Administration and the US DOE (total of approximate CZK 450 million.), the Czech Republic has become a pilot country, which will carry out such shipment from the NRI to the Russian Federation (RF) by means of special developed and tested casks, which are

compatible with the technology of research reactors of Russian design as well as the technology of the reprocessing plant in the RF [31].

Tender for such casks took place under the auspices of IAEA. Six famous manufacturers from the USA, RF, Germany, France and the Czech Republic participated therein. The ŠKODA JS a.s., which ensured manufacture of 16 casks, development of which was initiated 10 years ago by ŠKODA JS a.s. and the NRI under the auspices of the Ministry of Industry and Trade of the Czech Republic, was chosen as a supplier. Six ŠKODA VPVR/M casks were purchased by the NRI for shipment of LEU SNF; ten casks for shipment of HEU SNF were purchased by the US Administration (approximately USD 4 million) and as a gift to the NRI provided that the NRI shall provide these as well as its casks for the RRRFR program. Once the shipment of SNF from the NRI is carried out, all 16 casks will be further used for return shipments of SNF from other countries to the RF by agreement between the NRI and the US DOE taking account of experience of the NRI from preparation and implementation of the transport from the Czech Republic to the RF.

2.5 ŠKODA VPVR/M TRANSPORT AND STORAGE CASK

The ŠKODA VPVR/M cask (see Figure 2.6) is a type B(U) and S cask system designed and licensed for the transport and storage of SNF of Russian origin research reactors [36].

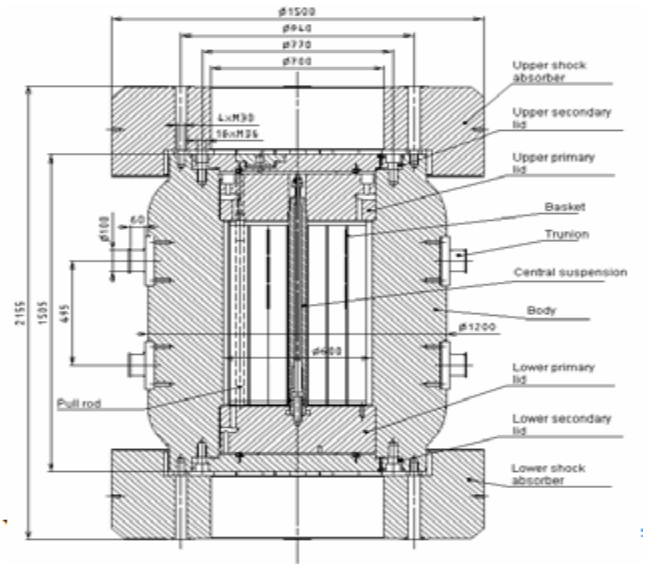

Figure 2.6: Scheme of the VPVR/M transport and storage cask

Figure 2.7: Manipulations in the manipulation frame

The VPVR/M cask loading procedure is divided into following activities:

− Cask transport in the ISO container to the SNF loading site

− Dismantling the cask in the manipulation frame (see Figure 2.7)

− Transport of the cask to the SNF storage facility (pool, hot cell)

− Putting the basket inside the loading facility (pool, hot cell)

− Loading the SNF into the basket, basket retraction into the cask

− Flushing of the cask with hot air, desiccation of the cask

− Cask completion, helium leaking test

− Cask sealing by IAEA and EURATOM seals

The specially designed basket handling tool is used for lowering the basket from the cask into the storage pool (see Figure 2.8, Figure 2.9). The basket is filled manually with the FAs by a special manipulation rod.

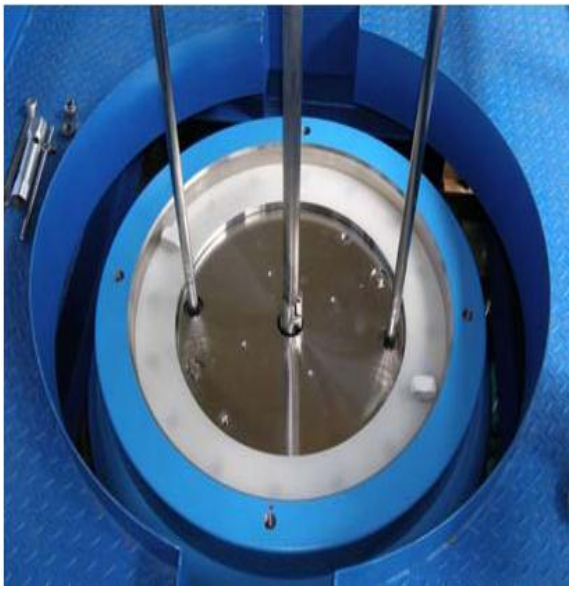

Figure 2.8: The attached central suspension/ hanger and centring fixture pull rods

Figure 2.9: Basket with lower lid in the storage pool.

The crane and lift fixtures are equipped with a digital dynamometer that is used to monitor the weight of the basket during reinstallation into the cask. It prevents the disruption of the central suspension/hanger [37].

The VPVR/M cask underwent three demonstrations to verify that the design was acceptable technically, for handling and loading SNF at the research reactor facilities and receipt and unloading at the Mayak facilities in RF. The demonstrations were held at the ŠKODA, NRI and Mayak facilities.

2.6 Demonstration of the VPVR/M cask at ŠKODA Manufacturing Facilities

The first demonstration was required by the DOE technical team to verify that the VPVR/M cask design was technically acceptable for use by the RRRFR Program. The demonstration was conducted in Plzen, the Czech Republic, at the ŠKODA JS company. The demonstration included a leak test, cask manipulation operation, simulating the unloading of the fuel basket at MAYAK (see Figure 2.10), loading the SNF, and

demonstrating the accidental failure of the central suspension/hanger resulting in the drop of the full basket [38].

2.7 Wet Run in the NRI Rez plc

The purpose of the NRI "wet run" was to: demonstrate that the handling equipment worked properly at the reactor site and at the HLWSF; demonstrate the detailed operating procedures; provide training for the NRI technicians; dry and seal the cask and prepare the cask for transport and loading it into the ISO container. The "wet run" was observed by representatives from the USA, Ukraine, Poland, Russian Federation, Bulgaria, Slovakia, and various organizations from the Czech Republic [36] [37] [38].

2.8 Mayak Dry Run

The third demonstration was performed at the Federal State Unitary Enterprise (FSUE) Mayak Production Association facilities, in Ozyorsk (see Figure 2.11). The purpose was to demonstrate the set-up of the cask handling and auxiliary equipment at the Mayak facilities; demonstrate that the detailed operating procedures were complete and operational; training of the Mayak technicians; and performing cask maintenance in preparation for loading the empty cask for transport and loading it into the ISO container, tying it down, and returning it to the originating facility. The dry run was attended by representatives from the Czech Republic (NRI and ŠKODA JS), DOE, FSUE "Mayak", "Sosny" R&D Company, and Rosatom [37] [38].

Figure 2.10: Basket being lifted out of cask using the central suspension/hanger

Figure 2.11: Basket inside the modified Mayak storage pool fuel handling cart

Currently available and feasible options that have been recognized by the International Atomic Energy Agency and practiced by overseas organizations have been considered for the spent fuel from GHARR-1 and are described below.

2.9 RBMK-1500 SPENT NUCLEAR FUEL CONTAINERS

Part of Ignalina Nuclear Power Plant (INPP) SNF is stored in the CASTOR and CONSTOR containers [39]. The metallic CASTOR cask is designed for transportation

and long term storage purposes, while heavy concrete based CONSTOR cask is usually used for the long term immobile storage. Both of these containers are designed for 50 years with possible extension up to 100 year depending on their safety conditions. To assess the radiation doses outside the containers and to evaluate their reliability after expire time, the composition of the SNF must be known and the transport of resulting source neutrons and γ quanta modeled properly. One has to note that the extension of storage time using these containers depends on the knowledge of the characteristics of SNF and resulting dose rates. Unfortunately, there are very little published data on RBMK SNF characteristics. Even the information on neutron fluxes in the fuel elements is not known precisely. Therefore, experimental measurements of dose rates outside the representative storage containers are indispensable despite of powerful modeling tools available today for radiation transport estimates.

A 3D model of the RBMK-1500 spent nuclear fuel storage container CASTOR has been created using the 3D MCNP5 geometry set-up (see Figure. 2.12 for details). The geometrical parameters, material properties and spent nuclear fuel filling history of the container were taken from the data of representative CASTOR container No.0067-14. The 2.08 m of diameter, 4.4 m of height and 30 cm of wall thickness cylindrical metallic container CASTOR is produced from cast iron. The container is filled with “32M" stainless steel basket where SNF assemblies are placed. This “32M” basket contains 51 fuel assemblies, each of them being divided into two parts (341 cm long each). The burnup of 2 % ^{235}U enrichment spent nuclear fuel in the container varies from 13 MWd/kg to 22 MWd/kg. In order to simplify their approach only 6 types of different fuel burnup assemblies were modeled. 102 different half-assemblies were located in the

specified places using MCNP5 hexagonal lattice option filled with appropriate assemblies (see Figure 2.12) as reported in the CASTOR container.

To perform the calculations several computational codes had to be combined. Modeling of SNF nuclide composition was done using Monteburns code [40]. Afterwards, the gamma and neutron source spectra were calculated with the ORIGEN-ARP code from the SCALE 5 codes package. Finally, MCNP5 was used for neutron and gamma transport and evaluation of radiation dose rates at the surface of CASTOR cask. For the input data MCNP5 requires detailed 3D geometry and particle source description, material composition, their densities and specific nuclear data. In this case, ENDF/B-VI data library was used for the fuel and structure materials, while JENDL-3.2 data files were employed for fission products.

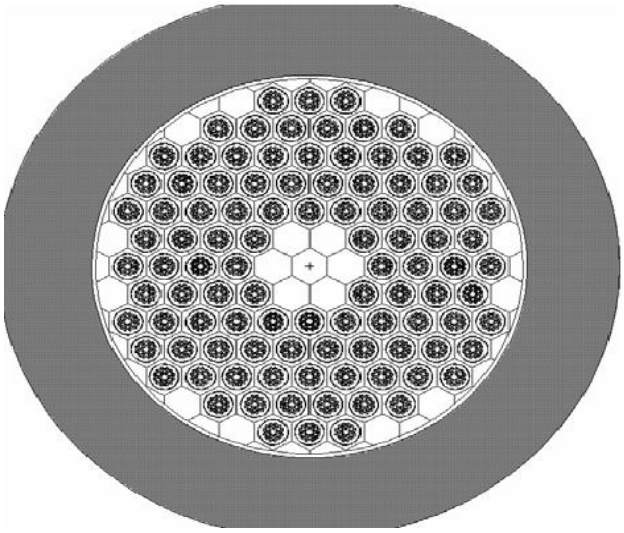

Figure 2.12: Cross-section of the SNF container CASTOR modeled with MCNP5

This particular container No.0067-14 was also examined experimentally with standard thermo-luminescence (TLD) and "Series 1000 MIN-RAD" dosimeters. The dose in the TLD attached at 8 points around the CASTOR container was accumulated during the

period of 167 hours, the total measurement uncertainty is below 10 % [41]. In addition, γ dose rates were also measured with MIN-RAD at 4 points at the CASTOR cask surface. The precision of MIN-RAD was somewhat worse compared to TLD but should be below 15 % [41].

The energy distribution of γ rays is very similar for every fuel burnup considered, but on the other hand, the γ rays intensity is changing with fuel burnup. The difference of total γ source intensity between 13 MWd/kg and 22 MWd/kg fuel is about 50 %.

The neutron spectra were also similar for different cases of fuel burnup . The difference between 13 MWd/kg and 22 MWd/kg fuel burnup results in the increase in the neutron source intensity nearly by one order of magnitude (~8 times).

The total γ source intensity in the cask is about $1.76 \cdot 10^{16}$ γ/s, and the total neutron source intensity is ~$7.62 \cdot 10^{7}$ n/s. These values were used in our further calculations for normalization of gamma and neutron doses calculated with MCNP5. The average intensity of the γ source from one fuel assembly is about $3.45 \cdot 10^{14}$ γ/s, which corresponds to 16 MWd/kg fuel burnup. The averaged intensity of the neutron source from one fuel assembly is $1.49 \cdot 10^{6}$ n/s corresponding to the fuel burnup between 16 MWd/kg and 17 MWd/kg.

The dose rate calculations were performed with MCNP5 using ring detector option for two different particle source descriptions: homogeneous gamma and neutron source distribution of 16 MWd/kg SNF in all 102 half-assemblies and heterogeneous distribution taking into account different burnup SNF assemblies from 13 MWd/kg to 22 MWd/kg according to the existing irradiation history.

Due to γ rays attenuation in CASTOR wall the photon flux decreases nearly by 10 orders of magnitude at the surface. In order to obtain a statistically significant result in a reasonable computing time specific variance reduction techniques were applied to increase the statistics of Monte Carlo calculations: the photon tracking transport importance in MCNP5 was gradually increased from 1 to 10^6 starting from the initial to the outside wall of the cask.

The results of γ dose rates at the surface of CASTOR cask are presented in Figure 2.13. The experimental data measured with TLD and MIN-RAD dosimeters are presented in circles and triangles, respectively. The MCNP5 modeling results are also compared to SCALE 4.3 predictions from [39]. We note that γ dose rates obtained from Monte Carlo simulations even taking into account the neighboring containers (we assumed the γ dose rate from the similar container surface at 1 m distance (11.8 μSv/h) and added to the calculated surface dose rate (26.8 μSv/h)) give a somewhat smaller average value of 38.6±0.4 μSv/h compared with measurements. All experimental γ dose points are ~1.6 times above the MCNP5 calculated average, especially for MIN-RAD measurement at 180º angle, where difference is almost 2.5 times. In our opinion, this result is rather good taking into account other uncertainties of our model (spent nuclear fuel composition, irradiation and cooling history, Co contents in the fuel cladding, etc.). In addition, this difference might also be due to the CASTOR container surface contamination with fission products from the cooling pool. In addition, the TLD are sensitive to the thermal neutron flux, which also might explain the increase in the measured γ dose.

On the other hand, the Monte Carlo calculations agree quite well with independent calculations performed with SCALE 4.3, which resulted in the 52 μSv/h dose rate after

10 years of cooling time [39] [42] [43]. The difference in the γ dose after ~13 years (our work) and 10 years [39] [42] [43] is determined mainly by ^{106}Rh (daughter of ^{106}Ru) high energy gammas, which have great influence on the γ dose due to the higher penetration through the cask walls, and by the ^{60}Co with its relatively short half-life ($T_{1/2}$ = 5.27 years).

Neutron dose rate at the surface of the CASTOR cask calculated with MCNP5 is presented in Figure 2.14. The two cases were considered: a) the case of a homogeneously distributed neutron source of 16 MWd/kg fuel burnup, and b) the case of a heterogeneously distributed neutron source taking into account fuel assemblies of higher burnup. The average neutron dose rate is about 75 μSv/h, and for the homogeneously distributed neutron source of 16 MWd/kg fuel burnup the neutron dose rate values vary from 68 μSv/h to 85 μSv/h. In addition, one sees that for the neutron source even a few assemblies with high burnup can cause observable anisotropy of neutron dose rates. This can be explained by lower neutron attenuation rates compared to gammas both in the absolute value and changes in energy spectra. For the heterogeneously distributed neutron source the average neutron dose rate is about 85 μSv/h, and the neutron dose rate values vary within the range from 76 μSv/h to 104 μSv/h. The local superposition of half-assemblies of higher burnup (16 MWd/kg - 22 MWd/kg) at the angles of 270º and 220º resulted in about 28 μSv/h increase in the neutron dose rate. This result confirms what neutron flux distribution is extremely sensitive to the fuel burnup and influences the neutron dose rate calculation results. In conclusion we would like to emphasize that neutron dose rate calculation should be performed with real SNF neutron source distribution in the container, because averaged burnup fuel (in our case 16 MWd/kg)

causes incorrect results. The measurements of neutron dose rates would be very useful to validate our predictions.

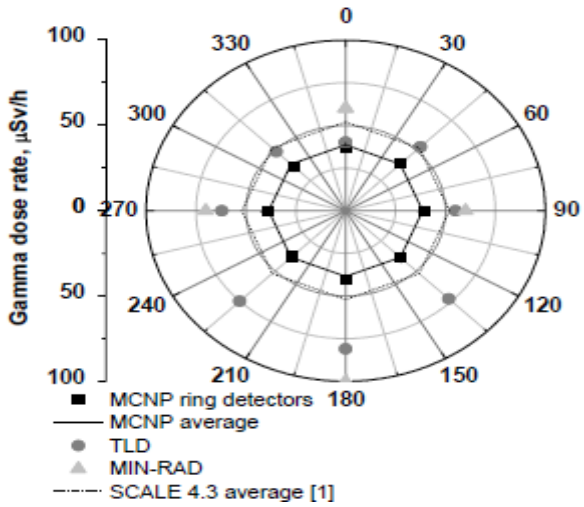

Figure 2.13: Angular gamma dose rate on the surface of castor cask calculated with MCNP5 against SCALE 4.3 predictions and experimental data measured with TLD and MIN-RAD dosimeter

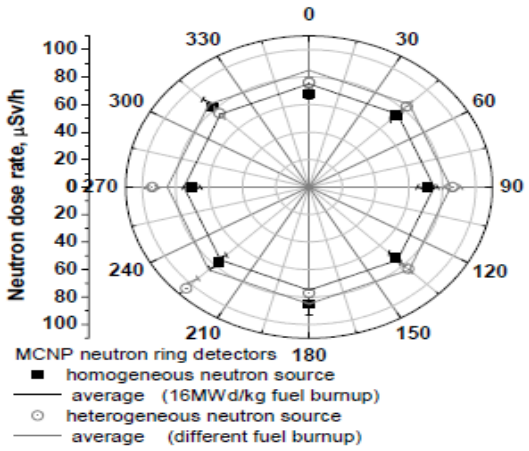

Figure 2.14: Angular neutron dose on the surface of castor cask calculated with MCNP5 in the case of homogeneously distributed neutron source and in the case of heterogeneously distributed neutron source

The neutron and gamma ray sources in the SNF storage cask CASTOR have been estimated using different radiation transport and material evolution code packages as ORIGEN-ARP, MCNP5 and Monteburns. The neutron dose rate from the surface of the

cask varies within the range between 76 μSv/h and 104 μSv/h. The anisotropy of dose rates is observed for neutrons and is explained by heterogeneous distribution of different burnup fuel assemblies inside the container. The estimated averaged gamma dose rate is 38.6±0.4 μSv/h, and is determined mainly by ^{137}Cs and ^{60}Co. This result underestimates the corresponding measurements performed with TLD and MIN-RAD dosimeters by ~50 %. The obtained discrepancies might be due to possible surface contamination, the partial gamma dosimeters sensitivity to neutron flux from the container, etc. Some additional investigations on this subject will be performed in the near future, although in general the agreement between our predictions and measurements is satisfactory. This work validates the methodology of the radiation shielding and dose rate calculations for RBMK SNF storage facilities. However, more experimental data are needed (in particular for other types of storage containers) in order to provide more precise uncertainties of the predicted values.

2.10 Immediate Dismantling

This is the option whereby the complete reactor assembly and ancillary systems are removed or decontaminated to a level that permits the property to be released for unrestricted use. This approach normally occurs shortly after the reactor is shutdown. If the facility or the reactor site is to be reused for future nuclear activities, restricted release may be prudent instead of unrestricted release [44].Some of the advantages of this method are

- Personnel with first-hand knowledge of the reactor are still available;
- Immediate reuse of property is possible;

- There is no liability for the reactor after decommissioning.

Disadvantages of this method includes

- Little decay period is available;
- Potential for higher radiation doses to workers during dismantling is increased;
- Dismantling and waste management costs may be higher due to higher activity level;
- Funds must be provided immediately.

2.11 Long Term Storage

Long Term Storage is one of the most popular methods for large reactors in which the nuclear facility is stored and maintained in a safe condition allowing it to decay sufficiently before dismantling. The storage period may last from several years to 140 years depending on the results of characterisation of the radioactive inventories at the time of shutdown [44]. Some of the merits of this method are

- More efficient and cost-effective dismantling techniques will be developed;
- Sufficient decay period would allow lower radiation exposure to operators during dismantling;
- Waste from dismantling can be handled safely due to the reduced activity levels;
- Active waste volume is low;
- Waste disposal cost is low.

Notable demerits of this method are

- Staff with first-hand knowledge of the reactor will not be available;

- Maintenance and surveillance must be carried out on a regular basis to prevent deterioration;
- Costs for care and maintenance will accumulate to a large sum;
- The site cannot be re-used until dismantled;
- The reactor owner will be liable for the safety of the reactor for a long time.

2.12 Entombment

The entombment is the method whereby the reactor structure is encased in a structurally stable material, such as concrete. The entombed structure is to be maintained and surveyed until the radioactivity decays to a level that permits unrestricted site release. This method is limited to the facilities where the appropriate decay of the nuclides in the nuclide vector is shorter that the expected life of the structure [38] [44]. Marked advantages include

- Initial waste disposal cost is low;
- Waste management is simplified;
- Overall decommissioning cost is low;
- Radiation hazards to operators during decommissioning are low;
- Special equipment or technology is not required.

Disadvantages

- It is not appropriate for most research facilities due to the presence of long-lived nuclides requiring several centuries to decay to an acceptable free release level;
- Long term liability and maintenance cost may cause a serious problem
- The reactor site cannot be reused.

2.13 Ghana Research Reactor-1

The Ghana Research Reactor-1 (GHARR-1) is a commercial version of the Miniature Neutron Source Reactor (MNSR) and belongs to the class of tank-in-pool type reactors [45] [46]. It is under-moderated with an H/U atom ratio of 197. The thermal power rate of the facility is 30 kW with a corresponding peak thermal neutron flux of 1.0×10E12 n/cm^2 s [46]. For fresh core, its cold clean excess reactivity is about 4 mk. Cooling is achieved by natural convection using light water. Presently, the GHARR-1 core consists of a fuel assembly HEU (U-Al alloyed) fuel elements arranged in ten concentric rings about a central control rod guide tube, which houses the reactor's only control rod. The control rod's reactivity worth is about -7 mk, providing a core shutdown margin of 3 mk of reactivity. The small core has a low critical mass. However, its relatively large negative temperature coefficient of reactivity is capable of boosting its inherent safety properties [46]. The small size of the core facilitates neutron leakage and escape in both axial and radial directions. To minimize such loses and thereby conserve neutron economy, the core is heavily reflected, respectively, on the side and underneath the fuel cage by a thick annulus and slab of beryllium alloy material. Adding regulated shims of beryllium to the top tray compensates for loss of reactivity due to axial neutron leakage, fuel burnup and samarium poisoning. Figures 2.15 and 2.16 is a schematic diagram of the GHARR-1 core. Table 2.2 also shows a summary of the pertinent design data for GHARR-1 fuel rods. Due to its inherent safety features, stability of flux and moderate cost, the MNSR has recently found enormous application in various fields of science [47] particularly in trace elements in matrices of biological and environmental samples [48] and soil fertility studies and geochemical mapping [49].

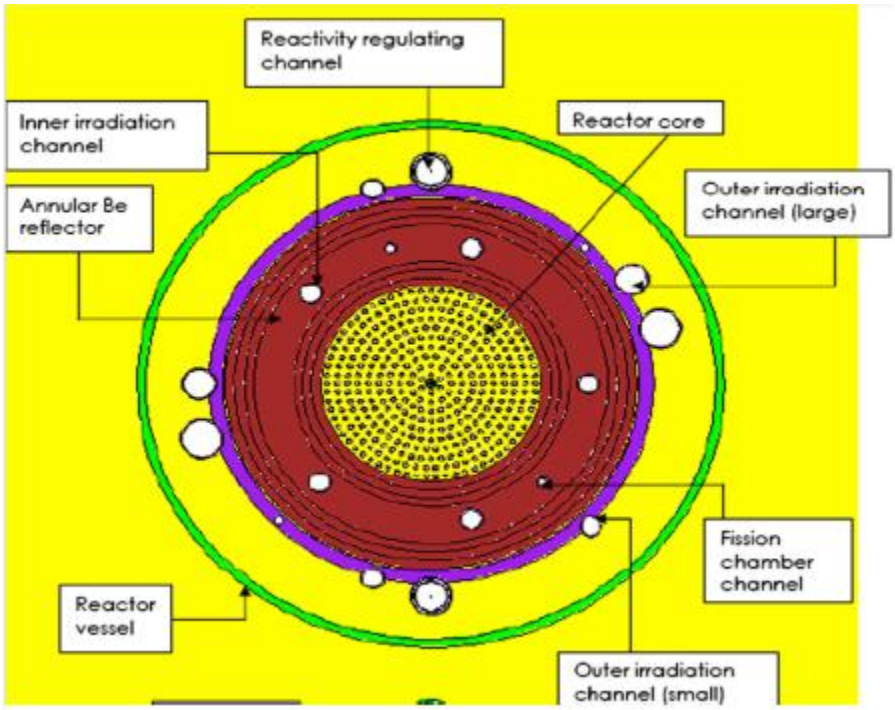

Figure 2.15: GHARR-1 core configuration showing fuel region.

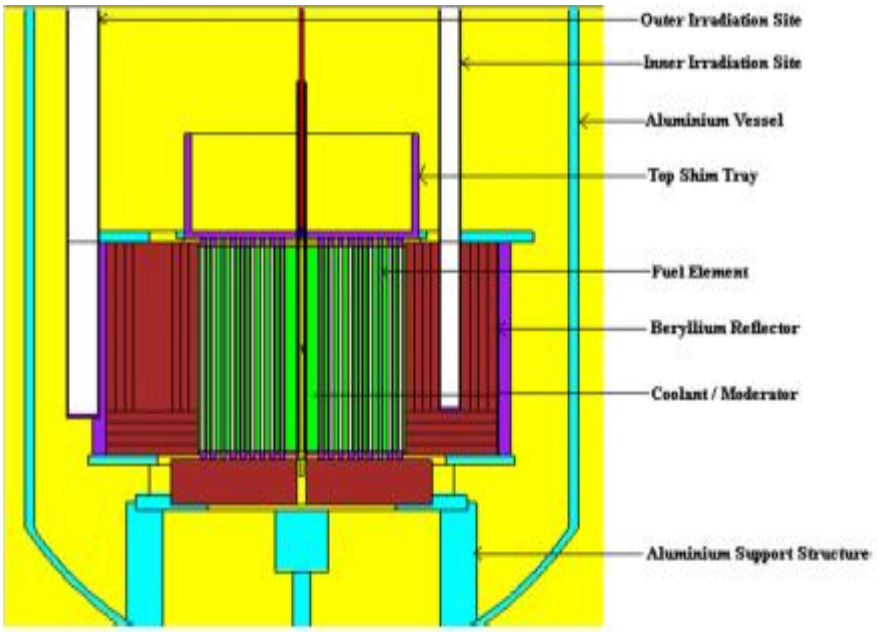

Figure 2.16: Vertical cross section of GHARR-1 reactor.

Table 2.2: Pertinent design data for GHARR-1 fuel rods are summarized

Parameter	**GHARR-1**
Reactor Power, kW	30kW
Number of rods in Core	344
Uranium density in fuel meat, g/cm^3	0.92
Enrichment,%	90.2
Fuel Meat, mm	4.3
Fuel rod, mm	5.5
^{235}U/rod	2.9011
^{238}U/rod	0.2902
Peak Rod Power, W	103.60
Anticipated Core Residence, FPEDs	750

The management of the spent fuel that will eventually confront us is a huge challenge. The design and construction of a temporary storage cask is very important to enable us store the fuel until we have a permanent storage for it. The cask was designed to ensure sub criticality as well as low radiation dose levels to the public and the environment. Another important feature is that the cask has a relatively small size taking into account the small size of the GHARR-1 core (radius of about 60cm). The cost of designing and fabricating such a cask was also put into consideration. Local materials that are readily

available are used in designing the cask thereby making it relatively cost effective. A conservative cask design (the spent nuclear fuel on the onset of discharge was used in the calculations) that constitutes multiple neutron and radiation shield was chosen as an ideal cask for this study. Taking into account the cylindrical nature of the GHARR-1 core, cylindrical cask is designed with materials that will ensure radiological safety and sub criticality. Among the materials used are, boron carbide for neutron absorption, resins for thermalisation of neutrons, lead for gamma attenuation and stainless steel for neutron absorption. Nitrogen was introduced in the aluminium canister containing the spent fuel for cooling. Aluminium canister is used instead of a fuel assembly basket to hold the spent fuel as the GHAAR-1 core is a once-through fuel and so there are no fuel assemblies. Tubular orifices were introduced at opposite sides of the cylindrical cask to ensure natural circulation (one tube is on the upper end of the cask whilst the second is on the lower end at the opposite side of the cask).

The imminent conversion of our HEU core to LEU shall undoubtedly leave us with spent HEU fuel to deal with. Due to the complex legal and administrative challenges involved in the take-back programmes, it is important to have a storage cask in place for the anticipated storage of the spent fuel before it is returned. Ghanaian serpentine is also used as the shielding material. Some designs of shield of the light water Reactors around the pressure vessels are made of ordinary concrete. It loses more than half of its water contents when temperature exceeds 90^{o}C [50]. Thus, the concrete must be cooled and maintained at temperature of 50^{o}C [51]. Such shields are provided with ducts for cooling when temperatures exceed 90^{o}C to avoid deterioration of its mechanical and attenuation properties. This situation is extremely precarious when they are used for high power

reactors. An alternative to the use of ordinary concrete is serpentine which in contained in a rock called serpentinite. It consist of a hydrous magnesium silicate with water of hydration ($3MgO.\ 2SiO_2.\ 2H_2O$). The rock also contains calcium and aluminium oxide [52]. Serpentine has higher percentage water content than concrete; which makes it suitable for shielding neutrons [53]. Since it loses its water of crystallization when heated above 480^oC such serpentine shield could be subjected to high temperature and there will be no need to provide complex and expensive cooling systems for radiation shielding. Serpentinite rocks are available elsewhere (Libya, Russian etc.). Three deposits have been found in Ghana which was located at Anum, Peki-Dzake and Golokwati [54]. They were investigated and found to be suitable for photon attenuation [55].

Serpentine slabs will be used in place of concrete in the proposed casks. Serpentine rocks will also be used to replace gravels as the course aggregate in concrete (SEPCRETE). Several numerical and computational methods or approaches based on nuclear reactor physics, nuclear engineering and mathematical theories exist for performing particle transport analysis. Over the years, both deterministic and stochastic methods have been employed in the performance of analysis of particle transport [56].

With improved mathematical and numerical computational methods, analysis of particle transport have even become more involving howbeit exacting in time, space and energy [57]. With the advent of advanced, powerful and sophisticated computers, innovative methods involving the extensive use computational codes or tools (e.g. Monte Carlo-based MCNP, SCALE, ANISON, MONK, RELAP5, MONTEBURN etc) [55] [42] [43] [58] and large scale computing facilities have now been adopted in analyzing complex nuclear and radiation transport processes as well as the design of appropriate storage

cask. The cask will seek to optimize shielding in its design in order to reduce radiation to as low as reasonably achievable. Also, the isotopic inventory of the core will be analyzed and predicted to verify information given by operators [57] [42] [43] [58].

It is also hoped that a cost analyses of the various casks designs will be evaluated and recommendation made. An overall safety assessment of the cask storage systems will be an integral part of this work.

Various computational tools were used in the calculations and analyses of the spent fuel cask. A general insight into how they are employed in solving the problems is given in the next chapter to help understand the way they work.

CHAPTER THREE

3 THEORY

A number of computational tools were used in the design of the cask. These codes are developed based on certain fundamental equations. The codes that were employed in this study include WIMSD4, ORIGEN2, REBUS3 and MCNP5. The codes are used for core depletion studies, particle transport and dose calculation.

The theoretical basis of the codes is investigated in this chapter.

3.0 ORIGEN2

In determining the time dependence of nuclide concentrations, ORIGEN2 is primarily concerned with developing solutions for the following equation

$$\frac{dN_i}{dt} = \text{Formation rate} - \text{Destruction rate} - \text{Decay rate} \qquad (3.1)$$

ORIGEN [59] considers radioactive disintegration and neutron absorption (capture and fission) as the processes appearing on the right-hand side of Eq. (3.1). The time rate of change of the concentration for a particular nuclide, N_i, in terms of these phenomena can be written as

$$\frac{dN_i}{dt} = \sum_j \gamma_{ji}\sigma_{f,j}N_j\phi + \sigma_{c,i-1}N_{i-1}\phi + \lambda_i' N_i' - \sigma_{f,i}N_i\phi - \sigma_{c,i}N_i\phi - \lambda_i N_i \qquad (3.2)$$

where (i = 1, ... I), and

$\sum_j {}_i\ \gamma_{ji}\sigma_{f,j}N_j\phi$ = yield rate of N_i due to the fission of all nuclides N_j;

$\sigma_{c,i-1}N_{i-1}\phi$ = rate of transmutation into N_i due to radiative neutron capture by nuclide N_{i-1};

$\lambda_i' N_i'$ = rate of formation of N_i due to the radioactive decay of nuclides N_i'

$\sigma_{f,i}N_i\phi$ = destruction rate of N_i due to fission

$\sigma_{c,i}N_i\phi$ = is the destruction rate of N_i due to all forms of neutron absorption other than fission ((n,γ), (n,α), (n,p), (n,2n),(n,3n));

$\lambda_i N_i$ = radioactive decay rate of N_i

Equation (3.2) is written for a homogeneous medium containing a space-energy-averaged neutron flux, φ, with flux-weighted average cross sections, σ_f and σ_c, representing the reaction probabilities. The flux is a function of space, energy, and time is dependent upon the nuclide concentrations. The mathematical treatment in ORIGEN2 assumes that the space-energy-averaged flux can be considered constant over a sufficiently small time interval, Δt. Similarly, it is assumed that a single set of flux weighted neutron cross sections can be used over the same time step. For a given time step, these assumptions are necessary if Eq. (3.2) is to be treated as a first-order, linear differential equation. The time-dependent changes in the flux and weighted cross sections are simulated in ORIGEN2 by providing a capability of updating the values for the space-energy-averaged flux and, therefore, for the weighted cross sections for each successive time step, Δt_k, Δt_{k+1}, ..., Δt_n. These values are derived from lattice cell analyses using physics

transport methods available in SCALE to update cross sections that represent the lattice geometry, conditions, and the nuclide concentrations.

3.0.1 SOLUTION WITH THE MATRIX EXPONENTIAL METHOD

Proceeding with the description of the ORIGEN2 analytical model, for all nuclides Ni, Eq. (3.2) represents a coupled set of linear, homogeneous, first-order differential equations with constant coefficients. As such, Eq. (3.2) can be written in matrix notation as

$$\underset{\sim}{\dot{N}} = \underset{\approx}{A}.\underset{\sim}{N} \qquad (3.3)$$

where $\underset{\sim}{\dot{N}}$ is a vector of nuclide concentrations and $\underset{\approx}{A}$ is the transition matrix containing the rate coefficients for radioactive decay and neutron absorption. Equation (3.3) has the known solution

$$\underset{\sim}{\dot{N}} = \exp\left(\underset{\approx}{A}t\right).\underset{\sim}{N}(o) \qquad (3.4)$$

where N(o) is a vector of initial nuclide concentrations. Analogous to a series expansion for the exponential function, the matrix exponential function, $\exp\left(\underset{\approx}{A}t\right)$ appearing in Eq. (4), is defined as

$$\exp\left(\underset{\approx}{A}t\right) \equiv \underset{\approx}{I} + \underset{\approx}{A}t + \frac{\left(\underset{\approx}{A}t\right)^2}{2} + ... = \sum_{m=0}^{\infty} \frac{\left(\underset{\approx}{A}t\right)^m}{m!} \qquad (3.5)$$

with $\underset{\approx}{I}$ being the unit matrix. Equations (3.4) and (3.5) constitute the matrix exponential method, which yields a complete solution to the problem. However, in certain instances related to limitation in computer precision, difficulties occur in generating accurate values of the matrix exponential function.

Under these circumstances, alternative procedures using either the generalized Bateman [60] equations or Gauss-Seidel iterative techniques are applied. These alternative procedures will be discussed after the section on the matrix exponential method.

A straightforward solution of Eq. (3.4) through the expansion in Eq. (3.5) would require the storage of the complete transition matrix. To avoid excessive memory storage requirements, a recursion relation has been developed. Substituting for the matrix exponential function in Eq. (4) would give

$$\underset{\sim}{N} = \left[\underset{\approx}{I} + \underset{\approx}{A}t + \frac{\left(\underset{\approx}{A}t\right)^2}{2!} + \frac{\left(\underset{\approx}{A}t\right)^3}{3!} + ... \right] \underset{\sim}{N}(o) \qquad (3.6)$$

The recursion relation may be observed by considering the solution of Eq. (3.6) for a particular nuclide, N_i. The result is a series of terms which arise from the successive post-multiplication of the transition matrix by the vector of nuclide concentration increments produced from the computation of the previous terms. Within the accuracy of the series expansion approximation, physical values of the nuclide concentrations are obtained by summing a converged series of these vector terms. The elements of the transition matrix, a_{ij}, are the first-order rate constants for the formation of nuclides i from nuclides j.

The solution in terms of these rate constants is written as

$$N_i = N_i(o) + t\sum_j a_{ij} N_j(o) + \frac{t}{2}\sum_k \left[a_{ik} t \sum_j a_{kj} N_j(o) \right] + \frac{t}{3}\sum_m \left\{ ai_m . \frac{t}{2}\sum_k \left[a_{mk} t \sum_j a_{kj} N_j(o) \right] \right\} + ... \quad (3.7)$$

where the range of indices, j, k, m, is 1 to M for a size M × M of matrix $\underset{\approx}{A}$. The recursion relation is developed from Eq. (3.7) by defining the terms C_1^n

$$C_1^o \equiv N_i(o), C_i^{n+1} = \frac{t}{n+1}\sum_j a_{ij} C_j^n \qquad (3.8)$$

which yields the solution for N_i as

$$N_i = \sum_{n=0}^{\infty} C_i^n \qquad (3.9)$$

The use of Eq. (3.9) in obtaining the solution for the system of nuclides given in Eq. (3.4) requires the storage of only two vectors, $\underset{\sim}{C}^n$ and $\underset{\sim}{C}^{n+1}$ in addition to the current value of the solution.

Various tests are conducted in ORIGEN2 to ensure that the summations indicated in Eq. (3.9) do not lose accuracy owing to relative magnitudes or small differences between positive and negative rate constants. Nuclides with large rate constants are removed from the transition matrix and treated separately. For example, in the decay chain A → B → C, if the decay constant for B is large, a new rate constant is inserted in the matrix for A → C. This technique was originally employed by Ball and Adams [61].

The determination of which transitions are to be reduced from the matrix involves the calculation of the matrix norm. The norm of the matrix $\underset{\approx}{A}$ is defined by Lapidus and

Luus [62] [63] as being the smaller of the maximum-row absolute sum and the maximum-column absolute sum. That is, the norm, [A], is given by

$$[A] = \min\left\{\max\sum_i |a_{ij}|, \max\sum_j |a_{ij}|\right\} \qquad (3.10)$$

In order to maintain precision in performing the summations of Eq. (3.9), the matrix norm is used to balance the user-specified time step, t, with the precision associated with the word length employed in the machine calculation. Lapidus and Luus have shown that the maximum term in the summation for any element in the matrix exponential function cannot exceed ([A]t)n/n! where n is the largest integer not larger than [A]t. In the ORIGEN2 program, [A]t is restricted by

$$[A]t \le -2\ln(0.001) = 13.8155 \qquad (3.11)$$

This value restricts the size of the maximum term to approximately 10^5.

3.0.2 SOLUTION TO THE NUCLIDE CHAIN EQUATIONS

Nuclides with short half-lives are removed from the transition matrix and treated separately. This separate treatment involves the solution of the nuclide chain equations. In conjunction with maintaining the transition matrix norm below the prescribed level, a queue is formed of the short-lived precursors of each long-lived isotope. These queues extend back up the several chains to the last preceding long-lived precursor. The queues include all nuclides whose half-lives (loss due to decay and neutron absorption) are less than 10% of the time interval. A generalized form of the Bateman equations developed by Vondy [58] is used to solve for the concentrations of the short-lived nuclides at the

end of the time step. For an arbitrary forward-branching chain, Vondy's form of the Bateman solution is given by

$$N_i = N_i(o)e^{-d_i t} + \sum_{k=1}^{i-1} N_k(o)\left[\sum_{j=k}^{i-1} \frac{e^{-d_j t} - e^{-d_i t}}{(d_i - d_j)} a_{j+1,j} \prod_{\substack{n=k \\ n\neq j}}^{i-1} \frac{a_{n+1,n}}{d_n - d_j}\right] \qquad (3.12)$$

where N_1 (o) is the initial concentration of the first precursor, N_2 (o) that of the second precursor, etc.

As in Eq. (3.7), a_{ij} is the first-order rate constant and d_i is equal in magnitude to the diagonal element, or $d_i = -a_{ii}$. Bell [54] has recast Vondy's form of the solution through multiplication and division by $\prod_{n=k}^{i-1} d_n$

Rearranging terms he obtains

$$N_i = N_i(o)e^{-d_i t} + \sum_{k=1}^{i-1} N_k(o) \prod_{n=k}^{i-1} \frac{a_{n+1,n}}{d_n}\left[\sum_{j=k}^{i-1} \frac{e^{-d_j t} - e^{-d_i t}}{(d_i - d_j)} \prod_{\substack{n=k \\ n\neq j}}^{i-1} \frac{d_n}{d_n - d_j}\right] \text{.....(3.13)}$$

The first product over isotopes n is the fraction of atoms that remain after the k^{th} particular sequence of decays and captures. If this product falls less than 10^{-6}, the contribution of this sequence to the concentration of nuclide i is neglected. Indeterminate forms arising when $d_i = d_j$ or $d_n = d_j$ are evaluated using L'Hopital's rule. These forms occur when two isotopes in a chain have the same diagonal element.

The solution given by Eq. (3.13) is applied to calculate all contributions to the "queue end-of-interval concentrations" of each short-lived nuclide from initial concentrations of

all others in the queue described above. Also, Eq. (3.13) is applied to calculate the contributions from the initial concentrations of all short-lived nuclides in the queue to the long-lived nuclide that follows the queue in addition to the total contribution to its daughter products. These values are appropriately applied in the program, either before or after the matrix expansion calculation is performed, to make the concentration of the long-lived nuclide or the total of its daughters the correctly computed quantity. Equation (3.13) is applied in making adjustments to certain elements of the final transition matrix, which now excludes the short-lived nuclides. The value of the element must be determined for the new transition between the long-lived precursor and the long-lived daughter of a short-lived queue.

The element is adjusted such that the end-of-interval concentration of the long-lived daughter calculated from the single link between the two long-lived nuclides (using the new element) is the same as what would be determined from the chain including all short-lived nuclides. The method assumes zero concentrations for precursors to the long-lived precursor. The computed values asymptotically approach the correct value with time as successive time intervals are executed. (For this reason, at least five to ten time intervals during the decay of discharged fuel are reasonable, because long-lived nuclides have built up by that time.). In the instance that a short-lived nuclide has a long-lived precursor, an additional solution is required.

First, the amount of short-lived nuclide i due to the decay of the initial concentration of long-lived precursor j is calculated as

$$N(t)_{j\to i} = N_j(o)a_{ij}\frac{e^{-a_{jj}t}}{a_{ii}-a_{jj}} \qquad (3.14)$$

from Eq. (3.13) with $a_{kk} = d_k$ and assuming $\exp(-d_{it}) << \exp(-d_{jt})$. However, the total amount of nuclide i produced depends upon the contribution from the precursors of precursor j, in addition to that given by Eq. (3.14). The quantity of nuclide j not accounted for in Eq. (3.14) is denoted by $N_j^{'}(t)$ the end-of-internal concentration minus the amount which would have remained had there been no precursors to nuclide j,

$$N_j^{'}(t) = N_j(t) - N_j(o)e^{-a_{jj}t} \qquad (3.15)$$

Then the short-lived daughter and subsequent short-lived progeny are assumed to be in secular equilibrium with their parents, which implies that the time derivative in Eq. (3.2) is zero.

$$\dot{N} = o = \sum_j a_{ij}N_j \qquad (3.16)$$

The queue end-of-interval concentrations of all the short-lived nuclides following the long-lived precursor are augmented by amounts calculated with Eq. (3.13). The concentration of the long-lived precursor used in Eq. (3.15) is that given by Eq. (3.14). The set of linear algebraic equations given by Eq. (3.16) is solved by the Gauss-Seidel iterative technique. This algorithm involves an inversion of the diagonal terms and an iterated improvement of an estimate for N_i through the expression

$$N_i^{k+1} = -\frac{1}{a_{ii}}\sum_{j\neq i} a_{ij}N_j^k \qquad (3.17)$$

3.1 REBUS 3

REBUS-PC has been subjected to an ongoing process of validation, where new changes are introduced and verified against expected benchmark results from older versions of the code, or against REBUS 8.0 or REBUS 9.0. Also, it has been routinely operated on WINDOWS and linux platforms with no changes to the source code. Four sample problems are available for user testing and verification. A linux script is used to automate the comparison of old and new results, and to isolate any differences. The reactor analyst needs information in useful form for understanding the physical variables and their effects on his reactor model. The *Mathematica* software was used to program (outside of REBUS) the cubic spline algorithms and the polynomial fit algorithms for the purposes of comparison, and to assist in debugging of new FORTRAN-77 coding in REBUS-PC. Experience is being gained as to the relative advantages and disadvantages of polynomial fits versus spline fits. There is essentially no difference in running time, since the computational time involved in processing burnup dependence is only a few tenths of a percent of the total job time. One advantage of the spline fit process is that the fits actually go through the data points smoothly. This is of particular value for fresh, unburned reactivity calculations. Two basic types of analysis problems are solved: 1) the infinite-time, or equilibrium, conditions of a reactor operating under a fixed fuel management scheme, or 2) the explicit cycle-by-cycle, or nonequilibrium operation of a reactor under a specified periodic or non-periodic fuel management program. For the equilibrium type problems, the code uses specified external fuel supplies to load the reactor. Optionally, reprocessing may be included in the specification of the external fuel cycle and discharged fuel may be recycled back into the reactor. For non-equilibrium

cases, the initial composition of the reactor core may be explicitly specified or the core may be loaded from external feeds and discharged fuel may be recycled back into the reactor as in equilibrium problems. Both equilibrium and non-equilibrium problems using a number of different core geometries including triangular and hexagonal mesh are handled by REBUS. The neutronics solution may be obtained using finite difference or nodal diffusion-theory methods. Microscopic cross sections are permitted to vary as a function of the atom density of various reference isotopes in the problem as appropriate for thermal reactor systems. The previous capability where neutron capture and fission processes were fitted to low-order polynomials as functions of burnup is retained. The total reactor burn cycle time is divided into one or more subintervals, the number of which is specified by the user. An explicit burnup is performed in each region of the reactor over each of these subintervals using the average reaction rates over the subinterval. These average reaction rates are based on fluxes obtained from an explicit 1-, 2-, or 3-dimensional diffusion theory neutronics solution computed at both the beginning and end of the subinterval. The transmutation equations are solved by the matrix exponential technique. The isotopes to be considered in the burnup equations, as well as their transmutation reactions, are specified by the user [64].

3.2 WIMS-ANL

The user must decide which transport solution is most appropriate for the cell being modeled. For most applications, the user usually selects either the PERSEUS (collision probability) or DSN (discrete Sn) transport solution methods. Either of these two methods can be used for single or MULTICELL models in either slab or annular geometry. The other transport solution options available, which have not been used at

ANL, are the PIJ-PERSEUS, and PRIZE-PERSEUS. These options model detailed rod-cluster geometries using one-dimensional transport solutions. For smaller unit cells, the PERSEUS method is recommended for shorter running times and good quality flux solutions. The DSN method is recommended for larger unit cells that might be more difficult to converge using the PERSEUS method. Using the DSN method the user has more control over the accuracy of the flux solution by choices in the Sn order and mesh widths. The main transport solution convergence criterion is controlled by selection of the TOLERANCE parameter. The main transport group structure is usually less than the number of library groups and more than the desired broad-group structure for subsequent diffusion or transport core calculations. As few as five main transport groups have been found to be an adequate predictor of flux spectrum and cell reactivity for simple three-region HEU unit cells. With the reduction in enrichment and additional regions modeled in a unit cell, more groups are required to be nearly equivalent to the same flux solution with the full number of library groups. With a 69- group library, it is recommended that 30 main transport groups be routinely used for most analyses and depletion studies. [65]Approximately half of these groups will be in the thermal range below 4 eV and the remainder in the fast energy range. The difference in reaction rates and cell reactivity between the use of 30 and 69 main transport groups is usually very small. The selection of the number of mesh points in a given region is primarily dependent on the mean-free path of thermal neutrons in a material. Strong thermal absorbers require more mesh points than structural or coolant materials. Difficulties in convergence of the main transport calculation can be encountered for unit cells with more than 200 mesh points. This usually occurs in cells with large regions with very small or very large absorption

cross-sections. A word of caution should be added that these unconverged cases do not abort but simply keep searching for convergence for exceedingly long periods of time. The reaction rate edits are calculated for each cross-section type. They are nuclide, cell, group, region, and temperature dependent. The reaction rate group structure must have the same structure as the main transport solution or use fewer groups collapsed from the main transport group structure. Any number of isotopic reaction rates can be edited including all 36 fission products.

These reaction rates are edited at each depletion time step unless selectively omitted. A reaction rate summary table is calculated at the end of each edit for all isotopes present in the reaction rate edit.

The summary is normalized to one neutron absorbed in the cell, regardless of which materials are included in the reaction rate edits.

There are two different time step types for fuel depletion calculations. One has no change in flux spectrum between time steps; the other is a recalculation of the flux spectrum for each time step interval. The recalculation of flux spectrum for each depletion step is the recommended method. Another equally important consideration is the selection of time step interval. In principle, the shorter the time step interval the more accurate depletion one obtains. It is recommended that one uses a very fine time step case to check any coarser time step depletion case.

During the rapid buildup of equilibrium xenon, short time steps are needed. Comparisons with other codes suggested that smaller time steps may be needed with WIMS. One should also be cautious about increasing the time step interval near end of life. One

should seek to find a maximum acceptable cell reactivity decrease per time step that will yield results nearly identical to the fine time step depletion mode. It is recommended to use close to the maximum number of 100 flux renormalization time steps for high burnup cross-section generation with data saved for only selected time steps. The fuel depletion model uses 35 active fission products with the remaining fission products placed into one lumped fission product material. Experience has shown that for long fuel lifetimes this fission product model is acceptable. For shorter fuel lifetimes additional fission products may be needed.

The depletion characteristics of any composition are determined by the geometry of the lattice and the information on the POWERC card. It is now possible to deplete with either fission power only or with fission and capture power combined. The cross-section library determines the depletion isotopics.

WIMS generates cell-averaged, broad-group macroscopic cross-sections as in a SCRAMBLE output format. In order to use WIMS cross-section data in the codes

DIF3D, REBUS, and TWODANT, it was necessary to create a data interface in WIMS-ANL to compute and write broad group microscopic or macroscopic cross-sections in the ISOTXS format. Most users request the microscopic option for generating ISOTXS data at selected burnup steps.

The microscopic ISOTXS format allows the user to model each neutron reaction that is available on the cross-section library. The original WIMS cross-section library did not provide for this possibility so a secondary WIMS library was added such that each neutron reaction could be modeled in subsequent diffusion or transport theory core

calculations. The primary WIMS-D4 library format remains unchanged, while the secondary library expands the information that can be put into ISOTXS data files. Not only are more neutron reactions modeled, but also energy-per-capture data have been added for each material in the library. The energy per fission is present in the primary library.

The library cross-section data are collapsed over the fine and intermediate group spectra to the selected broad group structure. The microscopic transport cross-sections are collapsed using the Travellli method. [66] This method insures that the microscopic cross-sections combined with their corresponding number densities will reproduce the proper macroscopic transport data. The Travelli method, however, can lead to microscopic transport cross-sections which are larger than the corresponding total cross-section data for some energy groups and for some isotopes. This does not constitute a real problem, and users seeing this in the ISOTXS edits should not be concerned. Again, this is only an artifact of the Travelli method. The user is allowed up to 6000 cross-section sets to be saved in one depletion case with any number of neutron groups. The number of cross-section sets is determined by the product of the number of isotopes saved at each timestep and the number of timesteps in which cross-sections will be saved on IBURN cards [65].

3.3 MCNP5

Two basic ways are used in Monte Carlo methods for solving the transport equation: mathematical method for numerical integration and computer simulation for physical processes. Mathematical approach is useful for importance sampling, convergence, variance reduction, random sampling technique and eigen value calculation scheme [67]

whilst the simulation approach is useful for collision physics tracking, tallying and so on. Monte Carlo methods solve integral problems (ie. the integral form of Boltzman equation). Most theory on Monte Carlo deals with fixed source problems. Eigen value problems are needed for criticality and reactor physics calculation. The key to Monte Carlo methods is the notion of random sampling. When Monte Carlo is used to solve integral Boltzman transport equation, it models the outcome of physical events (eg. Neutron collision, fission process, source etc). The geometrical geometry models the arrangement of materials [68]. The time dependent linear Boltzman transport equation

$$\psi(r,v) = \int\left[\int \psi(r',v')C(v' \to v, r')dv' + Q(r',v)\right].T(r' \to r, v)dv' \qquad (3.18)$$

where

$\psi(r,v)$ = particle collision density

$Q(r',v)$ = source term

$C(v' \to v, r')$ = collision kernel, change velocity at fixed position

$T(r' \to r, v)$ = transport kernel, Change in position at a fixed velocity

$$\text{Angular Flux} = \psi(r,v) = \frac{\psi(r,v)}{\sum(r,|v|)} \qquad (3.19)$$

$$\text{Scalar Flux} = \phi(r,|v|) = \int_{\Omega} \frac{\psi(r,v)}{\sum(r,|v|)} d\Omega, v = |v|\Omega \qquad (3.20)$$

Source term for the Boltzman equation

$$Q(r,v)=\begin{Bmatrix} S(r,v) \\ S(r,v)+\int \psi(r,v')F(v' \rightarrow v,r)dv' \\ \frac{1}{\kappa}\int \psi(r,v')F(v' \rightarrow v,r)dv' \end{Bmatrix} \qquad (3.21)$$

where

$S(r,v)$ = Fixed source

$F(v' \rightarrow v,r)$ = creation operator (due to fission particle at (r,v') creates particle at (r,v)

κ = eigen value

The Monte Carlo methods make some assumptions in solving the Boltzman equation. The assumption made include

- A static homogeneous medium
- Time dependent system
- Markovian (ie. the next event depends only on the current (r, v, E) and not on previous event.
- Particles do not interact with each other
- Neglect relativistic effects
- No long range forces (Particles fly in straight lines between events)
- Material properties are not affected by particle reactions

The particle histories after repeated substitution for ψ_κ will give

$$\psi_\kappa(p)=\int \psi_{\kappa-1}(p').R(p' \rightarrow p)dp' \qquad (3.22)$$

$$\psi_\kappa(p)=\int \psi_0(p_0).R(p_0 \rightarrow p_1).R(p_1 \rightarrow p_2)...R(p_{\kappa-1} \rightarrow p)dp_0...dp_{\kappa-1} \qquad (3.23)$$

The history is a sequence of states; (P_0, P_1, P_2, P_3,…) [68].

When a particle starts out from a source, a particle track is created. If that track is split 2 for 1 at a splitting surface or collision, a second track is created and there are now two tracks from the original source particle, each with half the single track weight. If one of the tracks has an (n,2n) reaction, one more track is started for a total of three. A track refers to each component of a source particle during its history. Track length tallies use the length of a track in a given cell to determine a quantity of interest, such as fluence, flux, or energy deposition. Tracks crossing surfaces are used to calculate fluence, flux, or pulse-height energy deposition (surface estimators). Tracks undergoing collisions are used to calculate multiplication and criticality (collision estimators). [69]

Within a given cell of fixed composition, the method of sampling a collision along the track is determined using the following theory [70]. The probability of a first collision for a particle between l and $l + dl$ along its line of flight is given by

$$p(l)dl = e^{-\sum_t l}\sum_t dl \qquad (3.24)$$

where $\sum_t$ is the macroscopic total cross section of the medium and is interpreted as the probability per unit length of a collision. Setting ξ the random number on [0, 1], to be

$$\xi = \int_0^1 e^{-\sum_t s}\sum_t ds = 1 - e^{-\sum_t l} \qquad (3.25)$$

It follows that

$$l = -\frac{1}{\sum_t}\ln(1-\xi) \qquad (3.26)$$

But, because is distributed in the same manner as $1-\xi$ and hence may be replaced by ξ, we obtain the well-known expression for the distance to collision,

$$l = -\frac{1}{\sum_t} \ln(\xi) \qquad (3.27)$$

Having gone through the physics of how the codes work, an outline of the methodologies that employed the codes is very important for the sake of users who would want to utilize the codes in a similar manner. The next chapter gives a detailed account of the methods that were used.

CHAPTER FOUR

4 METHODOLOGY

A number of codes were applied in the design of the spent fuel transport cask. Each code used has a specific assignment that contributes to the eventual design of the cask. Transport, fuel depletion, cross section generation and burnup calculation are among the vast capabilities of the codes that were applied in this study. WIMS-ANL, REBUS3, ORIGEN2 and MCNP5 were the main codes utilized in this study.

The Winfrith Improved Multigroup Scheme (WIMS) code has been used extensively throughout the world for power and research reactor lattice physics analysis. There are many WIMS versions currently in use [71]. It was chosen for the accurate lattice physics capability and for an unrestricted distribution privilege. The code and its 69-group library tape 166259 generated in Winfrith were obtained from the Oak Ridge National Laboratory, Radiation Safety Information Computational Center (RSICC) in 1992 [72]. The first was the capability to generate up to 20 broad-group burnup-dependent macroscopic or microscopic ISOTXS cross-sections for each composition of the unit cell [73], an ENDF/B-V based nuclear data library [74] (later updated to ENDF/B-VI), and a SUPERCELL option [73]. As a result of these modifications and other minor ones, the code was named WIMS-D4M [75] [76]. The code is variably dimensioned and can accommodate cross section libraries with greater than 69 energy groups. ENDF/B-VI cross-section libraries with both 69 and 172 energy group structures are now in use with the code. WIMS uses transport theory to calculate the neutron flux as a function of energy and spatial location in a one-dimensional cell.

The input deck for WIMS was set up and run. The input deck comprises 3 main sections, the prelude data, the main card and the edit data. The prelude section contains information about the type of problem, the main transport routine, the number of broad energy group as well as the number of few energy groups to be used. It also provides specification on the number of materials, the maximum number of cell regions and the number of nuclides to be included in the edit chain.

The main card section specifies the annulus region in the current cell being considered. Every region is assigned a number. Every material is assigned a number as well and their outer radii are entered. The bell factor that aid in the calculation of cross sections is also specified based on geometry (ie. 1.40 for slabs and 1.16 for cylinders). The specific mesh intervals in the current cell type are also specified with the more sensitive parts having more meshes. The material compositions and the partitioning of library groups into few groups are also specified. The manner in which the fuel depletes in each burn up step is also entered.

The edit data section provides information on the specific number of thermal groups. In this case, the few groups were partitioned into 2 groups (ie. fast and thermal). The specific nuclides to be included in the ISOTXS files are also specified. The number of burnup steps and the use of secondary libraries are entered as input. The section also shows how neutron few group are partitioned into broad group.

After all the necessary pieces of information are entered, the deck was run to produce the ISOTXS file to be used in the REBUS3 code.

The REBUS-PC code has evolved away from its roots as a design tool for fast reactors to encompass the needs of thermal reactor design and analysis. Since its conception in the 1960's, REBUS (the REactor BUrnup System) has always been a general-purpose tool [77] [78] [79] [80] [81] [82] [83]. It was originally designed and coded for the capabilities of large main-frame computers, some of which had "small core memory" and "large core memory." As a result the code was written in modular style, using specialized Argonne Reactor Code (ARC) system routines for file management, memory management, input processing, and so on. The evolution of work stations such as those created by SUN, DEC, and IBM offered cost-effective alternatives to main-frame computing. Over the past ten years, advances in personal computer architecture, hardware, software, and FORTRAN compilers have made using PC's under WINDOWS or linux operating systems the method of choice for many scientific and engineering purposes. The Reduced Enrichment Research and Test Reactor Program (RERTR) has determined that its reactor analysis software, when compiled by the Lahey Fortran 95 [84] (WINDOWS and linux), is very effective even for huge problems when run on present- generation PC's using Pentium IV processors. REBUS-PC is written in FORTRAN 77, as a stand-alone code. Modular features of Lahey Fortran 95 are not used.

ORIGEN2 computes time-dependent concentrations and radiation source terms of a large number of isotopes, which are simultaneously generated or depleted through neutronic transmutation, fission, and radioactive decay. Provisions are also provided to simulate input feed rates, and physical or chemical removal rates from a system. The calculations may pertain to fuel irradiation within a nuclear reactor, or the storage, management, transportation, or subsequent chemical processing of spent fuel elements.

ORIGEN2 is widely used in nuclear reactor and processing plant design studies, design studies for spent fuel transportation and storage, burnup credit evaluations, decay heat and radiation safety analyses, and environmental assessments. The matrix exponential expansion model of the ORIGEN (**O**ak **R**idge **I**sotope **GEN**eration) code is unaltered in ORIGEN2. In addition, the code will perform integration of actinide or fission product decay energies and radiation sources over any decay interval, by applying the Volterra integral method as an alternate solution to the matrix exponential method.

ORIGEN2 is the depletion and decay module in code system. It may be called from a control module, or it may be run as a stand-alone program. The primary objective in the design of ORIGEN2 is to make it possible for the depletion calculations to utilize multi-energy-group cross sections processed from any standard ENDF/B formatted nuclear data library. This function has been implemented through the execution of physics codes within either the SCALE system or the AMPX system, both developed and maintained at Oak Ridge National Laboratory (ORNL). These codes compute problem-dependent neutron-spectrum-weighted cross sections that are representative of conditions within any given reactor fuel assembly, and convert the data into a cross-section library format that can be used by ORIGEN. Time-dependent cross-section libraries may be produced that reflect fuel composition variations during irradiation.

MCNP is a 3-D transport theory code based on statistical simulation of particle transport. It uses combinatorial geometry description and continuous energy cross section to simulate time dependent transport processes [85]. To accurately simulate transport and interaction of particles and because of the material heterogeneity it is important to use the

transport theory methods. There are two types namely the deterministic method and the Monte-Carlo [86].

The Monte-Carlo method can exactly represent the physical model using a combinatorial geometry and can perform particle transport based on continuous energy nuclear cross sections [85]. However, it is expensive with time (ie it takes a great deal of time to run the code).

4.0.1 Core Life Estimate Based on REBUS3 Model

The core life was estimated based on the REBUS3 model. A detailed input deck was developed and run. The REBUS input deck allows for specification of the various regions. The reactor is represented in a Cartesian plane. The dimensions of the various radii of the components (x axis) of the reactor are specified and the dimensions of the height(y axis) are also specified. The components are divided into subsections for the sake of analyses. The more nodes you desire, the more the axial sections.(eg. The beryllium reflector was divided into 5 sub sections). Mesh intervals are specified in the deck. The mesh intervals were chosen with respect to the stability of the regions. In areas where there are many variations, a finer mesh is used in order to capture every detail. Since the output will bring out a lot of nuclides, the specific ones you want to track are specified in the deck. The nuclides Xe, Pm and I are very important poisons that need to be tracked because they are time dependent. The rest are not as important but they still affect your output. The homogenization of every fuel ring is very important. The flux profile is a cosine function whilst the U-235 concentration is a Bessel function. Therefore, the reaction rate turns out to be flat thereby providing a desirable condition in the reactor. The constituents of the reactor components are specified. The code allows for

the user to end the run after the neutronic calculation or continue doing burnup calculation. In reactors where fuel management is practiced, you are able to assign the homogenized fuel to a particular fuel management path. The input also contains the number of days the reactor is operated, the power at which the reactor is operated, the beginning of a particular stage of operation and the end of that particular stage of operation. The deck also specifies when the neutronic calculation should be done. In order words, it divides the number of hours for which the reactor runs into sub intervals based on the run time of the reactor.

The procedure used is based on a simple reactivity rundown calculation. It assumes that the top beryllium shim tray is filled up to the maximum of 10.95 cm for the fresh core. A constant power level at 30 kW was used for the depletion. The REBUS3 excess reactivity rundown curve is then adjusted for (i) the bias (-0.47 mk) between MCNP5 model and the REBUS3 model, and (ii) the equilibrium xenon worth (3.81 mk at 30 kW and 2.00 mk at 15 kW). The end of core life is reached when the excess reactivity of the core goes down to 2.3 mk. For a core operated at full power of 30 kW, the estimated core life is ~750 full-power-equivalent-days (FPEDs). In terms of practical reactor operational schemes, assuming the core is operated at 30 kW for 2 hours per day, 4 days per week, and 48 weeks per year, the estimated core life of 750 FPEDs is equivalent to 46.88 years [750/(2*4*48/24) =46.88]. This estimate of the core life is fairly consistent with a previous cycle-by-cycle estimate of ~ 48 years. In the previous study, top Be shims were added cycle-by-cycle such that the core excess reactivity at the begin-of-cycle (BOC) is 4.0 mk and depleted down to 2.3 mk at end-of cycle (EOC) for every cycle until the total Be shim reaches 10.95 cm. The small difference in these two procedures indicated that

the simple reactivity rundown calculation with full top Be shim loaded to the fresh core is an acceptable alternative to the much more elaborate and tedious cycle-by-cycle simulation of the real operational scheme for top Be shim addition.

4.0.2 Radionuclide Activities in Peak Burnup Fuel Rods for GHARR-1 Core

An input deck was set up and calculations were performed to obtain the inventory of halogens, noble gases, alkaline metals, and actinides in the peak power fuel rods for the core operated at typical power level. The peak burnup fuel rods were evaluated. The fuel rods have a fuel meat of 90.2 % enriched U-Al alloy. . The inventory data reported here can be used in SSDOSE code for radiological assessment of accident scenarios involving the release of radioactive material (e.g., maximum hypothetical accidents, or MHA). The burnup value obtained from the ORIGEN run was compared to that obtained from the REBUS run.

The ORIGEN deck was set up to calculate multiplication based on total vector mass. The nuclide composition and continuous nuclide feed rate were specified for nuclides of interest. The cut off fraction was over ridden to give way for output summary table. Two vectors were set up in the deck and nuclide concentration data in one vector were moved into the other vector depending on the calculation of interest. The decay and cross section libraries were specified so that the code works with those selected data. The input data can be printed out. The code was instructed to control the printing of the input data libraries (only relevant ones were printed). The deck was also set up to track photon production rate in 18 energy groups. Since the code was written for nuclear power plants, the code was instructed to read nuclide identifiers for replacement decay and cross section data cards in order to suit the MNSR. The average burnup, flux and specific

power for an irradiation was calculated. Neutron flux and power were specified for irradiation of a single interval. Decay of a single interval was also specified. The table type to be printed (element, nuclides or summary) was specified for actinides, activation products and fission products.

Nuclide inventory data were calculated with ORIGEN2 code package, a zero-dimensional isotope decay and transmutation code. The code solves the transmutation equations using libraries of radioactive decay data and 1-group cross section data. The base code libraries allow the tracking of over 100 actinides and nearly 900 fission product nuclides. Pre-calculated libraries of 1-group cross section data are available for use in ORIGEN2 for several reactor systems. A standard library for an oxide-fueled LWR, the so-called bwrus library, represents the closest potential match to the basic neutronics characteristics of the core. It is preferable to replace cross section data for some or all of the nuclides in the library with data that are more appropriate for the particular system under analysis. For the present analysis, 1- group cross section data were calculated for the fuel rods using the WIMS-ANL code. Replacement cross section data were calculated for only a dozen also selected actinides and fission products. The calculated 1-group capture and fission cross sections at the mid-core life.

ORIGEN-2 code tracks radioactive nuclide inventories for 3 material groups, i.e., activation products, actinides and daughters, and fission products. The radioactive nuclide activities (in curies) are produced both during the irradiation period and cooling period afterward. A large amount of nuclide inventory data is available for analysis. For a bounding hypothetical accident radiological dose evaluation, the maximum value of the

radionuclide activities over the whole core life history (including both irradiation period and cooling period) must be extracted if needed.

4.1 MCNP5 deck development and run

The cell numbers and material numbers were specified in the MCNP input deck. The densities of the materials that make up of the reactor in grammes/cm^3 were entered in the cell card section. The surface card section contains the dimensions of the various parts of the reactor were specified in the x-y-z plane. The constituents of the various materials were also outlined in the data card section.

The specific amount of radionuclides remaining after 750FPED was obtained after both REBUS and ORIGEN runs in order to mimic the exact isotopic content of the fuel when the fuel is spent. The values are fed into the already developed MCNP5 cask input deck and run to obtain multiplication factor. Transport simulations were run for 200,000000 particle histories (500,000 particles and 400 criticality cycles) with an initial criticality (k_{eff}) guess of 1.004. The transport of both neutron and photons were simulated. Various tally cards were used in order to obtain different results. For example F5 tally was employed for photon transport whilst F4 and F6 tallies were utillised for flux and energy deposition respectively.

Various schemes have evolved for classifying radioactive waste according to the physical, chemical and radiological properties that are of relevance to particular facilities or circumstances in which radioactive waste is managed. These schemes have led to a variety of terminologies, which may differ from State to State and even between facilities in the same State. In some instances, this has given rise to difficulties in establishing

consistent and coherent national waste management policies and implementing strategies, and can lead to less than optimal levels of safety. It also makes communication on waste management practices difficult nationally and internationally, particularly in the context of the Joint Convention on the Safety of Spent Fuel Management and on the Safety of Radioactive Waste Management [87]. In order to address these issues, the classification of radioactive waste has been the subject of international standards on the safety of radioactive waste management. According to the IAEA Safety Series on the protection of people and environmental classification of radioactive waste, there are six categories. The spent fuel from GHARR-1 is classified as Intermediate level waste (ILW) as it contains particularly long lived radionuclides that require a greater degree of containment and isolation than that provided by near surface disposal.

However, ILW needs no provision, or only limited provision, for heat dissipation during its storage and disposal. ILW may contain long lived radionuclides, in particular, alpha emitting radionuclides that will not decay to a level of activity concentration acceptable for near surface disposal during the time for which institutional controls can be relied upon [87].

The heat generation rates from radioactive decay of fission products shall be assumed to be equal to 1.2 times the values for infinite operating time in the ANS Standard (Proposed American Nuclear Society Standards—"Decay Energy Release Rates Following Shutdown of Uranium-Fueled Thermal Reactors." Approved by Subcommittee ANS-5, ANS Standards Committee, October 1971) [88].

Radioactive waste is generated in a number of different kinds of facilities and it may arise in a wide range of concentrations of radionuclides and in a variety of physical and chemical forms. These differences result in an equally wide variety of options for the management of the waste. There is a variety of alternatives for processing waste and for short term or long term storage prior to disposal. Likewise, there are various alternatives for the safe disposal of waste, ranging from near surface to geological disposal.

Because radioisotopes of all half-life lengths are present in nuclear waste, enough decay heat continues to be produced in spent fuel rods to require them to spend a minimum of one year, and more typically 10 to 20 years, in a spent fuel pool of water, before being further processed. However, the heat produced during this time is still only a small fraction (less than 10%) of the heat produced in the first week after shutdown [89]. Calorimetric and gamma radiation methods are used for decay heat measurements on spent nuclear fuel [90].

The amount of heat generated is dependent upon the types and amounts of radionuclides in the waste (e.g. half-life, decay energy, activity concentration and total activity). Furthermore, consideration of heat removal is very important (e.g. thermal conductivity, storage geometry and ventilation). Therefore, the significance of heat generation cannot be defined by means of a single parameter value. The impact of heat generation can vary by several orders of magnitude, depending on the influencing factors and the methods in place for heat removal. Management of decay heat should be considered if the thermal power of waste packages reaches several Watts per cubic meter [87]. More restrictive values may apply, particularly in the case of waste containing long lived radionuclides. However, the measurement of heat decay is beyond the scope of this thesis.

All the computational tools proved very helpful in the neutronic and burnup calculations as well as in the analyses and evaluation of the results obtained from the simulations. The key results are presented and discussed in the next chapter. The results showed that the proposed casks were feasible and safe to fabricate.

CHAPTER FIVE

5 RESULTS AND DISCUSSION

5.0 Core life Estimation

A simple reactivity rundown was done to obtain an estimate of the core lifetime of Ghana Research Reactor-1 using REBUS3 code. This is in order to obtain the isotopic inventory of the fuel required at the point of discharge which is at 2.3mk. A graph of excess reactivity against full power equivalent days is shown below in figure 5.1 to depict the exact number of days that it will take the 344 HEU core of GHARR-1 to reach an excess reactivity of 2.3mk from an initial value of 4mk.

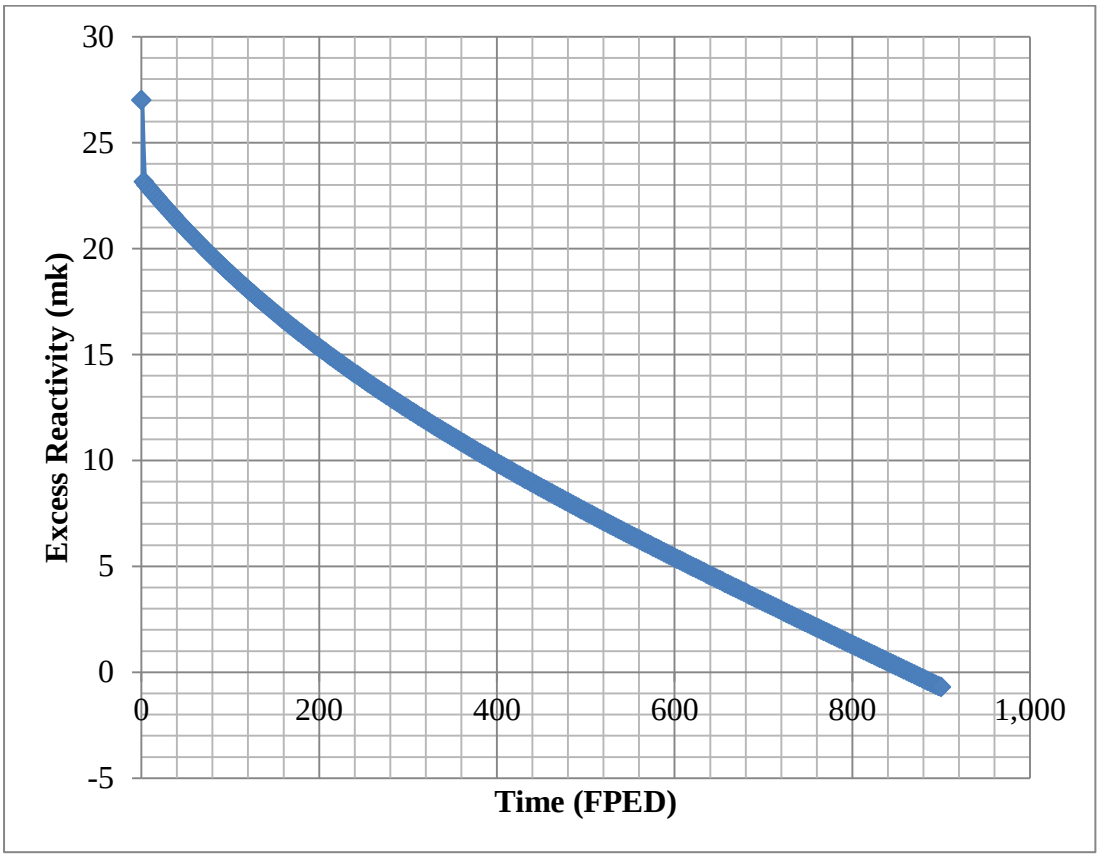

Figure 5.1: GHARR-1 Core Life Estimate Based on REBUS3 Model Using Simple Reactivity Rundown Calculations for Fresh Core Loaded with 10.95 cm Top Be Shims and Operated at Power Levels 30 kW

As the fuel burns, the excess reactivity of the core reduces gradually from 4mk to 2.3mk over the period it stays in the core. When the core excess reactivity reduces below the 2.3mk value, a beryllium shim of a particular thickness is added to the shim tray to compensate for the neutron population loss. The specific thickness of beryllium shim added is based on the reactivity versus beryllium thickness graph and other reactor physics calculations. The normal practice is that a beryllium shim of a particular thickness is added to bring reactivity back to 4mk when it goes below 2.3mk Another shim is added again when the reactivity drops again until the beryllium shim tray becomes full. A REBUS model with a beryllium shim tray filled to the top (10.95cm) is used. The former model uses top beryllium shims that are added cycle-by-cycle such that the core excess reactivity at the begin-of-cycle (BOC) is 4.0 mk and depleted down to 2.3 mk at end-of cycle (EOC) for every cycle until the total Beryllium shim reaches 10.95 cm. This is a more tedious cycle-by-cycle simulation of the real operational scheme for top Be shim addition. However, the gradient of both models are approximately the same for the two sets of results as shown in a previous study for 345 HEU Generic MNSR core by a group of experts working on a Coordinated Research Project at Argonne National Laboratory in the United States. [91]

The results obtained from the runs were adjusted to take care of the bias in the effects of equilibrium xenon as well as the bias between the REBUS code and the MCNP5 code. During a simple run down, the saturation xenon accumulated during the operations in the week are absent because over the weekend the reactor does not operate therefore the saturation xenon is allowed to decay. Hence the need for the biasing assuming reactivity remains same. The REBUS3 model is intended for burnup reactivity calculation to enable

core life time estimation. The diffusion theory model is rather crude and many detail features such irradiation channels, control rod guide tubes, regulators, etc. are not modeled. Such a deficiency can be overcome by biasing the REBUS3 calculated reactivity against the MCNP5 value. It is like the calibration of instrument (REBUS3) against the standard (MCNP5). You need to try various homogenization schemes and generate cross sections for them to see how they improve the comparison between REBUS3 and MCNP5 results. The REBUS3 result is improved to match the MCNP5 results to within 0.25 mk difference (bias). Experience indicated that the differences in k-effectives (delta k = k1 - k2) are pretty much the same whether you are using REBUS3 or MCNP5 values. Therefore we can rely on REBUS3 for reactivity calculations, even though the absolute values of k-effective between REBUS3 and MCNP5 are off by some bias value. A simple run down at 30kW resulted in an estimated core life of approximately 750 full-power-equivalent-days. Assuming in real operational terms the reactor operates for 2hours a day, 4 days a week and 48 weeks in a year then the estimated core life of the reactor is equivalent to [750/(2*4*48/24) =46.88years]. The value obtained from this simulation is compared with that obtained from ORIGEN2 that helps estimate the burnup and isotopic inventories.

5.0.1 Radionuclide Activities in Peak Burnup Fuel Rods for GHARR-1

Calculations were performed by the ORIGEN2 code to obtain the inventory of halogens, noble gases, alkaline metals, and actinides in the peak power fuel rods for GHARR-1 operated at 30kW. The core peak burnup fuel rods were evaluated. The inventory data reported in tables A1 –A4 can be used in SSDOSE code for radiological assessment of accident scenarios involving the release of radioactive material.

For a bounding hypothetical accident radiological dose evaluation, the maximum value of the radionuclide activities over the whole core life history (including both irradiation period and cooling period) must be extracted. The bounding maximum radioactivity values (for input to the SSDOSE code) are summarized in Table 5.1 for halogens, noble gases, alkaline metals and actinides.

Table 5.1: Maximum Activities (Ci) for MNSR Peak Power Fuel Rods Over the Entire Core Life Time

Radioactive Radionuclides	**Concentration (Curies)**
Halogens	
Br-84	2.54 E+02
Br-85	3.16 E+02
Br-86	2.39 E+02
Br-86M	2.41 E+02
Br-87	5.44 E+02
I-131	7.20 E+02
I-132	1.08 E+03
I-133	1.69 E+03
I-134	1.91 E+03
I-135	1.58 E+03
I-136	7.68 E+02
Te-132	1.07 E+03
Noble Gases	
Kr-85M	3.19 E+02
Kr-87	6.45 E+02
Kr-88	9.12 E+02
Kr-89	1.16 E+03

Xe-133	1.69 E+03
Xe-135	1.52 E+03
Xe-135M	2.85 E+03
Xe-137	1.50 E+03
Xe-138	1.57 E+03
Alkaline Metals	
Ba-140	1.56 E+03
Ce-141	1.48 E+03
Ce-143	1.48 E+03
Ce-144	1.14 E+03
La-140	1.57 E+03
Mo-99	1.50 E+03
Nb-95	1.61 E+03
Nd-147	5.72 E+02
Pm-147	2.31 E+02
Pr-143	1.45 E+03
Ru-103	7.91 E+02
Sr-89	1.20 E+03
Actinides	
U-237	6.79 E-02
Np-238	1.87 E-01
Np-239	4.68 E-01
Pu-238	2.93 E-06
Pu-239	7.59 E-06
Pu-240	4.23 E-07
Pu-241	3.32 E-06

These bounding maximum activities were extracted from the detail data shown in the Table A-1 through Table B-4 for the peak rod as shown in the appendix. The bounding maximum radioactivity values are always found near the beginning of the irradiation period (75 FPEDs) for halogens and noble gases. However, the bounding maximum activities for alkaline metals and actinides and daughters are almost always found at the end of irradiation period (750 FPEDs).

For the halogen and noble gas radioactivities, the concentrations (activity can be obtained from the concentrations) of these shorter-lived nuclides reaches a saturation point within ~ 100 days of operation, as production from fission and destruction by radioactive decay balance. For the alkaline metals and actinides, the concentrations do not generally reach saturation during the irradiation because of their longer half-lives. Therefore in order to obtain the bounding hypothetical accident radiological dose evaluation, the maximum values of the radionuclide activities over the whole core life history (including both Irradiation and cooling period) must be examined. This implies that all the results reported in the appendix A1-A4 and B1- B4 should be examined.

U-238 undergoes a neutron capture to form U-239, which quickly decays by β^- emission to Np-239. Subsequent transmutations of Np-239 lead to even higher actinides and their daughters.

The major contributors, Np-239 and U-237, to the actinide activities at end of irradiation are short-lived radionuclides with half-lives on the order of days. Within a few weeks after shutdown, these nuclides will have largely decayed to longer-lived Pu-238 and Pu-

239. This can be seen in Table 5.2 which provides the actinide activity inventories in the peak burnup rods after one year of post-irradiation cooling.

Table 5.2: Peak Power Rod Actinide Activities (Ci) after Constant Operation for 750 FPED for GHARR-1 followed by 1 Year of Cooling

Actinides	Discharge	1day	5days	10days	30days	90days	365days
U-237	6.64E-02	5.99E-02	3.97E-02	2.38E-02	3.05E-03	6.43E-06	7.76E-11
Np-238	5.42E-04	3.91E-04	1.05E-04	2.05E05	2.93E-08	4.83E-14	4.80E-14
Np-239	1.36E-01	1.02E-01	3.15E-02	7.22E-03	2.01E-05	5.38E-13	1.08E-13
Pu-238	2.92E-06	2.93E-06	2.95E-06	2.95E-06	2.95E-06	2.95E-06	2.93E-06
Pu-239	7.58E-06	7.59E-06	7.61E-06	7.61E-06	7.62E-06	7.62E-06	7.62E-06
Pu-240	4.23E-07	4.23E-07	4.23E-07	4.23E-07	4.23E-07	4.23E-07	4.23E-07
Pu-241	3.32E-06	3.32E-06	3.32E-06	3.31E-06	3.31E-06	3.28E-06	3.16E-06

For the purpose of assessing the bounding radiological consequences of a release of actinides from fuel material, the maximum doses would be obtained at the time of discharge. Unless the hypothetical accident scenario assumes that it happens right at the precise moment at discharge, it should be reasonable to consider some level of cooling has occurred for accidents involving any kind of operational core access events or maintenance activities. Therefore any level of cooling assumed after discharge would be helpful to reduce the radiological dose levels due to the decay away of those short lived actinides.

5.0.2 Peak Power Pin Photon Source During Irradiation Period

Nuclide inventories as well as photon density generally increase with burn-up. The photon density in the fission products are the highest followed by the actinides and activation products in that order. Fission products are also high alpha emitters. As the

fission products are born out of fission, they strive to achieve a more stable radionuclide. In an attempt to achieve stability, they give off photon emissions until they reach this stable state. For example, Caesium-137 is one such radionuclide. It has a half-life of 30 years, and decays by pure beta decay to a metastable state of barium-137 (Ba-137m). Barium-137m has a half-life of minutes and is responsible for all of the gamma ray emission. The ground state of barium-137 is stable.

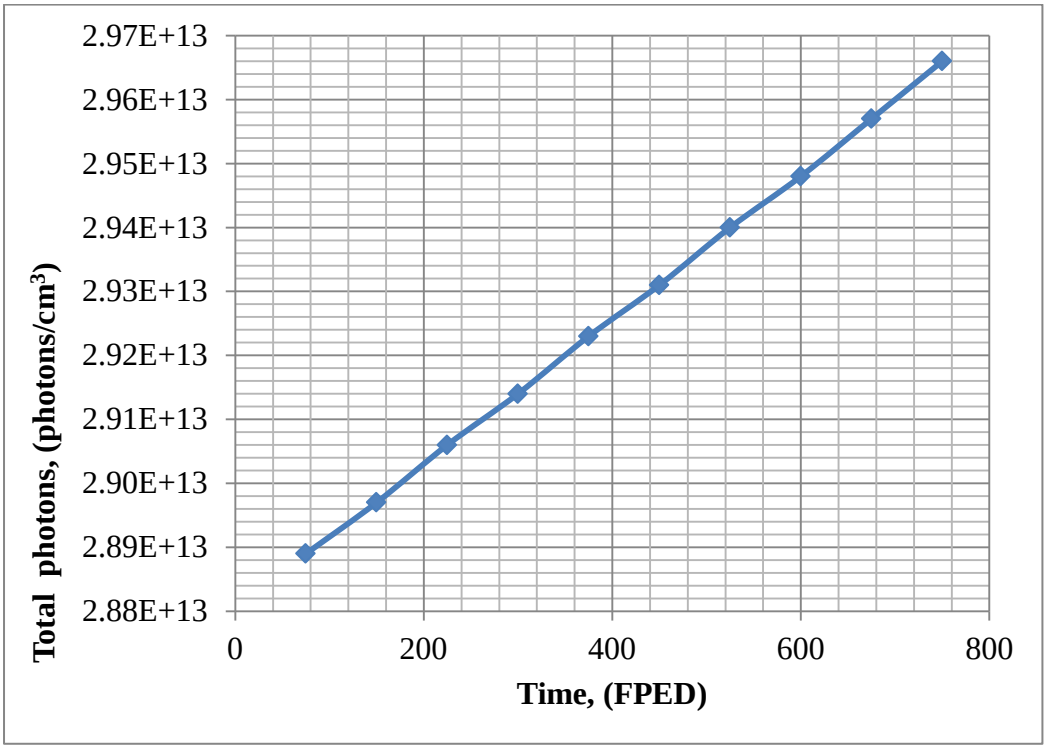

Figure 5.2: Photon density in actinides during irradiation period

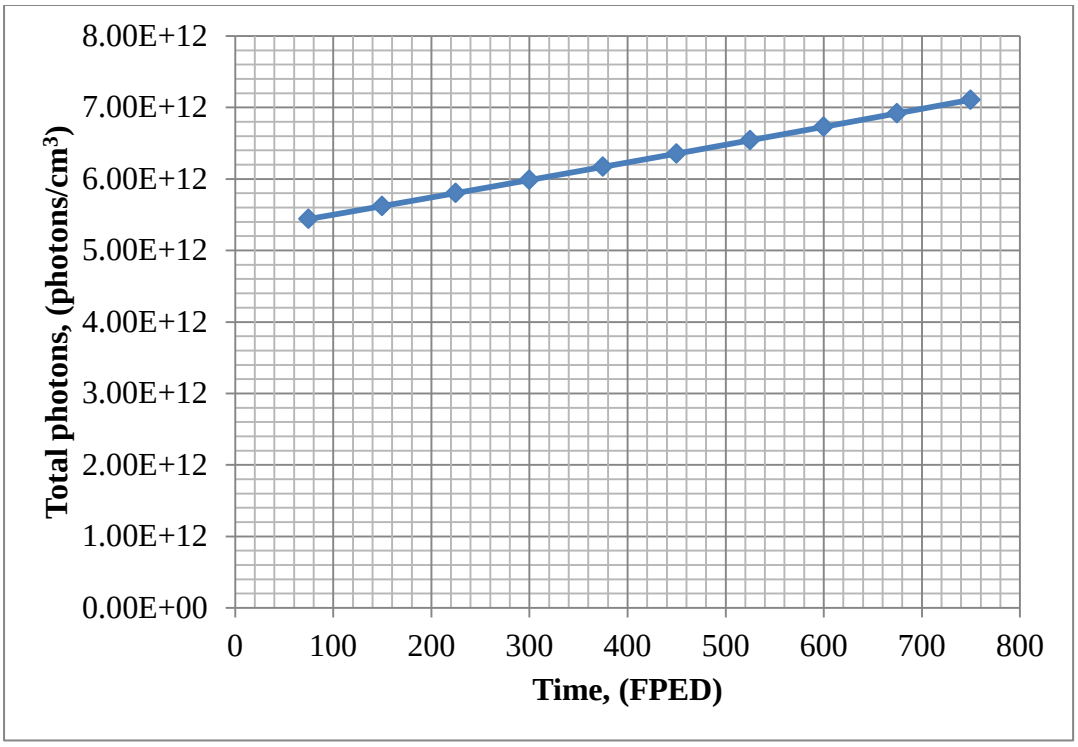

Figure 5.3: Photon density in activation products during irradiation period

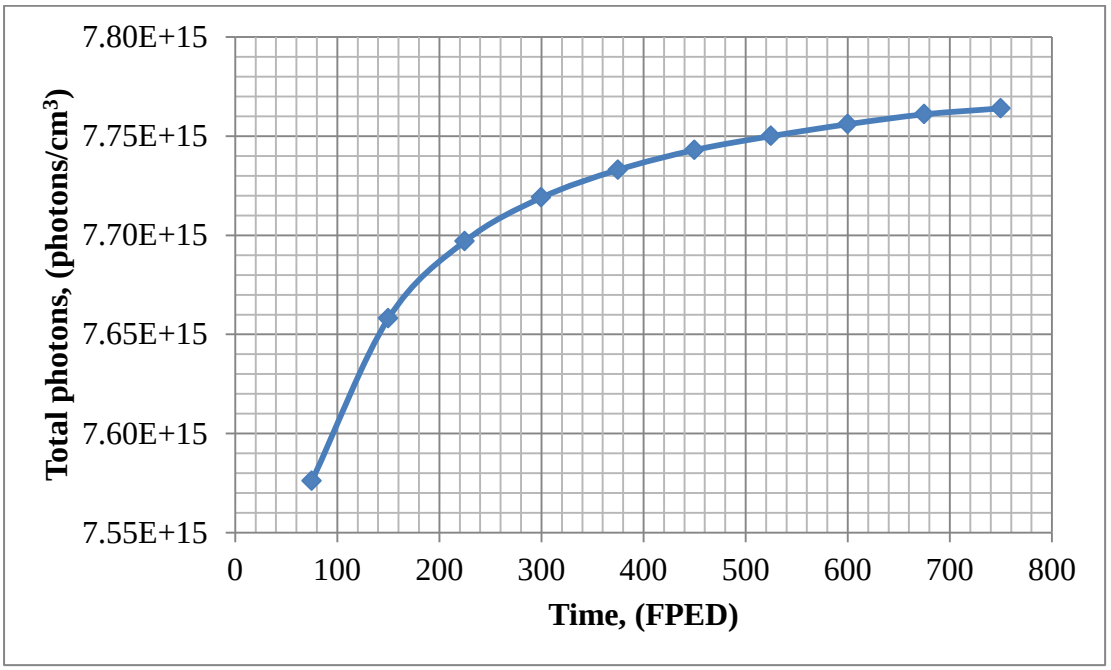

Figure 5.4: Photon density in fission products during irradiation period

For a bounding hypothetical accident radiological dose evaluation, the maximum values of the photon spectra over the whole core life history (including both irradiation period and cooling period) must be extracted. The results are shown in Appendix Tables C1, C2, and C3 respectively in the appendix. The bounding maximum photon spectral values are always found at the end of the irradiation period for activation products, actinides and fission products. The history of buildup of photon source during irradiation period is shown in figures 5.2, 5.3 and 5.4. For all the radionuclides, the total photon source reaches its maximum at the end of irradiation period.

Figures 5.5, 5.6 and 5.7 shows the GHARR-1 peak power pin photon source for fission products, actinides and activation products during cooling period for 8,000 calendar days.

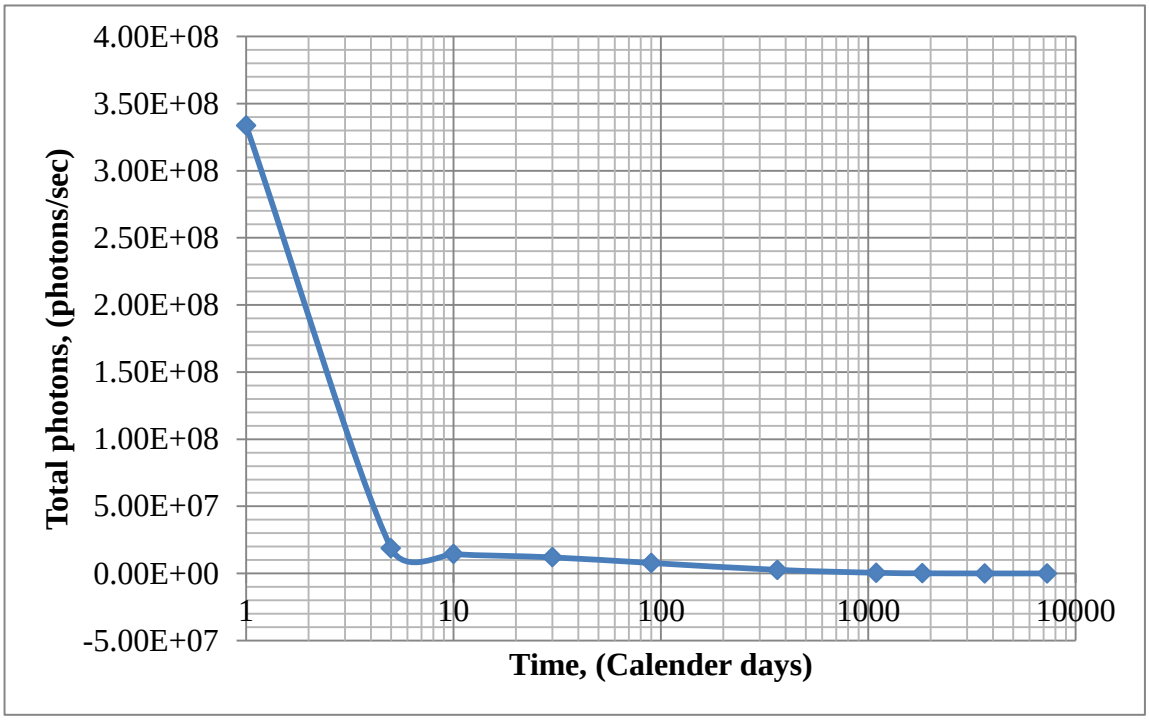

Figure 5.5: A log graph of GHARR-1 Peak Power Pin Photon Source for Activation Products During Cooling Period for 8,000 Calendar Days

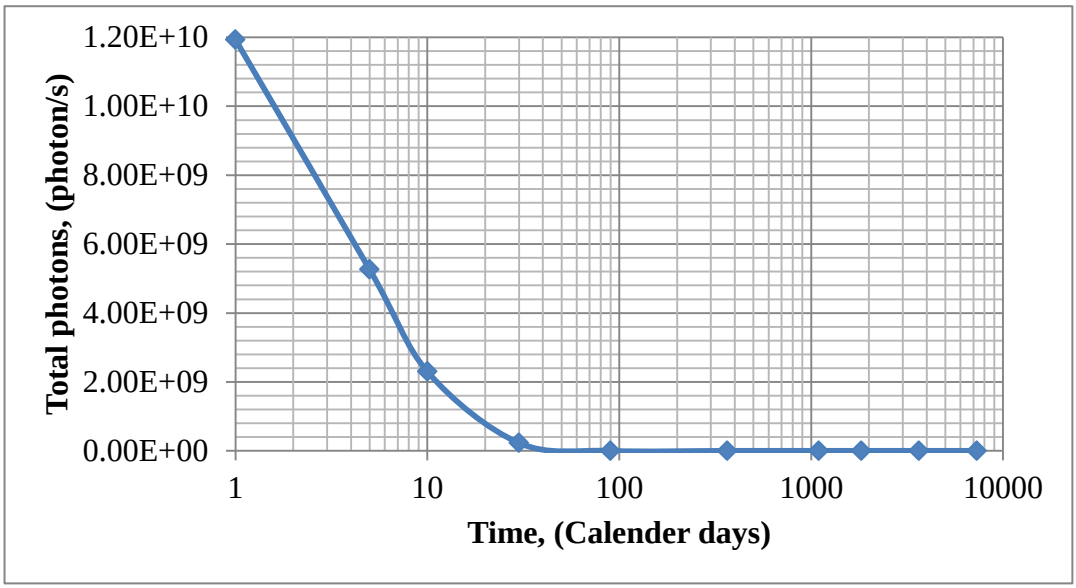

Figure 5.6: A log graph of GHARR-1 Peak Power Pin Photon Source for Actinides During Cooling Period for 8,000 Calendar Days

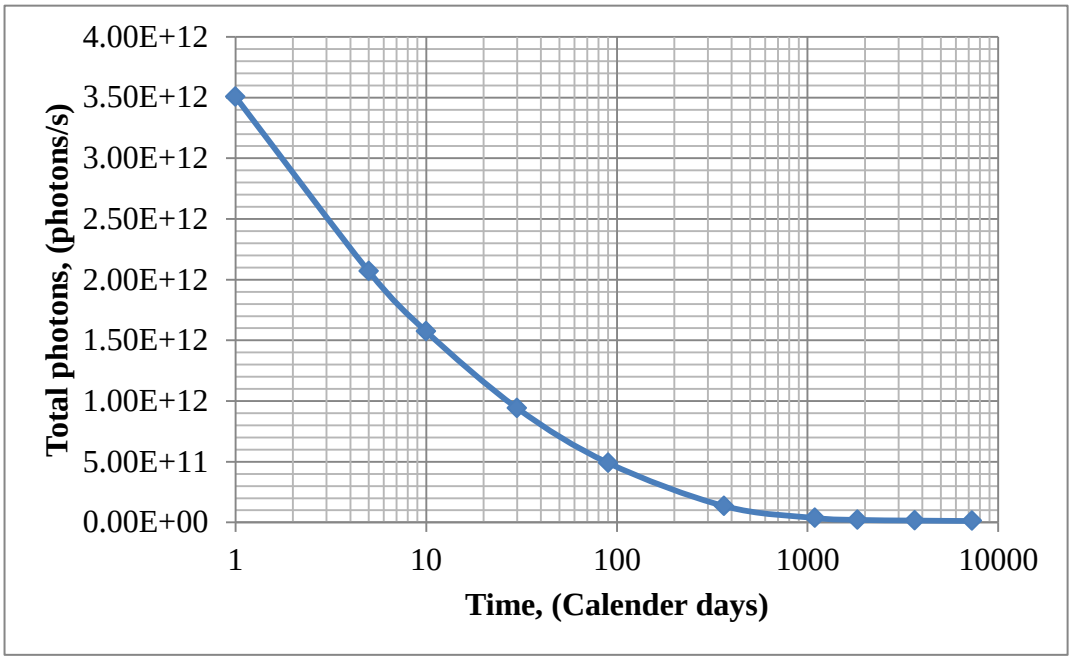

Figure 5.7: A log graph of GHARR-1 Peak Power Pin Photon Source for Fission Products During Cooling Period for 8,000 Calendar Days

The photon energies are higher for fission products followed by actinides and activation products respectively during spent fuel cooling. The total photon source decays quickly during the initial cooling period within ~ 30 days. After that the decay rate slows down progressively. Since almost 99% of the photon energy are produced by the fission products, the bounding radiological dose due to hypothetical accidents can be evaluated at the end of irradiation (discharge time) when the photon source is at its maximum in the entire core life history. This assumption is the most conservative approach to obtain the maximum radiological doses in any hypothetical accident scenario

5.1 Fuel Depletion and Plutonium Production in the GHARR-1

The depletion of U-235 and the production of Pu-239 were analyzed for the GHARR-1 using both REBUS3 and ORIGEN2 code packages for comparison. The results of the comparison are shown in figure 5.8. The figure shows that the U-235 burnup weight percent for the both the ORIGEN2 and the REBUS3 are very comparable. The ORIGEN2 code recorded U-235 burnup weight percent of 2.90% whilst that of the REBUS3 was 2.86%.

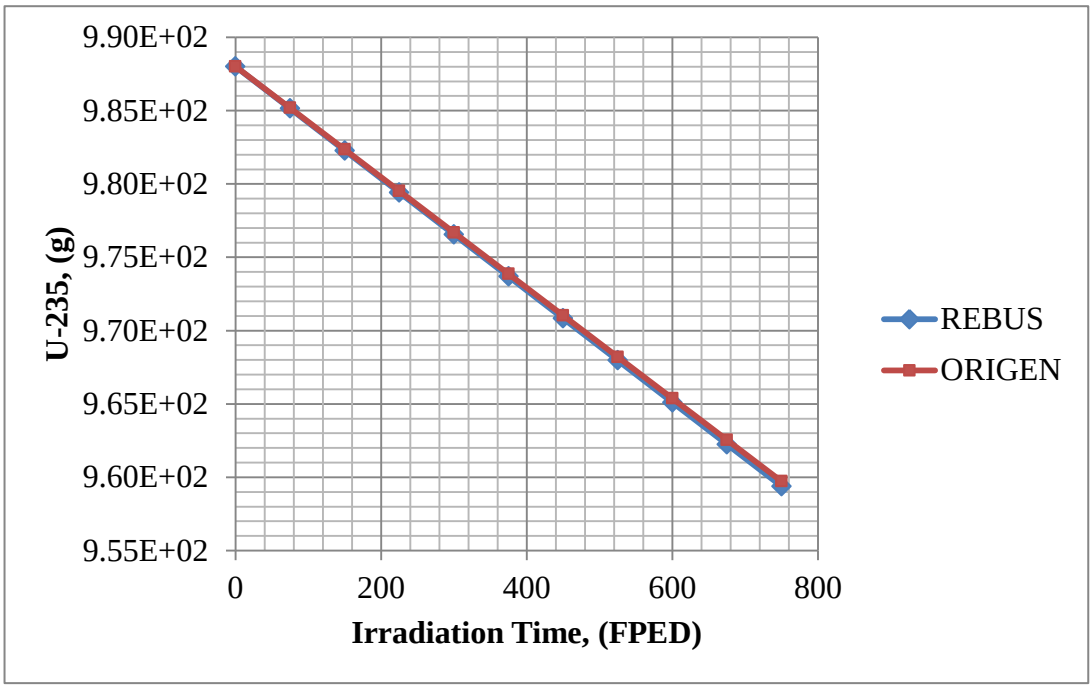

Figure 5.8: A graph showing the U-235 burnup weight percent using ORIGEN2 and REBUS3

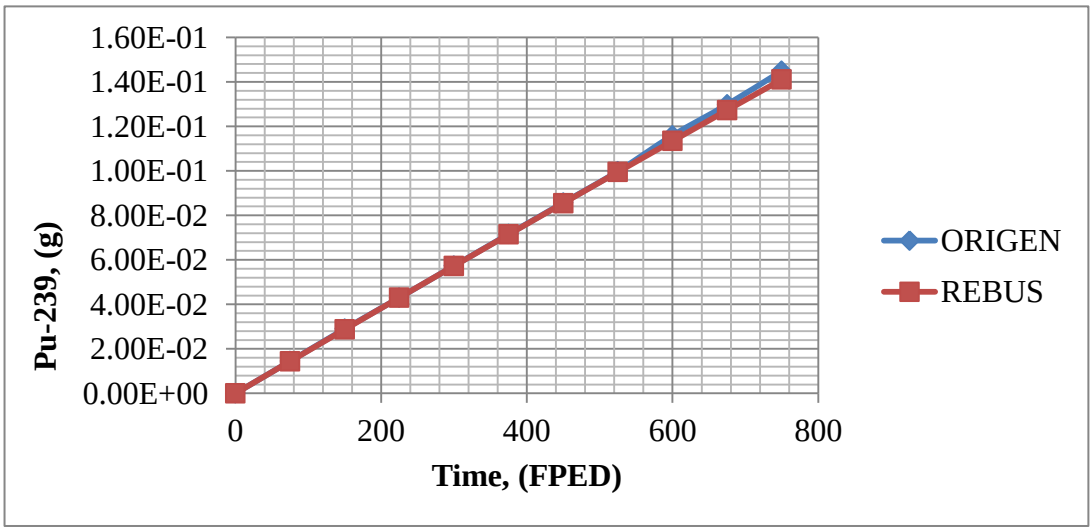

Figure 5.9: Comparison of Pu-239 Production from REBUS3 and ORIGEN-2 for GHARR-1

The production of plutonium-239 is also very comparable based on the ORIGEN2 and the REBUS3 results. The amount of Pu-239 peaks at the end of the irradiation period around a value of 1.45E-01grammes as shown in figure 5.9. The value is understandable since burnup is low hence making the production of Pu-239 also low.

5.2 Criticality and Neutron Distribution in Cask

The isotopic inventory obtained from the run of the REBUS3 and the ORIGEN2 runs were used in setting up an MCNP deck in order to perform neutronic calculations as well as dose calculations. In all, six casks of various materials compositions and material arrangements were designed to achieve the best cask design. Figures 5.10, 5.11, 5.12 and 5.13 are two examples of the casks designs showing the x-z and x-y cross sectional views of each cask.

Table 5.3: Composition & Arrangement of Cask Material with Reference to Spent Nuclear Fuel

Cask A	Cask B	Cask C	Cask D	Cask E	Cask F
Al canister	B P	Resin	Resin	Al canister	Liquid nitrogen
Lead	Lead	BP	Boron carbide	Boron carbide	Al canister
Steel	Stainless steel	Lead	Lead	Lead	Boron carbide
S C	S C	Stainless steel	Stainless steel	Stainless steel	Resin
Stainless steel	Stainless steel	S C	S C	S C	Boron carbide
lead	lead	Stainless steel	Stainless steel	Stainless steel	Lead
		lead	lead	lead	Stainless steel
					S C
					Stainless steel
					Lead

Al-Aluminium SC-Serpentine Concrete BP-Borated Polyethylene

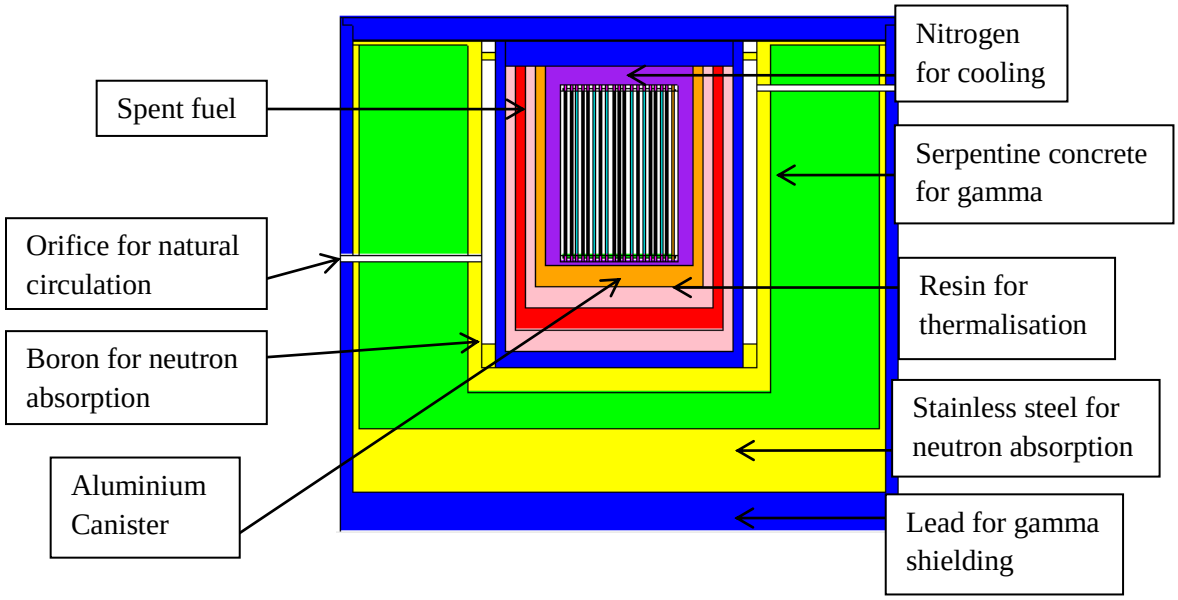

Figure 5.10: X-Z Cross sectional View of Cask Design F.

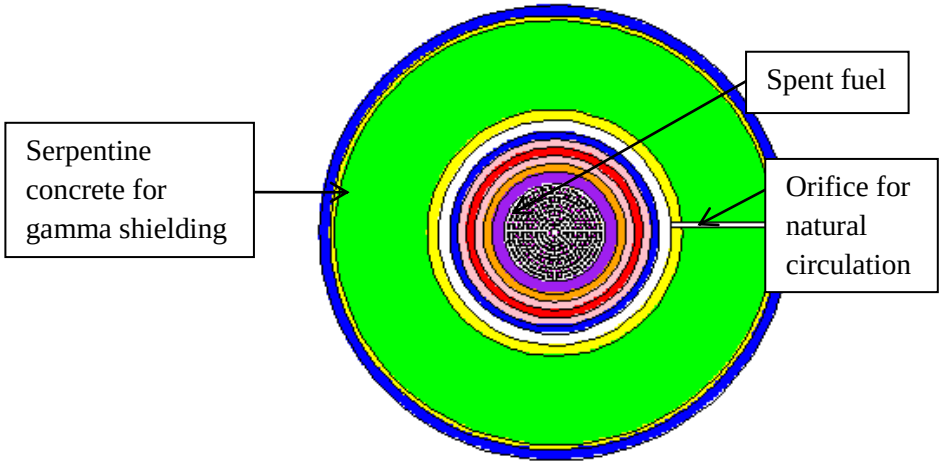

Figure 5.11 : X-Y Cross sectional View of Cask Design F.

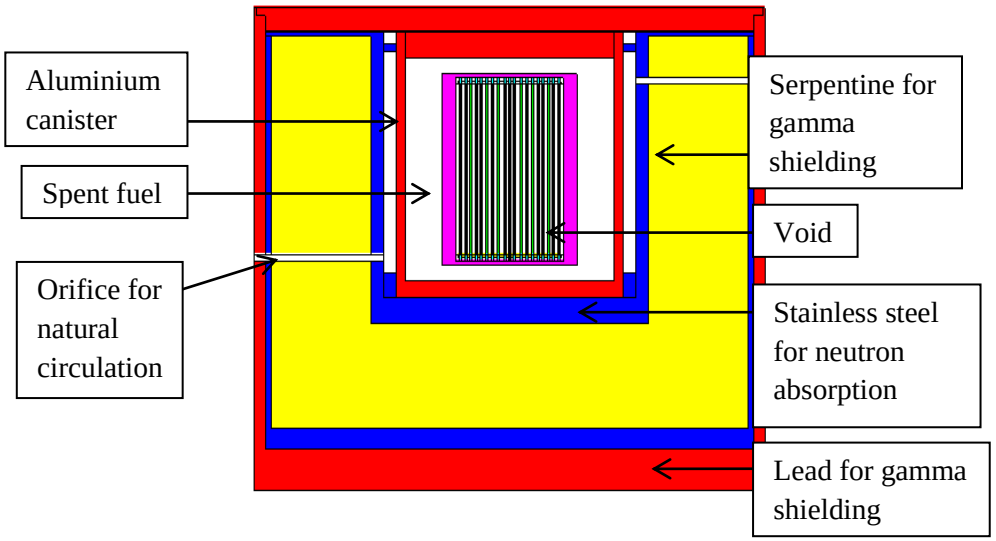

Figure 5.12: X-Z Cross Sectional View of Cask Design A.

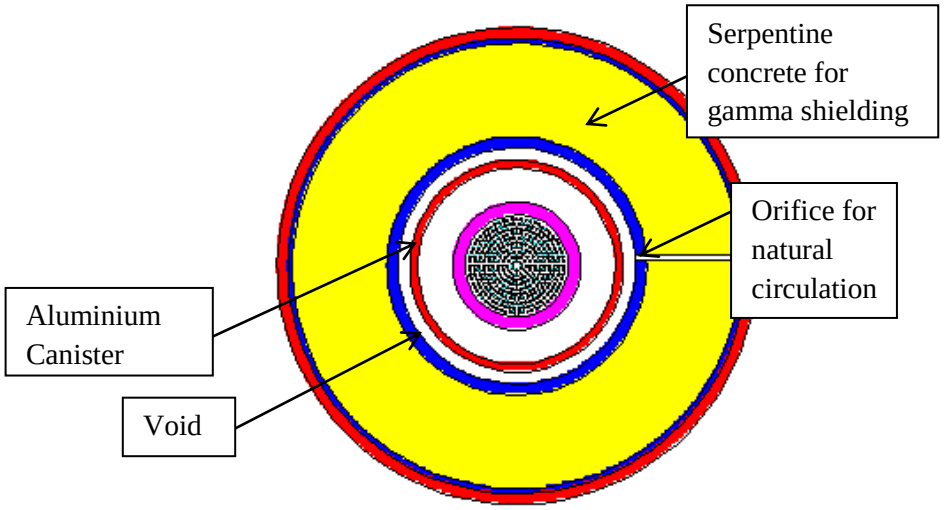

Figure 5.13: X-Y Cross sectional view of Cask Design A.

The casks were designed to include multiple layers of neutron and photon absorbers. All the cask designs were modeled with external radius specification of approximately 60cm and height of 75.462cm. All casks were cooled using natural circulation. **Cask A** is composed of the GHARR-1 spent fuel core (the spent fuel was placed in the cask just after discharge; consideration was not given to wet storage for all designs) in an aluminium canister and surrounded by five layers of lead, steel, serpentine concrete, stainless steel and lead respectively. Each material was selected because of its ability to shield either neutrons or gamma from personnel and the environment. The availability of serpentine in Ghana as well as its shielding ability made it a preferable choice for concrete material. The results obtained for the MCNP simulation of **cask A** produced a multiplication factor 0.02969±0.00001. The results showed that the **design A** could keep the fuel sub critical even without previous cooling. The neutron flux profiles in the various layers were also obtained. Figures 5.14 to 5.18 show the neutron flux distribution in the various layers.

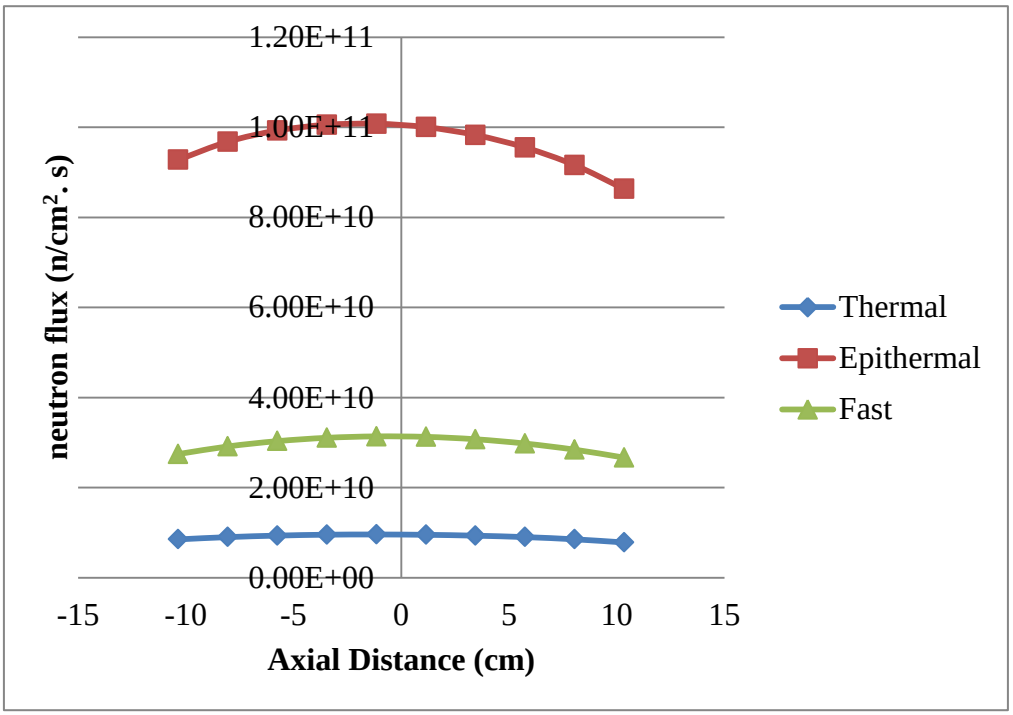

Figure 5.14: Neutron Flux Distribution in first Layer of Cask A

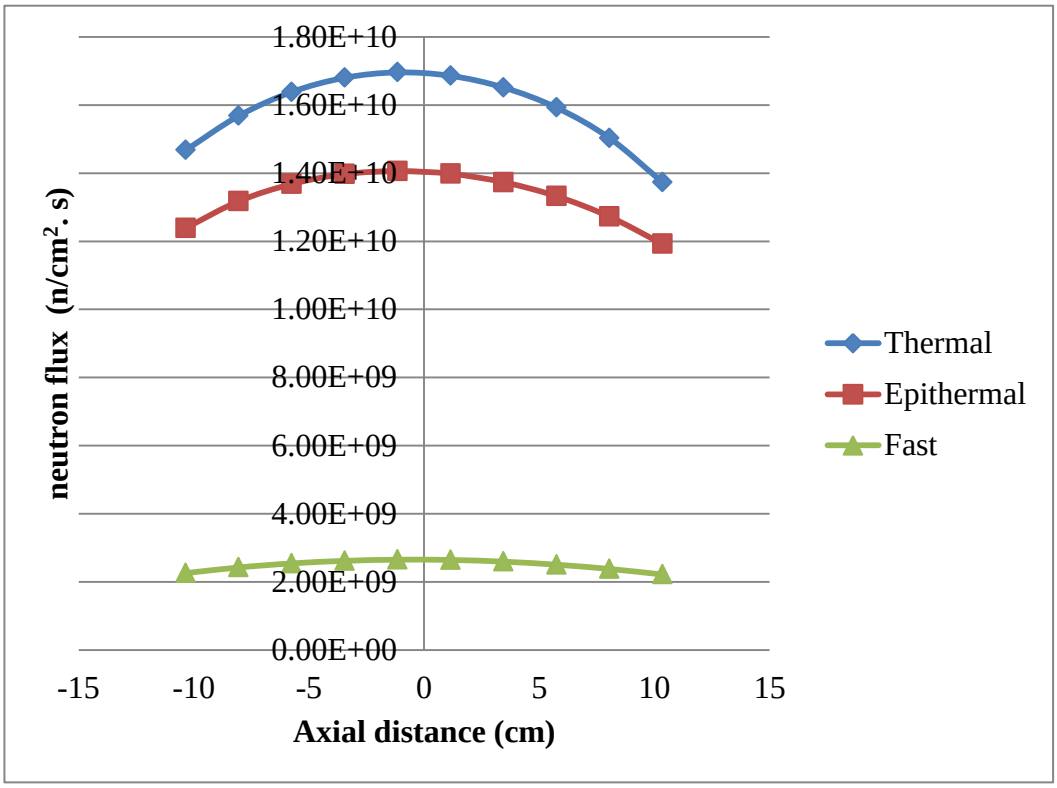

Figure 5.15: Neutron Flux Distribution in Second Layer of Cask A

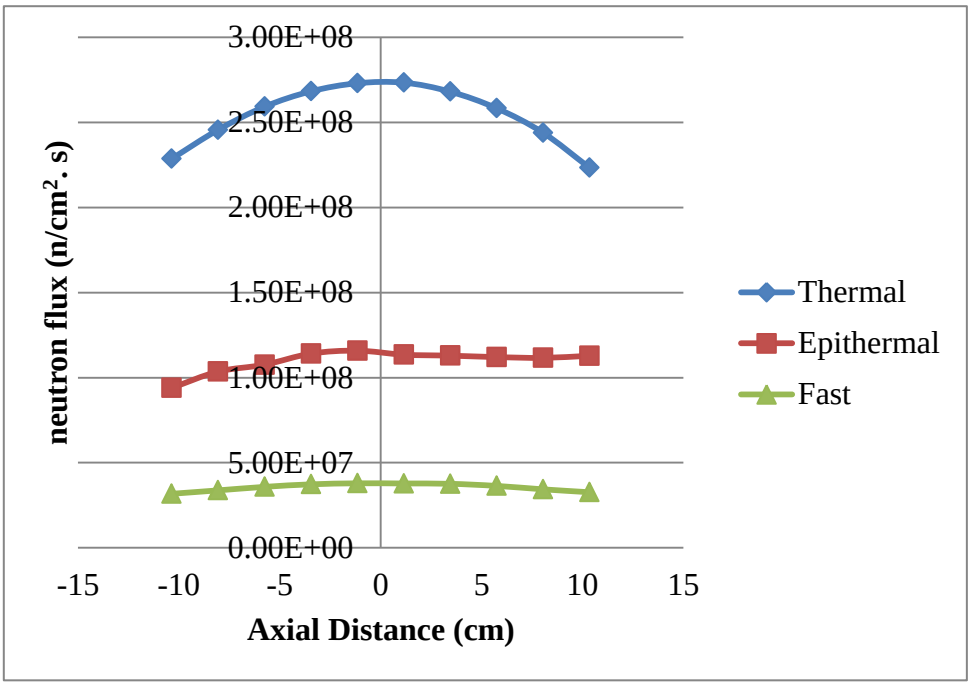

Figure 5.16: Neutron Flux Distribution in Third Layer of Cask A

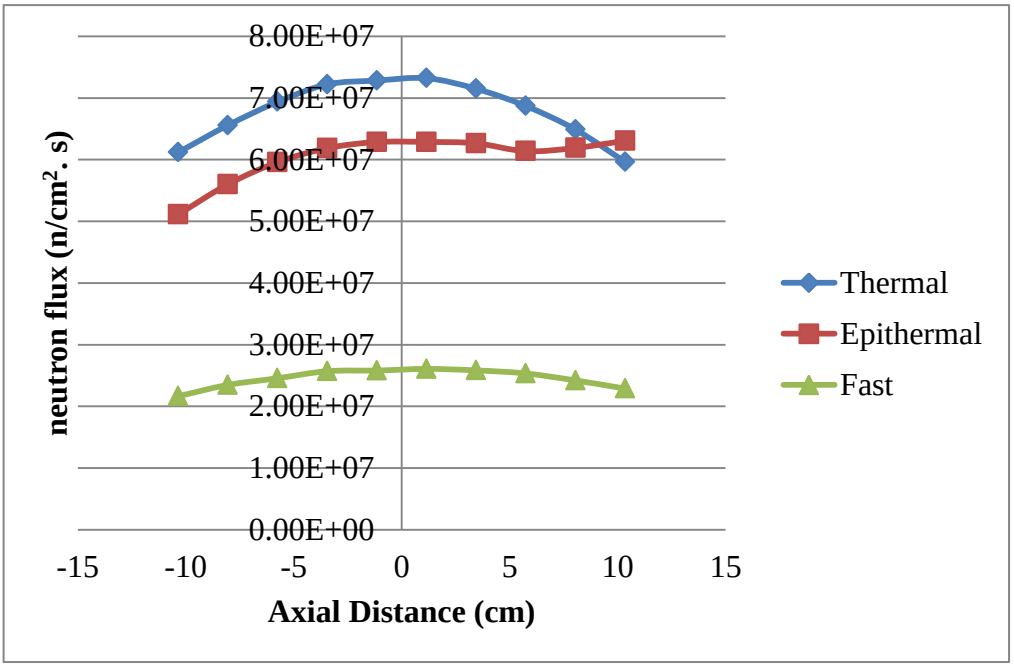

Figure 5.17: Neutron Flux Distribution in Fourth Layer of Cask A

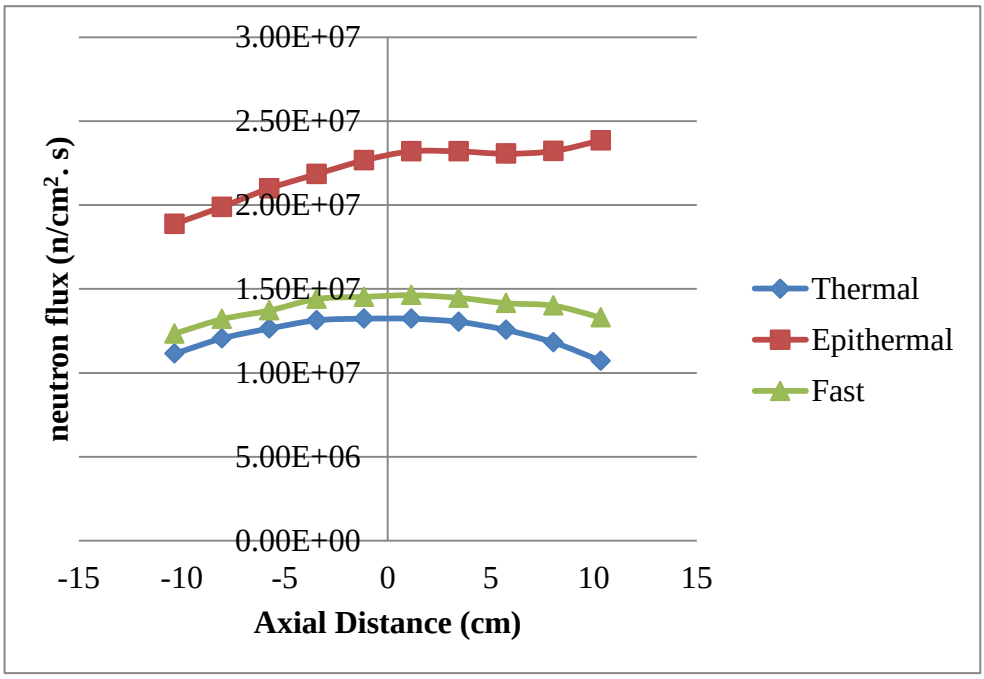

Figure 5.18: Neutron Flux Distribution around Cask A

The profile in the first layer of cask A shows that the epithermal neutrons are the highest followed by the fast and the thermal flux respectively. The neutrons which are born fast have interacted or collided with quite a few materials; therefore most of them have slowed down to the epithermal neutron energy range. This could account for the high level of epithermal neutrons. As the flux interacts with multiple materials, the thermal flux increases whilst the epithermal flux decrease. This is due to more collisions by the neutrons with multiple shielding materials. Generally, the flux profile from the bottom to the top in all materials increase to a peak value in the region around the center of the cask before dipping to lower values around the top. This could be attributed to the fact that the spent fuel occupies the mid portion of the cask and so the flux is most dense in that region. The area around the cask produced more epithermal flux than fast flux due to lack of interaction or collision with other materials. The flux profile of the total neutron flux distribution from the first layer to the surface of the cask shows a decrease in intensity of

the flux. The materials and design chosen for cask **A** was able to maintain sub criticality as well as reduce the neutron to some extent.

Cask **B** consists of the spent fuel in aluminium canister with cylindrical layers of borated polyethylene, lead, stainless steel, serpentine concrete, stainless steel and lead. The neutron flux profiles are shown in Figures 5.19 to 5.23.

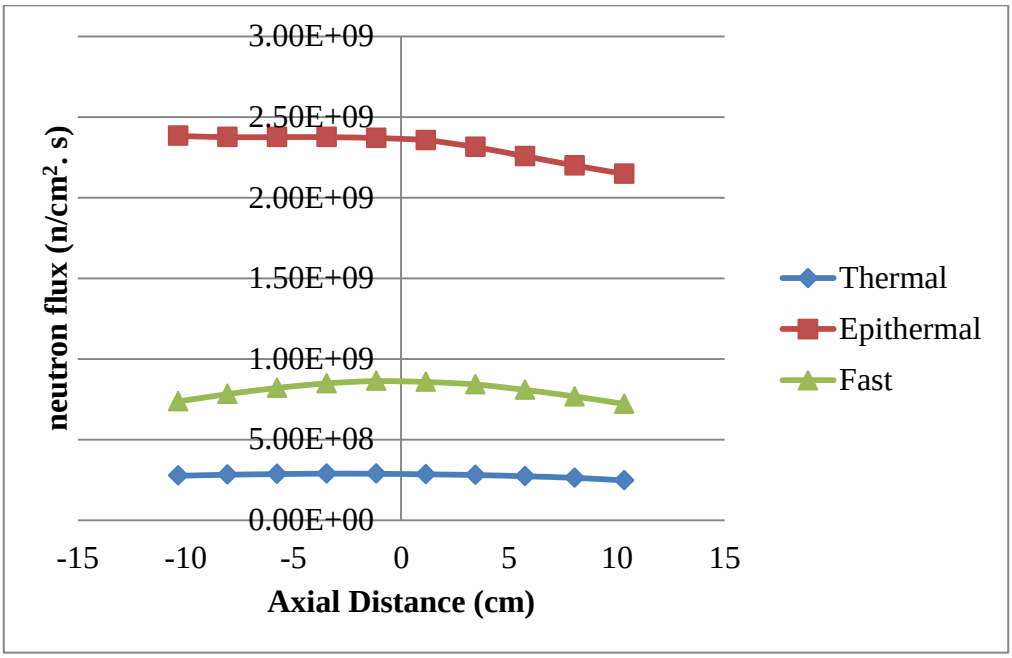

Figure 5.19: Neutron Flux Distribution in first Layer of Cask B

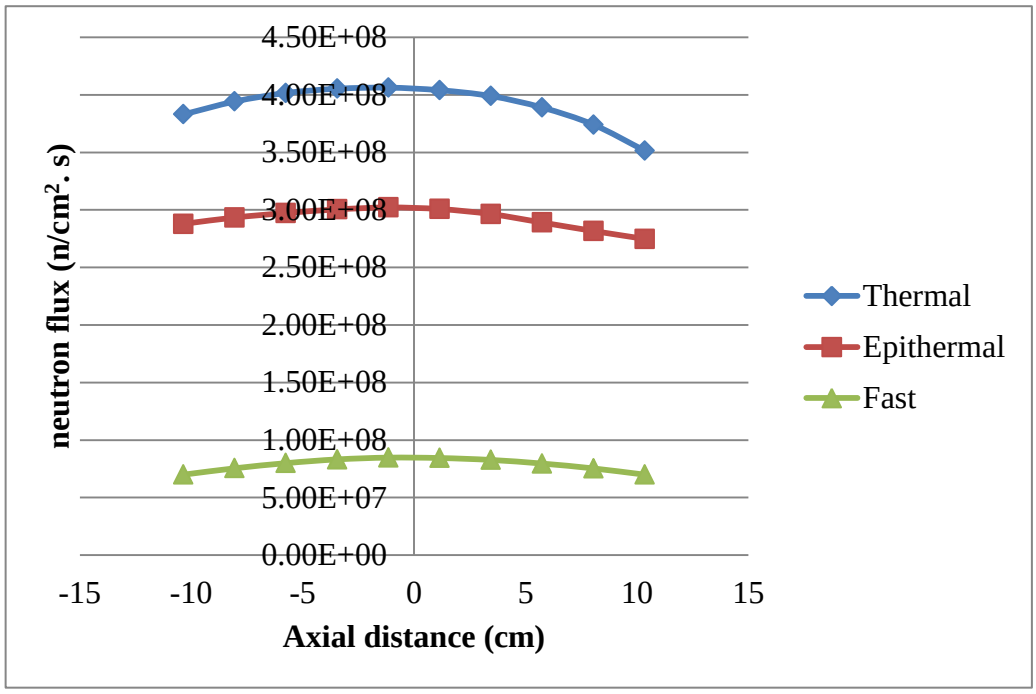

Figure 5.20: Neutron Flux Distribution in Second Layer of Cask B

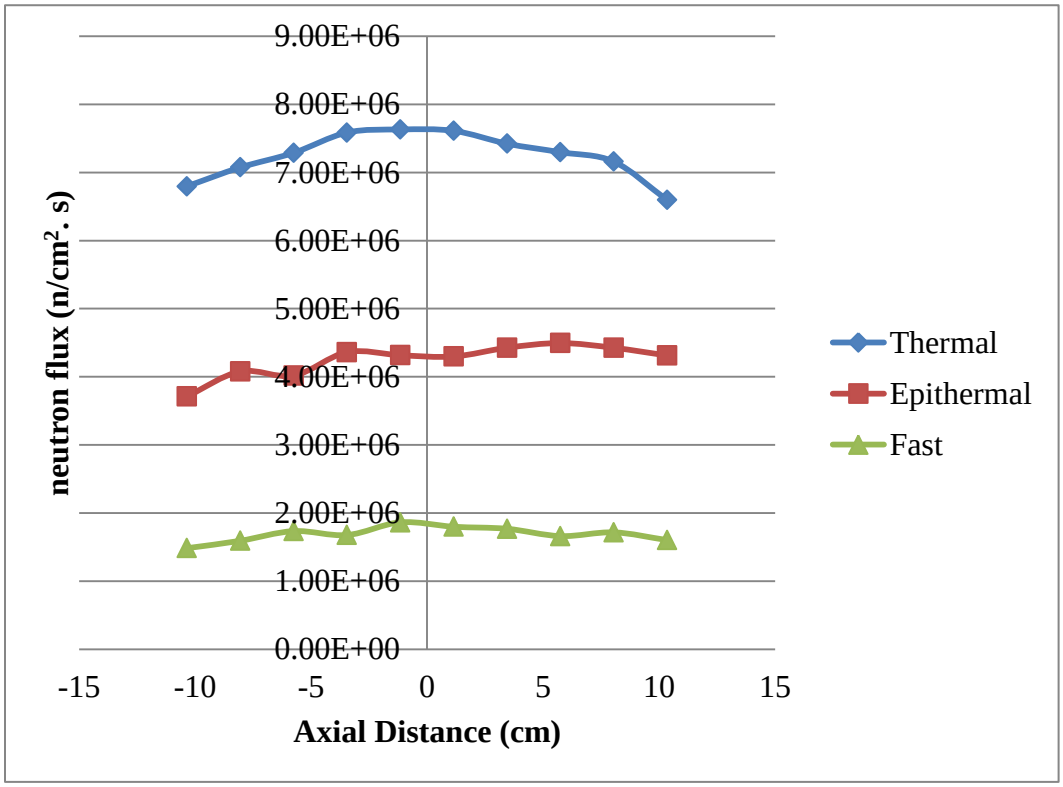

Figure 5.21: Neutron Flux Distribution in Third Layer of Cask B

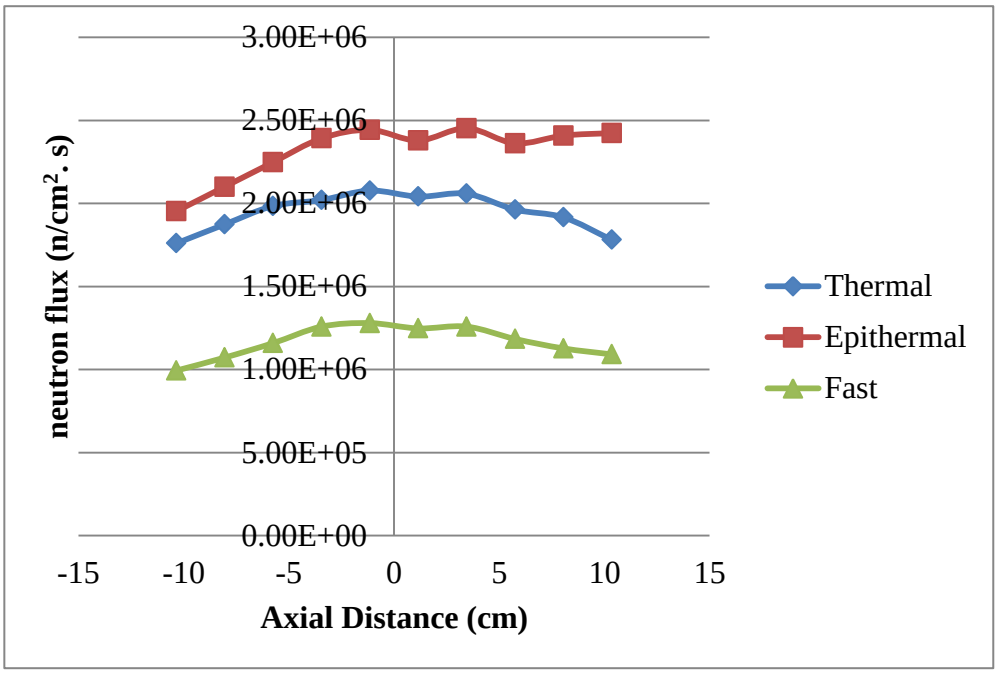

Figure 5.22: Neutron Flux Distribution in fourth Layer of Cask B

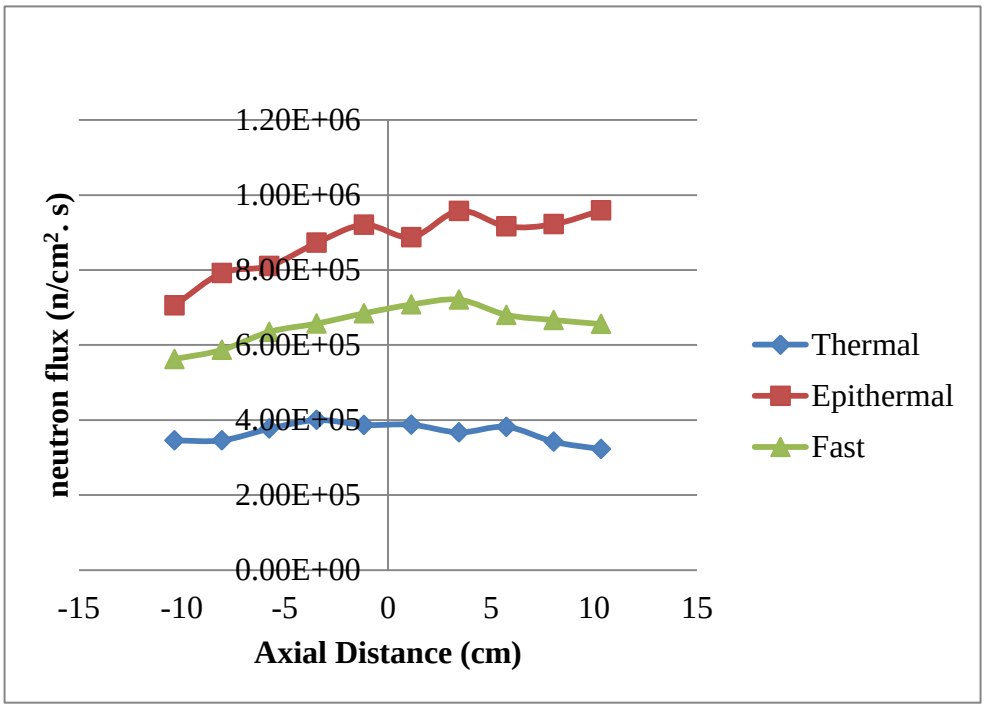

Figure 5.23: Neutron Flux Distribution around the Cask B

The flux profile in the various layers followed the same trend as in cask A. The total neutron distribution decreased from the first layer to the surface of the cask. However, the

values recorded on the surface of cask design B were lower than that of cask design A. This could be explained as being as a result of the borated polyethylene which is a known neutron absorber. The cask maintained a sub critical system with multiplication factor of 0.06304 ± 0.0002. The magnitude of the k_{eff} in cask B could be explained by the fact that due to the high absorption cross section of the borated polyethylene, more neutrons are retained in the system thereby giving a higher k_{eff}.

Cask C also comprised the spent fuel in a container containing resins, surrounded by cylindrical layers of borated polyethylene, lead, stainless steel, serpentine concrete, stainless steel and lead respectively. Figures 5.24 to 5.28 show the neutron flux distribution in the design.

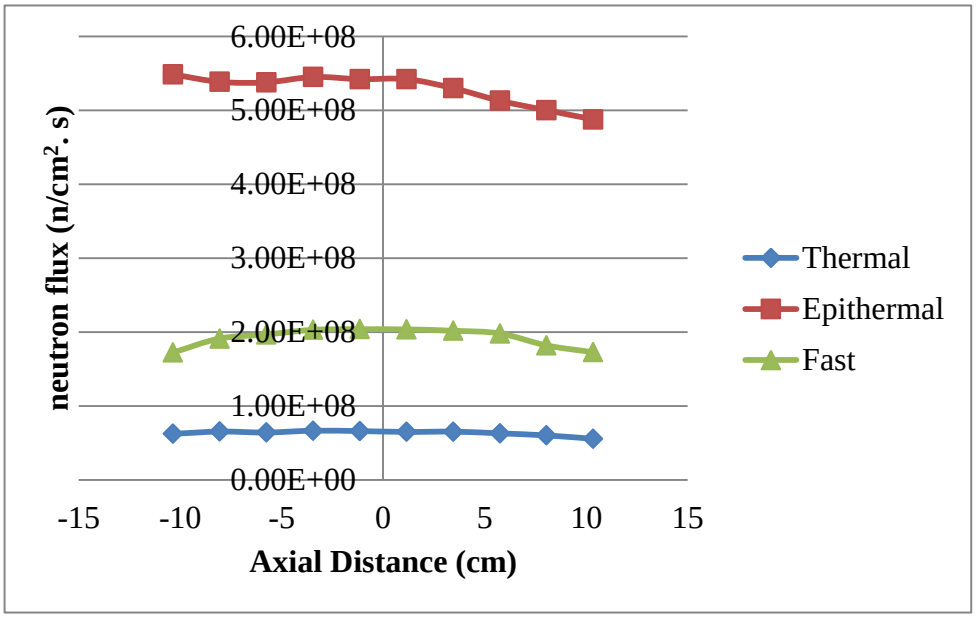

Figure 5.24: Neutron Flux Distribution in the First Layer of Cask C

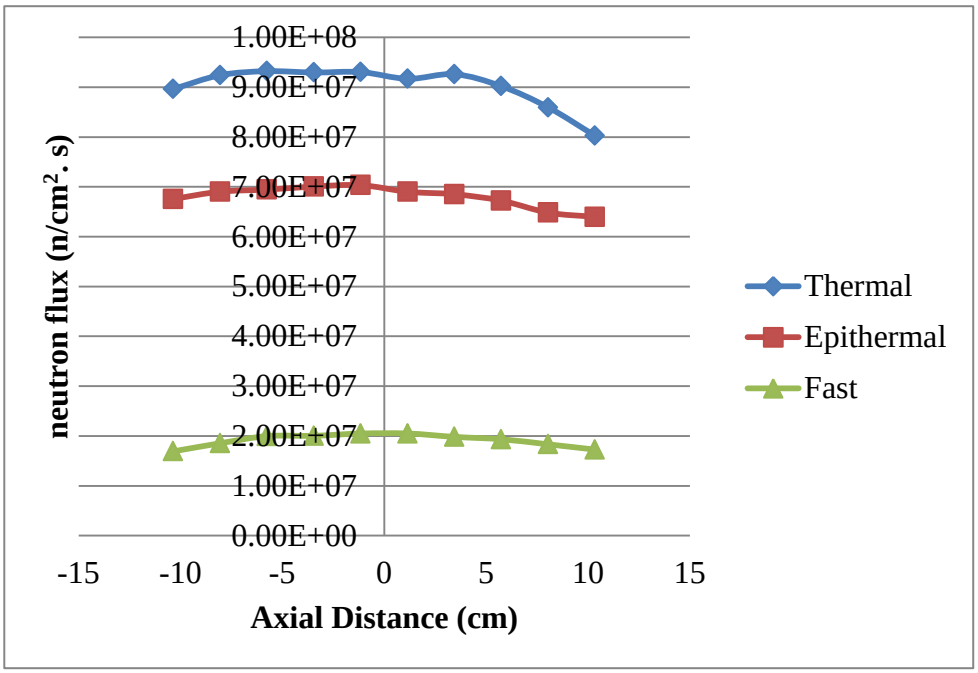

Figure 5.25: Neutron Flux Distribution in the Second Layer of Cask C

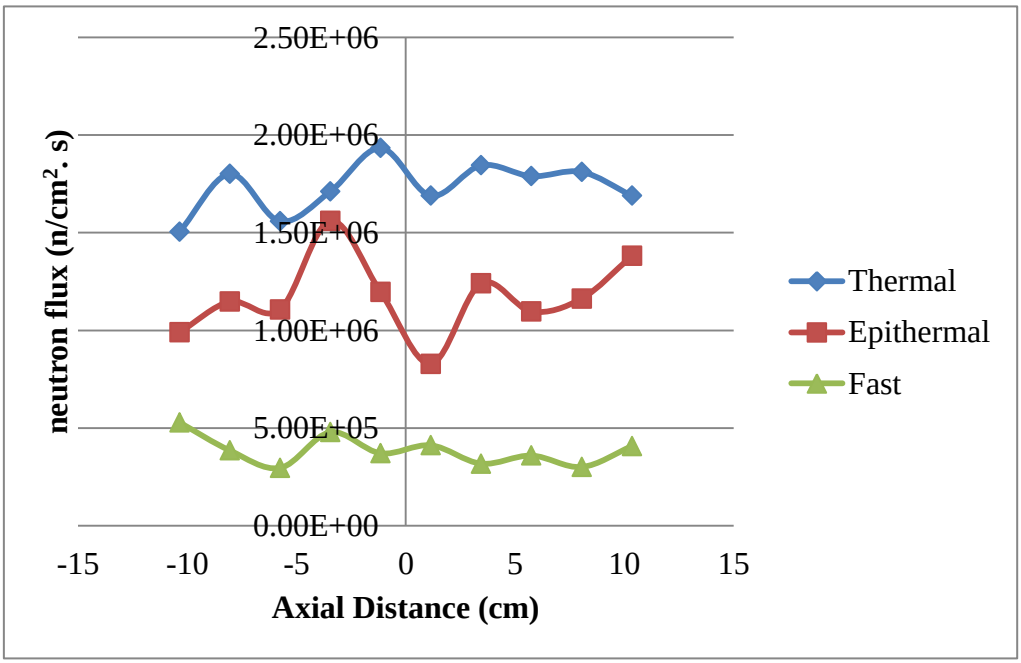

Figure 5.26: Neutron Flux Distribution in the Third Layer of Cask C

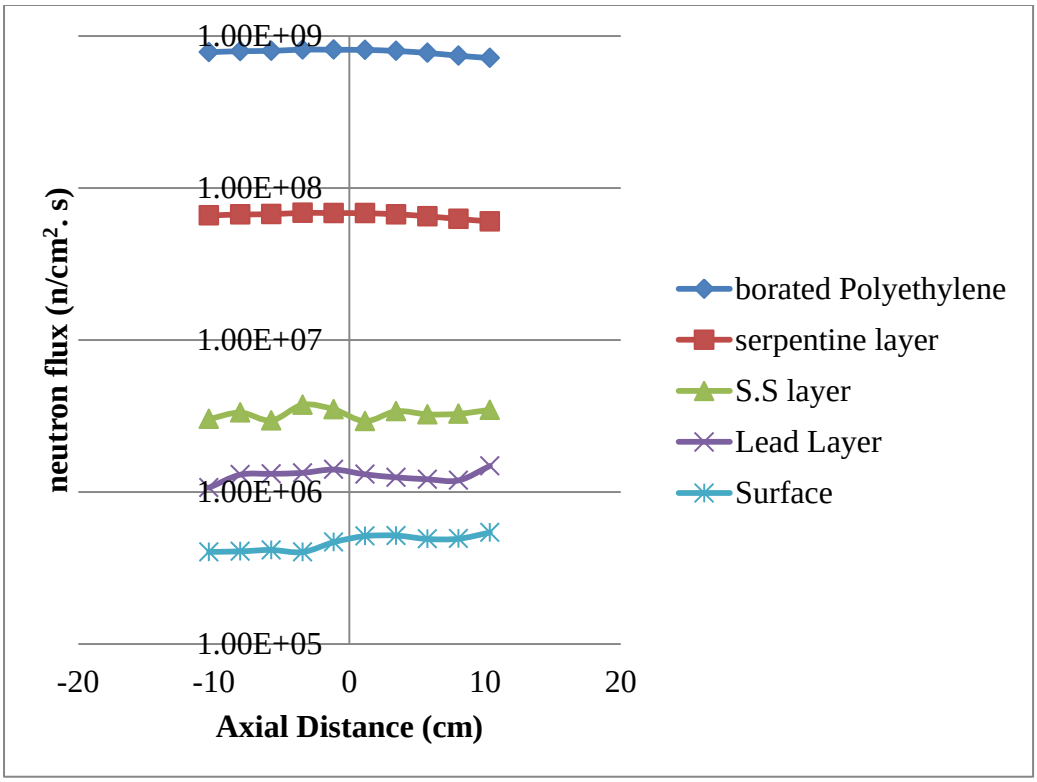

Figure 5.27: Total Neutron Flux Distribution in the various Layers of Cask C

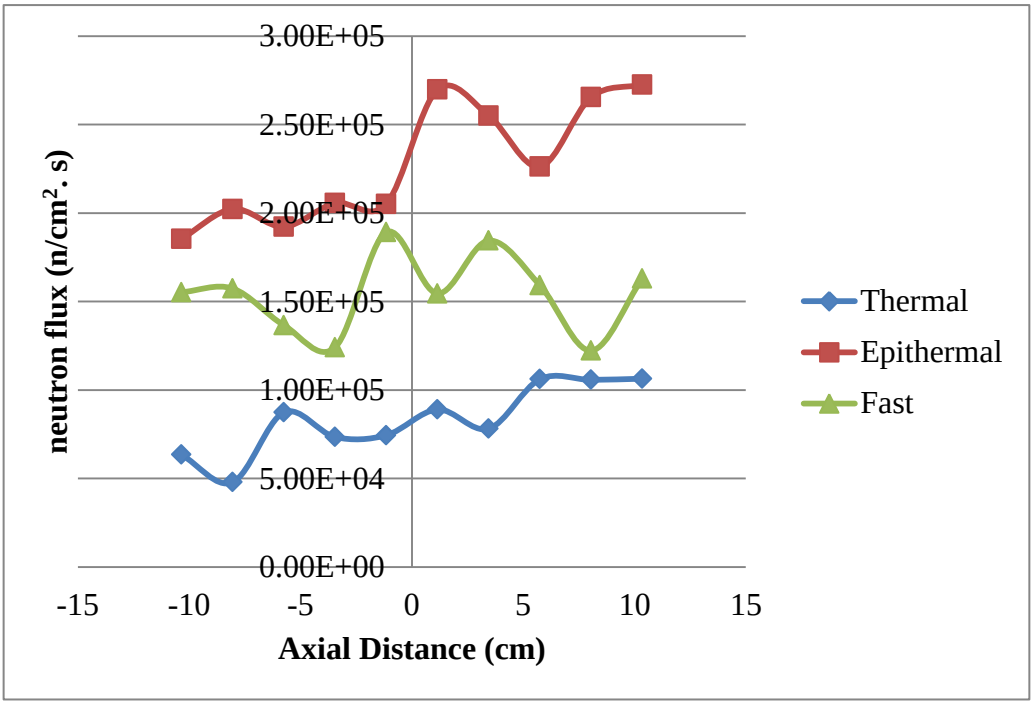

Figure 5.28: Neutron Flux Distribution around of Cask C

The neutron flux profile in the cask design C followed the same trend in the first, second and third layers as observed in the initial cask designs. They recorded lower flux values than previously observed. The region around the cask also recorded higher epithermal neutron flux due to insufficient scattering by target nuclei. The multiplication factor was 0.19809 ± 0.00027. Even though this cask design is able to maintain sub criticality, it recorded a higher value than previous designs. As usual, the total flux decreases from layer to layer until it reaches the surface.

Cask D consists of the spent fuel in a container containing resins, surrounded by cylindrical layers of boron carbide, lead, stainless steel, serpentine concrete, stainless steel and lead respectively. Figure 5.29 shows the total neutron flux distribution profile in the design. The graph shows the decrease in neutron intensity from the source to the region around the cask (10^9 to 10^6). The layer to layer neutron flux distribution followed the trend of values obtained in cask design C. However, the cask D recorded higher flux values in the region around the surface than in cask C thereby making cask C preferable to cask D with respect to neutron flux. The multiplication factor was 0.15393 ± 0.00025.

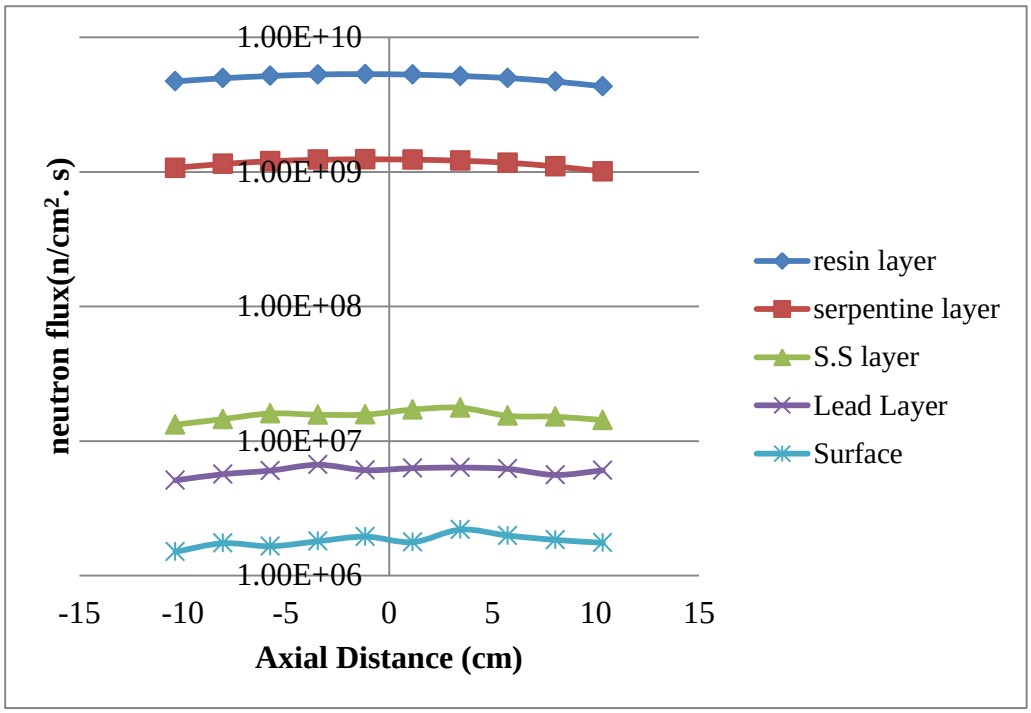

Figure 5.29: Total Neutron Flux Distribution in the various Layers of Cask D

Cask E consists of the spent fuel in an aluminium canister, surrounded by cylindrical layers of boron carbide, lead, stainless steel, serpentine concrete, stainless steel and lead respectively. Figure 5.30 shows the total neutron flux distribution in the various layers of cask design E.

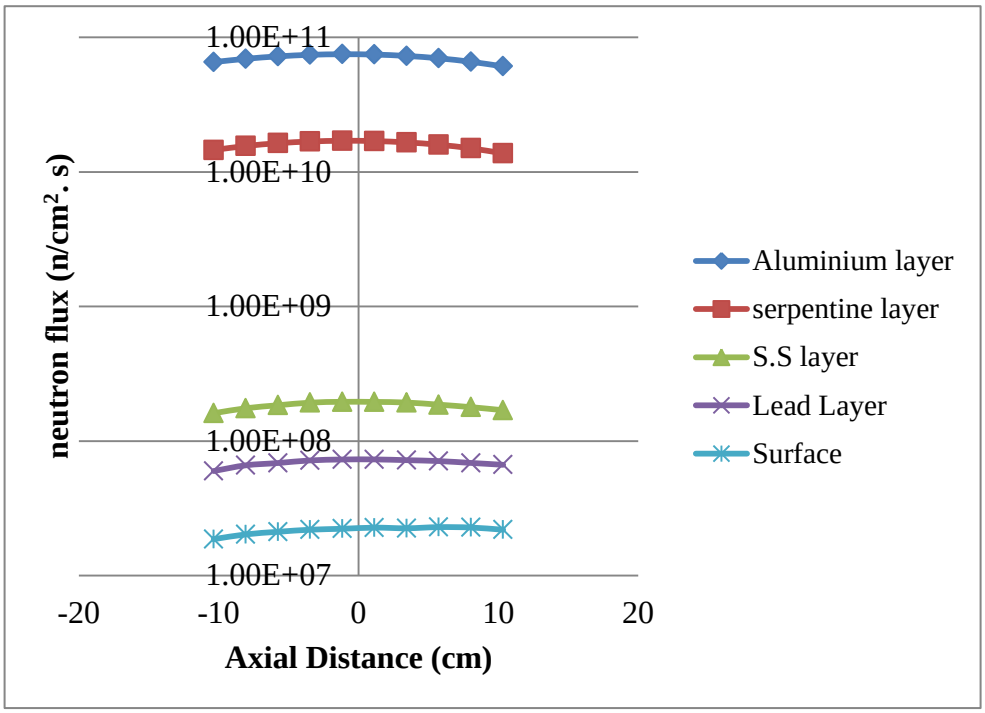

Figure 5.30: Total Neutron Flux Distribution in the various Layers of Cask E

The neutron flux at the surface of the cask is reduced but only to order 10^7. Comparatively, the cask C design is better in terms of neutron shielding. The k_{eff} was recorded as 0.02028 ± 0.00001 at the MCNP run showing that this design can also keep spent fuel sub critical.

More layers were introduced in the Cask F. The layers were rearranged and the external radius was maintained. In this design, liquid nitrogen was introduced to cool the spent fuel in the aluminium canister. Layers of boron carbide for neutron absorption, resin for thermalisation, boron carbide, lead, stainless steel and serpentine concrete for neutron and gamma shielding were used. Figure 5.31 shows the total flux distribution from each layer as well as the region around the cask. The neutron flux reduced from order 10^{10} at the source to 10^5 on the surface making it the best in terms of neutron shielding.

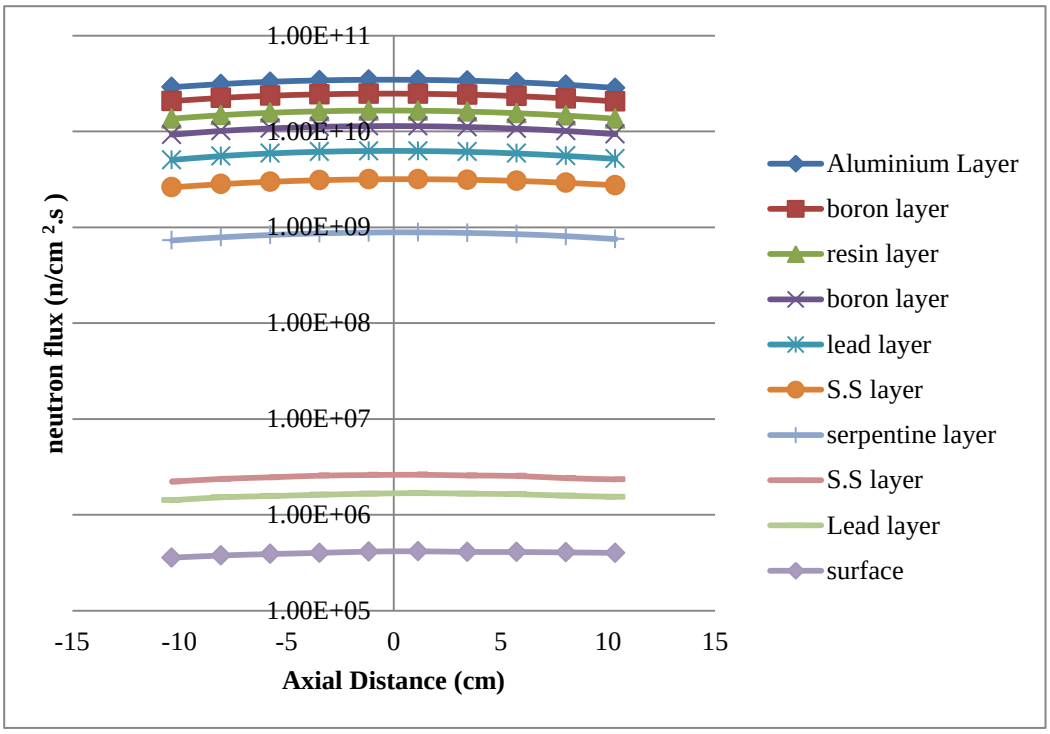

Figure 5.31: Total Neutron Flux Distribution in the various Layers of Cask F

The neutron flux in the first seven layers is relatively high (of the order 10^8 to10^{10}). The neutron energies are reduced as a result of interaction with multiple layers. However, there is a big drop in neutron flux intensity when the neutrons encounter the serpentine layer due to its high scattering cross section. Further interaction with the final lead layer adds up to the decrease in intensity due to its high atomic number. The k_{eff} was recorded as 0.01717 ± 0.00001 after the MCNP run showing that this design can also keep spent fuel sub critical.

5.3 DOSE CALCULATION

The amount of absorbed dose given off at the surface of the various cask were also obtained using MCNP.

Radiation damage depends on the absorption of energy from the radiation and is approximately proportional to the mean concentration of absorbed energy in irradiated

tissue. For this reason, the basic unit of radiation dose is expressed in terms of absorbed energy per unit mass of tissue [92]. The human body is made up of 70–80% water. Basic dose distribution data are usually measured in water phantom which closely approximates the radiation absorption and scattering properties of muscle and other soft tissue [93]. Values of linear absorption attenuation coefficient were obtained from the National Institute of Standards and Technology database [94].The cell that was used determine the dose rate were filled with water in the MCNP input deck . The F4: P tally was used in the simulation to obtain the photon flux. The results were normalized and converted to absorbed dose using the equation

$$\frac{\phi \frac{photons}{cm^2.s} * E \frac{MeV}{photons} * 1.6 * 10^{-13} \frac{J}{MeV} * \mu_m cm^{-1}}{\rho_m \frac{kg}{cm^3} * 1 \frac{J/kg}{Gy}} \qquad (5.1)$$

The absorbed dose in the water can be used to represent the dose of that person. The values obtained from the various cask designs are found in the table 5.4 below.

Table 5.4: A table of Axial Distance (cm) and Dose rate (Gy/h)

Axial dist.	Cask A	Cask B	Cask C	Cask D	Cask E	Cask F
-10.35	4.33E+01	1.59E+00	4.25E-01	1.89E+00	4.33E+01	3.22E-01
-8.05	4.57E+01	1.63E+00	4.24E-01	2.01E+00	4.57E+01	3.44E-01
-5.75	4.78E+01	1.68E+00	4.72E-01	1.87E+00	4.78E+01	3.57E-01
-3.45	4.91E+01	1.71E+00	4.08E-01	1.87E+00	4.91E+01	3.70E-01
-1.15	4.98E+01	1.76E+00	4.87E-01	2.07E+00	4.98E+01	3.77E-01
1.15	5.00E+01	1.74E+00	4.65E-01	2.09E+00	5.00E+01	3.82E-01
3.45	4.95E+01	1.77E+00	4.96E-01	2.09E+00	4.95E+01	3.81E-01
5.75	4.84E+01	1.75E+00	4.68E-01	1.86E+00	4.84E+01	3.77E-01
8.05	4.69E+01	1.71E+00	4.43E-01	1.98E+00	4.69E+01	3.69E-01
10.35	4.50E+01	1.66E+00	4.18E-01	1.85E+00	4.50E+01	3.57E-01

The results show that the cask design F has the highest gamma shielding ability. The cask design C also has a good gamma shielding ability as the results obtained from the run show that it closely follows the Cask design F with the smallest gamma intensity. Considering the fact that the spent fuel was placed in the cask immediately after discharge, the values recorded are quite good. Normally, spent fuel undergoes wet storage for between 6 months to a year. By which time, most of the short lived radioisotopes undergo decay. Wet storage reduces the amount of photon dose that is given off by the spent fuel.

CHAPTER 6

6 CONCLUSION AND RECOMMENDATION

International concerns on the use of HEU powered reactors for peaceful uses have driven the coordination of core conversion studies. The study has helped develop prospective LEU cores for MNSR that will ensure desirable power and flux. The Ghana Research Reactor-1, in any case, should have an onsite spent fuel cask to hold the spent fuel in the event that the core reaches its lifetime. Detailed studies of the design of appropriate casks were undertaken. A simple reactivity rundown was done to obtain an estimate of the core lifetime of Ghana Research Reactor-1 using REBUS3 code. A simple run down at 30kW resulted in an estimated core life of approximately 750 full-power-equivalent-days. Assuming in real operational terms the reactor operates for 2hours a day, 4 days a week and 48 weeks in a year then the estimated core life of the reactor is equivalent to [750/(2*4*48/24) =46.88years]. Inventory of halogens, noble gases, alkaline metals, and actinides in the peak power fuel rods for GHARR-1 operated at 30kW was obtained. The peak rod power used for the inventory analysis was 103.6W. The bounding maximum radioactivity values are always found near the beginning of the irradiation period (75 FPEDs) for halogens and noble gases. However, the bounding maximum activities for alkaline metals and actinides and daughters are almost always found at the end of irradiation period (750 FPEDs). For the halogen and noble gas radioactivities, the concentrations (and so, activity) of these shorter-lived nuclides reach a saturation point within ~ 100 days of operation, as production from fission and destruction by radioactive decay balance. For the alkaline metals and actinides, the concentrations do not generally reach saturation during the irradiation because of their longer half-lives. The major

contributors to the actinide activities at end of irradiation are short-lived radionuclides with half-lives on the order of days. Within a few weeks after shutdown, these nuclides will have largely decayed to longer-lived Pu-238 and Pu-239. For all the materials, the total photon source reaches its maximum at the end of irradiation period. The photon energies are higher for fission products followed by actinides and activation products respectively during spent fuel cooling. The total photon source decays quickly during the initial cooling period within ~ 30 days. The depletion of U-235 and the production of Pu-239 were analyzed for the GHARR-1 using both REBUS3 and ORIGEN2 code packages for comparison. The ORIGEN2 code recorded U-235 burnup weight percent of 2.90% whilst that of the REBUS3 was 2.86%. The amount of Pu-239 peaks at the end of the irradiation period around a value of 145 mg hence the plutonium production in GHARR-1 is small.

Various gamma and neutron shielding materials were selected in designing six spent fuel casks. After MCNP simulation, each cask design was able to maintain sub criticality. Effective multiplication factor values of Cask A, Cask B, Cask C, Cask D, Cask E and Cask F were recorded as 0.02969±0.00001, 0.06304 ± 0.0002, 0.19809 ± 0.00027, 0.15393 ± 0.00025, 0.02028 ± 0.00001 and 0.01717 ± 0.00001 respectively. The layer used in each cask design was able to reduce both neutron flux and gamma to the surfaces of the six cask designs. It was observed that when more layers (materials) were added to the cask F, it recorded the best results in terms of the neutron and gamma intensity on the surface of cask (from 10^{10} to 10^{5} n.cm^{2}. s^{-1} for neutron and mGy/h for gamma). However, the cask radius was still maintained at approximately 60cm and at a height of 75.46cm. The cask designs are small and portable which will make transporting easier. Clearly, the

cask design is feasible, cheaper and convenient as the cost of importation and clearing of a foreign cask is eliminated. The cask design is a very conservative one considering that the spent fuel was placed in the cask designs just after discharge. The cask F design which comprise, liquid nitrogen for cooling the spent fuel in the aluminium canister and multiple layers of boron carbide for neutron absorption, resin (composed of hydrogen, oxygen, carbon and boron) for thermalisation, boron carbide, lead, stainless steel and serpentine concrete for neutron and gamma shielding will be a good addition to the GHARR-1 facility as it will make the LEU spent fuel conversion more convenient. Its addition will also make spent fuel transportation to other locations on site and dry storage efficient. Serpentine, which is very abundant in parts of Ghana, can be used to form an effective gamma barrier (as part of the shielding layer in the cask). The results show that the inclusion of the serpentine concrete in the multiple layers contributes to the reduced neutron flux and photon dose rate around the cask. The use of serpentine concrete should be encouraged because its high attenuation coefficient and good neutron removal cross section.

6.0 RECOMMENDATION

After the successful completion of this research study, it was realized that some of the findings will help in other research activities like radiological consequence. Further studies will also be very valuable in tackling nuclear spent fuel management issues in Ghana. Recommendations following the completion of this work are outlined below

- Radioactivity results obtained from this study should be used in SS DOSE or any other appropriate code to calculate radiological consequence in accident scenarios.

- This study has shown that dry storage facility for GHARR-1 using serpentine concrete is feasible. However, wet spent fuel storage should be considered in further studies to help simulate a near real system rather than a conservative system.
- Work on permanent spent nuclear storage should also be encouraged to solve Ghana's long term Fuel management issues.
- Thermal Hydraulic studies should be carried out on the proposed cask to assist in the calculation of decay heat and other important parameters. The scope of this study did not include these important parameter.
- Since this study has been able to prove that dry storage for GHARR-1 is possible, the next step is to exhaust all other areas of this research so that we can fabricate a prototype. In the likely event of cask fabrication, transportation risks should be estimated in order to analyze the consequence and risk of a radioactive material transport.
- In the event that the cask is fabricated, impact characteristics and sensitivity analyses (i.e. the effect of natural disasters such as fire, floods, earthquakes etc.) should be investigated and verified against experimental result.
- The results showed that serpentine is a good shielding material and hence could be employed in shielding of radiation emitting sources.

7 REFERENCE

[1] IAEA, www.iaea.org/About/policy/GC/GC48/Documents/gc48inf.4_ftn1.pdf.

[2] INTERNATIONAL ATOMIC ENERGY AGENCY, "Safety Series No. 117," in *Operation of Spent Fuel Storage Facilities*, Vienna, IAEA, 1994.

[3] INTERNATIONAL ATOMIC ENERGY AGENCY, "Safety Assessment for Spent Fuel Storage Facilities," in *Safety Series No. 118*, Vienna, IAEA, 1994.

[4] INTERNATIONAL ATOMIC ENERGY AGENCY, "International Basic Safety Standards for Protection Against Ionizing Radiation and for the Safety of Radiation Sources-Interim Edition," in *Safety Series No. 115*, Vienna, IAEA, 1995.

[5] J.F. Briemeister, "MCNPTM-A Generl Monte Carlo N-Particle Transport Code," *Version 4c Manual*, Vols. LA-13709-M, USA:LANL, 2000.

[6] G. McKinney, "A Practical Guide to Using MCNP with PVM," *Trans. Am. Nucl. Soc.*, no. 71, p. 397, 1994.

[7] INTERNATIONAL ATOMIC ENERGY AGENCY, "Safety and Engineering aspects of Spent Fuel Storage," in *Proceedings of a Symposium*, Vienna, 10-14 October,1994, proceedings Series.

[8] INTERNATIONAL ATOMIC ENERGY AGENCY, "Nuclear Power, Nuclear Fuel Cycle and Waste Management: Status and Trends," in *IAEA Yearbook*, Vienna, IAEA, 1994, p. Part C.

[9] INTERNATIONAL ATOMIC ENERGY AGENCY, *INTERNATIONAL ATOMIC ENERGY AGENCY BULLETIN*, vol. 3, p. 35, 1993.

[10] J. Klein and D. Turner, "Issues relating to Spent Nuclear Fuel Storage:, DOE Spent Nuclear Fuel: Challenges and Initiatives Session: Quantity and Location of DOE'S Spent Nuclear Fuel," in *American Nuclear Society Conference*, Salt Lake City, Utah, December 13-16. 1994.

[11] USDOE, Office of Fissile Material Disposition, "Final environmental impact statement," *Comment response document*, vol. 3, no. Part A, November,1999.

[12] Nuclear Energy Agency; Organisation for Economic Coperation and Development, "Beneficial Uses and production of Isotopes," vol. NEA No. 5293, no. OECD 2005,

2004 Update.

[13] W. J. Quapp, "An Advanced Solution For The Storage, Transportation And Disposal Of Spent Fuel And Vitrified High Level Waste.," in *Global 99*, Jackson, Wyoming, August 29 - September 2, 1999.

[14] W. J. Quapp, P. A. Lessing ., "Radiation Shielding Composition". U.S.A Patent U.S. Patent No. 5,786,611, 28 July 1998.

[15] USDOE, Office of Science and Technology, Office of Environmental Management, Depleted Uranium: A DOE Management Challenge, U.S.A: DOE/EM-0262, October 1995.

[16] P. A. Lessing," Development of "DUCRETE", INEL-94/0029, March, 1995.

[17] W. J. Quapp et al, "Depleted Uranium Hexafluoride: The source material for Advanced Shielding Systems," in *Third International Uranium Hexafluoride Conference*, November 28 -December 1, 1995.

[18] W.J. Quapp to K Shirai, "Interviewee, *Personal Communication, CRIEPI, Research and Development on Depleted Uranium Concrete"*. [Interview]. 15 December 1997.

[19] R. T. Haelsig, "Depleted Uranium Concrete Container Feasibility Study", Packaging Technology Inc.,EGG-MS-11400, September 1994.

[20] J. E. Hopf, "Conceptual Design Report for the DUCRETE Spent Fuel Storage Cask System", INEL-95/0030, February, 1995.

[21] J. E. Hopf, Conceptual Design Report for a Transportable DUCRETE Spent Fuel Storage Cask System", INEL-95/0167, April, 1995.

[22] F. P. Powel," Comparative Economics for DUCRETE Spent Fuel Storage Cask Handling,Transportation, and Capital Requirements, INEL-95/0166, March, 1995.

[23] USDOE, Viability Assessment of a Repository at Yucca Mountain, DOE/RW-0508, December, 1998.

[24] USDOE," Proceedings of a Workshop on Uses of Depleted Uranium in Storage, Transportation and Repository Facilities", Las Vegas, NV: DOE/EM- 0349, July 15-17, 1997.

[25] USDOE, "Integrated Data Base Report: U.S. Spent Fuel and Radioactive Waste

Inventories, Projections, and Characteristics, Rev. 13," DOE/RW-0006, 1966.

[26] International Atomic Energy Commission, "Regulation for the Safe Transport of Radioactive Material," *IAEA Safety Standard Series No ST-1*, IAEA, 1996.

[27] U.S. 10. CRF part 71, "Packaging of the Transportation of Radioactive Material", 1997.

[28] Korea Atomic Energy Act, 1999.

[29] S. Y. Chung,P.K. Ji, B.I. Choi, H.Y. Lee, Y.S. Lee "Conceptual Design for KN-12 Spent Fuel Shipping Cask," in *International Conference on Structural Mechanics in Reactor Technology*,, Seoul-Korea, August 15-20, 1999.

[30] A. Travelli, "The US RERTR Program Status and Progress", Argonne National Lab, Argonne-Illinois, USA.: DOE.

[31] F.Svitak , V. Broz, M. Hrehor, M. Marek, P. Novosad, J. Podlaha, J Rychecky: "Present Experience of NRI Rez with Preparation of Spent Nuclear , Fuel Shipment to Russian Federation", Czech Republic: Nuclear Research Institute Rez plc, Husinec 130, CZ-25068.

[32] United States Nuclear Regulatory Commission, "Safety Evaluation Report Related to the Evaluation of Low-Enriched Uranium Silicide-Aluminum Dispersion Fuel for Use in Non-Power Reactors," US. Nuclear Regulatory Commission Report NUREG-1313, July, 1988.

[33] Executive Office of the President of the United States, "Trends in Health Care Cost Growth and the Role of the Affordable Care Act," November, 2031.

[34] U.S. Department of Energy,Assistant Secretary for Environmental Management, "Final Environmental Impact Statement on a Proposed Nuclear Weapons Nonproliferation Policy Concerning Foreign Research Reactor Spent Nuclear Fuel," DOE/EIS-02 18F, Februar,y 1996.

[35] M. Tyacke, S. František, R. Jiri, P. Miroslav, S. Alexey, K. Sergey, E. Bradley, A. Dudchenko and K. Golubkin, "Development of a New Transportation/Storage Cask System for Use by the DOE Russian Research Reactor Fuel Return Program," in *Proceedings of the 15th International Symposium on the Packaging and Transportation of Radioactive Materials (PATRAM)*, Miami, Florida, USA, October 21-26, 2007.

[36] P.Kotnour, Transport and Storage Cask VPVR SKODA JS, Plzen, Czech Republic, September 9, 2004.

[37] V. Broz and J. Rychecky, "Demo Test-Wet Run VPVR/M SKODA Transport Cask at the Nuclear Research Institute", Rez, plc, Rez, Czech Republic: DRS 1264, October 10, 2005.

[38] V. Broz and J. Rychecky," Evaluation of Demo Test-Wet Run VPVR/M SKODA Transport Cask at the Nuclear Research Institute", Rez, plc, Rez, Czech Republic: DRS 1270, November 26, 2005.

[39] A. Šmaižys, P. Poškas, D. Lukauskas and V. Remeikis, "Experimental determination of radiation safety of spent nuclear fuel dry storage casks CASTOR and CONSTOR," *Lithuanian Journal of Physics*, Vols. 41(4-6), pp. 547-550, 2001.

[40] R. Plukienė, A. Plukis, V. Remeikis and D. Ridikas, "Benchmark calculations of RBMK spent nuclear fuel isotopic composition using MCNP and ORIGEN codes," *Lithuanian Journal of Physics*, vol. 45, no. 4, pp. 281-287, 2005.

[41] A. Plukis, R. Plukienė, V. Remeikis, R. Davidonis, P. Kucinskas and D. Ridikas, "Evaluation of radiation shielding of RBMK-1500 reactor spent fuel containers," *Lithuanian Journal of Physics*, vol. 46, no. 3, pp. 367-374, 2006.

[42] A. Croff, ORIGEN2 — A Revised and Updated Version of the Oak Ridge Isotope Generation and Depletion Code, ORNL-5621,Oak Ridge National Laboratory, July 1980.

[43] J. Sterbentz and C. Wemple," Calculational Burnup Methodology and Validation for the Idaho National Engineering Laboratory Spent Nuclear Fuels", INEL- 96/0304, September,1996.

[44] K. Sungjoong, "Plan for Moata Reactor DecommissioningAnsto", Australian Nuclear Science and Technology Organisation, New Illawarra Road, Lucas Heights, N.S.W., 2234,Australia, skx@ansto.gov.au..

[45] J. Gao, General description of the Ghana MNSR, MNSR Training, China Institute of Atomic Energy, 1993.

[46] B.J.B. Nyarko, "Neutron activation analysis". University of Ghana, School of Nuclear and Allied Sciences, Department of Nuclear Engineering, Lecture, pp. 1–3., 2009.

[47] G. Kennedy, J. St.Pierre, K. Wang, Y. Zang, J. Preston, C. Grant and M. Vutchkov, "Activation constant for SLOWPLOKE and MNS reactors calculated from the neutron spectrum and k0 and Q0 values," *Journal Radioanalytical Chemistry,* p. 167, 2000.

[48] T. Su-De, "Multi-elemental analysis of Chinese biological standard reference materials by monostandard instrumental neutron activation analysis.," *Journal Radioanalytical Nuclear Chemistry,* p. 81, 1984.

[49] I. Umar, "The Potentials of MNSR in the Socioeconomic Development of Nigeria," in *ICENSIAEA Small Research Reactor Workshop,* University of West Indies, Jamaica., 2003.

[50] Assay Report 1096, "Ghana Geological Survey Department Lab Report," 1987.

[51] E.H.K. Akaho, G. Emi-Reynolds and E.O.Darko, "Theoretical Investigation of Ghanaian Serpentines for Shielding of Gamma Sources," Technical Report-GAEC-NNRI-RT-6, 1990.

[52] K. Hilsdofth, "A method to Estimate the Water Content of Concrete Shields," *Nuclear Science and Engineering,* vol. 6, 1967.

[53] F.G. Petterson, "Shielding properties of Ordinary Concrete as a Function of Temperature", H.W.-65572, 1960.

[54] E.G. Jaeger ;Editor, "Engineering Compendum on Radiation, IAEA Report," IAEA, 1968.

[55] T. S.Aklu and R. M. Megahid, "Attenuation of Fission Neutrons in Serpentine Sand and Serpentine Concrete," in *Proceedings of the Siminar on the use of Research Reactors in Fundermental and Applied Science*, Tajura-Tripoli, Libya, 1987.

[56] G.A.Vasilev, "The Attenuation of Reactor Radiation by Serpentine Concrete," *Journal of Nuclear Energy,* vol. 20, p. Parts A & B, 1966.

[57] SCALE, "Version 5,," *A Modular Code System for Performing Standardized Computer Analyses for Licensing Evaluations*, ORNL/TM-2005/39, April 2005, p. Vols. I–III.

[58] J.W. Sterbentz, "Radionuclide Mass Inventory, Activity, Decay Heat, and Dose Rate Parametric Data for TRIGA Spent Nuclear Fuels", INEL-96/0482, March, 1997.

[59] M. J. Bell, ORIGEN B—The ORNL Isotope Generation and Depletion Code, ORNL-462 (CCC-217), Union Carbide Corporation (Nuclear Division), Oak Ridge National Laboratory, May,1973.

[60] H. Bateman, "The Solution of Differential Equations Occurring in the Theory of Radioactive Transformations," in *Proc. Cambridge Phil. Soc.*, 1910, pp. 15,(423).

[61] S. Ball and R. Adams," MATEXP: A General Purpose Digital Computer Program for Solving Ordinary Differential Equations by the Matrix Exponential Method", ORNL/TM-1933, Union Carbide Corporation (Nuclear Division), Oak Ridge National Laboratory, August, 1967.

[62] L. Lapidus and R. Luus, "Optimal Control of Engineering Processes," Blaisdell Publishing Co., Waltham, Mass., 1967, p. 45–49.

[63] D. Vondy, "Development of a General Method of Explicit Solution to the Nuclide Chain Equations for Digital Machine Calculations", ORNL/TM-361, Union Carbide Corporation (Nuclear Division), Oak Ridge National Laboratory, October, 1962.

[64] A.P. Olson, "Version 1.4, ANL/RERTR/TM-32," in *A Users Guide for the REBUS-PC code*, Argonne National Laboratory, 9700 South Cass Avenue, Argonne, Illinois 60439-4815, ANL, December 21, 2001, pp. 7-15.

[65] J.R. Deen, C.I. Costescu, L.S. Leopando and W.L. Woodruff, "Rev. 6," in *WIMS-ANL User Manual*, ANL/TD/TM99-07, February, 2004, pp. 2-5.

[66] N. Hudson, F. Rahnema and H.D. Gougar, A.M. Ougouay, "Spectral History Correction of Microscopic Cross section for the PBR using Slow Down balance," *PHYSOR 2006, ANS Topical Meeting in Reactor Physics Organised and hosted by Canada Nuclear Society,Vancouver, Canada*, 10-14 September, 2006.

[67] T.E. Booth, "Monte Carlo Variance Reduction Approaches for Non-Boltzmann Tallies," Los Alamos National Laboratory report LA-12433, Dececmber,1992.

[68] L.L. Carter and E. D. Cashwell, "Particle Transport Simulation with the Monte Carlo Method," in *ERDA Critical Review Series*, TID-26607, 1975.

[69] R.A. Forster, "A New Method of Assessing the Statistical Convergence of Monte Carlo Solutions," *Trans. Am. Nucl. Soc*, vol. 64, p. 305, 1991.

[70] X-5 Monte Carlo Team, "Version 5," in *MCNP — A General Monte Carlo N-Particle Transport Code,Volume I: Overview and Theory*, ONL, April 24, 2003, p.

27.

[71] M.J. Marshall, "A Summary of WIMSD4M Input Options," *AEEW-M-1327, Atomic Energy Establishment, Winfrith- Dorcester*, 1980.

[72] WIMS-D4 Winfrith Improved Multigroup Scheme Code System, Radiation Shielding Information Center, CCC-576, Martin Marietta Energy Systems, Inc., Oak Ridge National Laboratory, 1990.

[73] C.I. Costescu, "Development of the WIMS-D4 Cell Code for HEU-LEU Fueled Research Nuclear Reactors," in *MSc Thesis, UIUC*, Urbana, IL, 1994.

[74] J.R. Deen, W.L. Woodruff and C.I. Costescu, "New ENDF/B-V Nuclear Data Library for WIMS-D4M," in *Proceedings ofInternational Meeting on Reduced Enrichment for Research and Test Reactors*, Oarai, Japan, October 3-7, 1993.

[75] J.R. Deen, W.L. Woodruff and L. C. Leal, "Validation of the WIMS-D4M Crosssection Generation Code with Benchmark Results," in *Proceedings International Meeting on Reduced Enrichment for Research and Test Reactors*, Williamsburg, VA USA, September 18-23, 1994.

[76] W.L. Woodruff, J.R. Deen and C.I. Costescu, "A Comparison of WIMS-D4 and WIMS-D4M Generated Cross-section Data with Monte Carlo," in *Proceedings of International Meeting on Reduced Enrichment for Research and Test Reactors*, Roskilde, Denmark, September 27 - October 1, 1992.

[77] L.J. Hoover, G.K Leaf, D.A. Meneley and P.M. Walker, "The Fuel Cycle Analysis System, REBUS," *Nucl. Sci. Eng.*, vol. 45, p. 53, 1971.

[78] A.P. Olson, J. P.Regis, D.A. Meneley and L.J. Hoover, "A User's Manual for the Reactor Burnup System, REBUS", Argonne-Illinois: FRA-TM-41, Argonne National Laboratory, September 28, 1972.

[79] A.P. Olson, "A User's Manual for the Reactor Burnup System, REBUS-2", Argonne-Illinois: FRA-TM- 62, Argonne National Laboratory, March 1, 1974.

[80] R. P. Hosteny, "The ARC System Fuel Cycle Analysis Capability, REBUS-2", Argonne-Illinois: ANL-7721, Argonne National Laboratory, October 1978.

[81] B.J. Toppel," A User's Guide for the REBUS-3 Fuel Cycle Analysis Capability", Argonne- Illinois: ANL-83-2, Argonne National Laboratory, 1983.

[82] K. L. Derstine, DIF3D, "A Code to Solve One-, Two-, and Three-Dimensional Finite-Difference Diffusion Theory Problems", Argonne-Illinois: ANL-83-64, Argonne National Laboratory, 1983.

[83] G. Palmiotti, E.E. Lewis and C.B Carrico, "VARIANT: VARIational Anistropic Nodal Transport for Multidimensional Cartesian and Hexagonal Geometry Calculation", Argonne-Illinois: ANL-95/40, Argonne National Laboratory, October, 1995.

[84] Lahey/Fujitsu Fortran 95 Language Reference, Revision F, Lahey Computer Systems, Inc. Incline Village, NV, (Linux Pro 6.0, 2000.

[85] J.K. Shultis and R.E. Faw, "An MCNP Primer", Manhattan-Kansas: Department of Mechanical and Nuclear Engineering, Kansas State University, Manhattan, KS66506..

[86] S. Glastone and A. Sesonske, "Nuclear Reactor Engineering., Reactor Design Basics", Fourth Edition, Vol. 1, 1994.

[87] IAEA, "Classification of Radioactive Waste," *Safety Series on Protecting People and Environment, General Safety Guide,* no. No. GSG-1.

[88] National Regulatory Commission, "10 CFR-ECCS Evaluation Models," *Appendix K to Part 50.*

[89] M. Ragheb,"Decay Heat Generation in Fission Reactors," *University of Illinois at Urbana-Champaign,* 22 March 2011.

[90] S. Kurnbranslehuntering AB, "Measurements of decay heat in spent nuclear fuel at the Swedish interim storage facility, Clab," *Swedish Nuclear Fuel and Waste Management Company,* Vols. ISSN 1402-3091, SKB Rapport R-05-62, pp. pp. 17-19, December 2006.

[91] R.G. Abrefah, B.J.B. Nyarko, J.J. Fletcher and E.H.K. Akaho, "Fuel Burnup Calculation of Ghana MNSR Using ORIGEN@ and REBUS# Codes," *Applied Radiation and Isotopes,* no. 80, pp. 12-16, 2013.

[92] Cember," Introduction to health physics", 4th ed_0071423087.pdf (27/05/2009, 01:07am)..

[93] M.F. Khan," The Physics in Radiation Therapy", second ed. Williams & Wilkins,Baltimore, USA, 176., 1994.

[94] National Institute of Standards and Technology: www.nist.gov.

8 APPENDICES

8.0 APPENDIX A1: Radioactivity in Curies of Nuclides in Peak Power Pin for HEU344 Core During Irradiation Period of Core Life (Halogens)

HALOGENS	75.0D	150.0D	225.0D	300.0D	375.0D	450.0D	525.0D	600.0D	675.0D	750.0D
BR 84	2.54E+02	2.54E+02	2.54E+02	2.54E+02	2.54E+02	2.54E+02	2.54E+02	2.54E+02	2.54E+02	2.54E+02
BR 85	3.16E+02	3.16E+02	3.16E+02	3.16E+02	3.16E+02	3.16E+02	3.16E+02	3.16E+02	3.16E+02	3.16E+02
BR 86	2.39E+02	2.39E+02	2.39E+02	2.39E+02	2.39E+02	2.39E+02	2.39E+02	2.39E+02	2.39E+02	2.39E+02
BR 86M	2.41E+02	2.41E+02	2.41E+02	2.41E+02	2.41E+02	2.41E+02	2.41E+02	2.41E+02	2.41E+02	2.41E+02
BR 87	5.44E+02	5.44E+02	5.44E+02	5.44E+02	5.44E+02	5.44E+02	5.44E+02	5.44E+02	5.44E+02	5.44E+02
I131	7.19E+02	7.20E+02	7.20E+02	7.20E+02	7.20E+02	7.20E+02	7.20E+02	7.20E+02	7.20E+02	7.20E+02
I132	1.08E+03	1.08E+03	1.08E+03	1.08E+03	1.08E+03	1.08E+03	1.08E+03	1.08E+03	1.08E+03	1.08E+03
I133	1.69E+03	1.69E+03	1.69E+03	1.69E+03	1.69E+03	1.69E+03	1.69E+03	1.69E+03	1.69E+03	1.69E+03
I134	1.91E+03	1.91E+03	1.91E+03	1.91E+03	1.91E+03	1.91E+03	1.91E+03	1.91E+03	1.91E+03	1.91E+03
I135	1.58E+03	1.58E+03	1.58E+03	1.58E+03	1.58E+03	1.58E+03	1.58E+03	1.58E+03	1.58E+03	1.58E+03
I136	7.68E+02	7.68E+02	7.68E+02	7.68E+02	7.68E+02	7.68E+02	7.68E+02	7.68E+02	7.68E+02	7.68E+02
TE132	1.07E+03	1.07E+03	1.07E+03	1.07E+03	1.07E+03	1.07E+03	1.07E+03	1.07E+03	1.07E+03	1.07E+03

8.1 APPENDIX A2: Radioactivity in Curies of Nuclides in Peak Power Pin for HEU344 Core During Irradiation Period of Core Life (Noble gases)

NOBLE GAS	75.0D	150.0D	225.0D	300.0D	375.0D	450.0D	525.0D	600.0D	675.0D	750.0D
KR 85M	3.19E+02	3.19E+02	3.19E+02	3.19E+02	3.19E+02	3.19E+02	3.19E+02	3.19E+02	3.19E+02	3.19E+02
KR 87	6.45E+02	6.45E+02	6.45E+02	6.45E+02	6.45E+02	6.45E+02	6.45E+02	6.45E+02	6.45E+02	6.45E+02
KR 88	9.12E+02	9.12E+02	9.12E+02	9.12E+02	9.12E+02	9.12E+02	9.12E+02	9.12E+02	9.12E+02	9.12E+02
KR 89	1.16E+03	1.16E+03	1.16E+03	1.16E+03	1.16E+03	1.16E+03	1.16E+03	1.16E+03	1.16E+03	1.16E+03
XE133	1.69E+03	1.69E+03	1.69E+03	1.69E+03	1.69E+03	1.69E+03	1.69E+03	1.69E+03	1.69E+03	1.69E+03
XE135	1.52E+03	1.52E+03	1.52E+03	1.52E+03	1.52E+03	1.52E+03	1.51E+03	1.51E+03	1.51E+03	1.51E+03
XE135M	2.85E+02	2.85E+02	2.85E+02	2.85E+02	2.85E+02	2.85E+02	2.85E+02	2.85E+02	2.85E+02	2.85E+02
XE137	1.50E+03	1.50E+03	1.50E+03	1.50E+03	1.50E+03	1.50E+03	1.50E+03	1.50E+03	1.50E+03	1.50E+03
XE138	1.57E+03	1.57E+03	1.57E+03	1.57E+03	1.57E+03	1.57E+03	1.57E+03	1.57E+03	1.57E+03	1.57E+03

8.2 APPENDIX A3: Radioactivity in Curies of Nuclides in Peak Power Pin for HEU344 Core During Irradiation Period of Core Life (Alkaline metals)

ALKALINE METALS	75.0D	150.0D	225.0D	300.0D	375.0D	450.0D	525.0D	600.0D	675.0D	750.0D
BA140	1.53E+03	1.56E+03	1.56E+03	1.56E+03	1.56E+03	1.56E+03	1.56E+03	1.56E+03	1.56E+03	1.56E+03
CE141	1.18E+03	1.42E+03	1.47E+03	1.48E+03	1.48E+03	1.48E+03	1.48E+03	1.48E+03	1.48E+03	1.48E+03
CE143	1.48E+03	1.48E+03	1.48E+03	1.48E+03	1.48E+03	1.48E+03	1.48E+03	1.48E+03	1.48E+03	1.48E+03
CE144	2.28E+02	4.17E+02	5.75E+02	7.07E+02	8.16E+02	9.08E+02	9.84E+02	1.05E+03	1.10E+03	1.14E+03
LA140	1.54E+03	1.57E+03	1.57E+03	1.57E+03	1.57E+03	1.57E+03	1.57E+03	1.57E+03	1.57E+03	1.57E+03
MO 99	1.50E+03	1.50E+03	1.50E+03	1.50E+03	1.50E+03	1.50E+03	1.50E+03	1.50E+03	1.50E+03	1.50E+03
NB 95	4.72E+02	1.01E+03	1.32E+03	1.48E+03	1.55E+03	1.58E+03	1.60E+03	1.60E+03	1.61E+03	1.61E+03
ND147	5.67E+02	5.72E+02	5.72E+02	5.72E+02	5.72E+02	5.72E+02	5.72E+02	5.72E+02	5.72E+02	5.72E+02
PM147	2.39E+01	5.27E+01	7.98E+01	1.05E+02	1.30E+02	1.52E+02	1.74E+02	1.94E+02	2.13E+02	2.31E+02
PR143	1.41E+03	1.45E+03	1.45E+03	1.45E+03	1.45E+03	1.45E+03	1.45E+03	1.45E+03	1.45E+03	1.45E+03
RU103	5.81E+02	7.35E+02	7.76E+02	7.87E+02	7.90E+02	7.91E+02	7.91E+02	7.91E+02	7.91E+02	7.91E+02
SR 89	7.74E+02	1.05E+03	1.15E+03	1.18E+03	1.20E+03	1.20E+03	1.20E+03	1.20E+03	1.20E+03	1.20E+03

8.3 APPENDIX A4: Radioactivity in Curies of Nuclides in Peak Power Pin for HEU344 Core During Irradiation Period of Core Life (Actinides)

ACTINIDES	75.0D	150.0D	225.0D	300.0D	375.0D	450.0D	525.0D	600.0D	675.0D	750.0D
U234	6.86E-02	6.85E-02	6.84E-02	6.84E-02	6.83E-02	6.82E-02	6.82E-02	6.81E-02	6.80E-02	6.79E-02
U235	2.13E-03	2.12E-03	2.12E-03	2.11E-03	2.11E-03	2.10E-03	2.09E-03	2.09E-03	2.08E-03	2.07E-03
U237	2.41E+00	4.63E+00	6.86E+00	9.11E+00	1.14E+01	1.36E+01	1.59E+01	1.82E+01	2.05E+01	2.28E+01
U239	4.56E+01	4.57E+01	4.59E+01	4.60E+01	4.61E+01	4.63E+01	4.64E+01	4.65E+01	4.67E+01	4.68E+01
NP238	1.84E-03	7.32E-03	1.65E-02	2.93E-02	4.59E-02	6.62E-02	9.04E-02	1.19E-01	1.51E-01	1.87E-01
NP239	4.56E+01	4.57E+01	4.59E+01	4.60E+01	4.61E+01	4.63E+01	4.64E+01	4.65E+01	4.67E+01	4.68E+01

8.4 APPENDIX B1: Radioactivity in Curies of Nuclides in Peak Power Pin for HEU344 Core During Cooling Period After Discharge (Halogen)

HALOGEN	DISCHARGE	1.0D	5.0D	10.0D	30.0D	90.0D	365.0D	1095.0D	1825.0D	3650.0D	7300.0D
BR 84	7.38E-01	1.92E-14	0.00E+00	0.00E+00	0.00E+00	0.00E+00	0.00E+00	0.00E+00	0.00E+00	0.00E+00	0.00E+00
BR 85	9.17E-01	0.00E+00	0.00E+00	0.00E+00	0.00E+00	0.00E+00	0.00E+00	0.00E+00	0.00E+00	0.00E+00	0.00E+00
BR 86	6.95E-01	0.00E+00	0.00E+00	0.00E+00	0.00E+00	0.00E+00	0.00E+00	0.00E+00	0.00E+00	0.00E+00	0.00E+00
BR 86M	7.01E-01	0.00E+00	0.00E+00	0.00E+00	0.00E+00	0.00E+00	0.00E+00	0.00E+00	0.00E+00	0.00E+00	0.00E+00
BR 87	1.58E+00	0.00E+00	0.00E+00	0.00E+00	0.00E+00	0.00E+00	0.00E+00	0.00E+00	0.00E+00	0.00E+00	0.00E+00
I131	2.09E+00	1.95E+00	1.39E+00	9.08E-01	1.62E-01	9.19E-04	4.65E-14	0.00E+00	0.00E+00	0.00E+00	0.00E+00
I132	3.14E+00	2.60E+00	1.11E+00	3.83E-01	5.44E-03	1.56E-08	0.00E+00	0.00E+00	0.00E+00	0.00E+00	0.00E+00
I133	4.91E+00	2.27E+00	9.25E-02	1.70E-03	1.92E-10	2.77E-31	0.00E+00	0.00E+00	0.00E+00	0.00E+00	0.00E+00
I134	5.56E+00	1.40E-07	0.00E+00	0.00E+00	0.00E+00	0.00E+00	0.00E+00	0.00E+00	0.00E+00	0.00E+00	0.00E+00
I135	4.58E+00	3.70E-01	1.58E-05	5.41E-11	0.00E+00	0.00E+00	0.00E+00	0.00E+00	0.00E+00	0.00E+00	0.00E+00
I136	2.23E+00	0.00E+00	0.00E+00	0.00E+00	0.00E+00	0.00E+00	0.00E+00	0.00E+00	0.00E+00	0.00E+00	0.00E+00
TE132	3.12E+00	2.52E+00	1.08E+00	3.72E-01	5.28E-03	1.51E-08	0.00E+00	0.00E+00	0.00E+00	0.00E+00	0.00E+00

8.5 APPENDIX B2: Radioactivity in Curies of Nuclides in Peak Power Pin for HEU344 Core During Cooling Period After Discharge (Noble gases)

NOBLE GASES	DISCHARGE	1.0D	5.0D	10.0D	30.0D	90.0D	365.0D	1095.0D	1825.0D	3650.0D	7300.0D
KR 85M	9.27E-01	2.29E-02	8.13E-09	7.05E-17	0.00E+00	0.00E+00	0.00E+00	0.00E+00	0.00E+00	0.00E+00	0.00E+00
KR 87	1.88E+00	3.95E-06	0.00E+00	0.00E+00	0.00E+00	0.00E+00	0.00E+00	0.00E+00	0.00E+00	0.00E+00	0.00E+00
KR 88	2.65E+00	7.57E-03	5.01E-13	9.44E-26	0.00E+00	0.00E+00	0.00E+00	0.00E+00	0.00E+00	0.00E+00	0.00E+00
KR 89	3.37E+00	0.00E+00	0.00E+00	0.00E+00	0.00E+00	0.00E+00	0.00E+00	0.00E+00	0.00E+00	0.00E+00	0.00E+00
XE133	4.92E+00	4.74E+00	3.07E+00	1.60E+00	1.15E-01	4.13E-05	6.82E-21	0.00E+00	0.00E+00	0.00E+00	0.00E+00
XE135	4.40E+00	1.68E+00	1.73E-03	1.88E-07	2.38E-23	0.00E+00	0.00E+00	0.00E+00	0.00E+00	0.00E+00	0.00E+00
XE135M	8.29E-01	5.93E-02	2.52E-06	8.67E-12	0.00E+00	0.00E+00	0.00E+00	0.00E+00	0.00E+00	0.00E+00	0.00E+00
XE137	4.37E+00	0.00E+00	0.00E+00	0.00E+00	0.00E+00	0.00E+00	0.00E+00	0.00E+00	0.00E+00	0.00E+00	0.00E+00
XE138	4.55E+00	0.00E+00	0.00E+00	0.00E+00	0.00E+00	0.00E+00	0.00E+00	0.00E+00	0.00E+00	0.00E+00	0.00E+00

8.6 APPENDIX B3: Radioactivity in curies of nuclides in peak power pin for HEU344 Core during Cooling Period after Discharge (Alkali metals)

ALKALINE METALS	DISCHARGE	1.0D	5.0D	10.0D	30.0D	90.0D	365.0D	1095.0D	1825.0D	3650.0D	7300.0D
BA140	4.54E+00	4.30E+00	3.46E+00	2.64E+00	8.93E-01	3.46E-02	1.16E-08	7.64E-26	0.00E+00	0.00E+00	0.00E+00
CE141	4.30E+00	4.23E+00	3.89E+00	3.50E+00	2.28E+00	6.35E-01	1.81E-03	3.14E-10	5.47E-17	6.92E-34	0.00E+00
CE143	4.31E+00	2.62E+00	3.49E-01	2.81E-02	1.17E-06	8.59E-20	0.00E+00	0.00E+00	0.00E+00	0.00E+00	0.00E+00
CE144	3.32E+00	3.32E+00	3.28E+00	3.24E+00	3.09E+00	2.67E+00	1.37E+00	2.30E-01	3.88E-02	4.53E-04	6.18E-08
LA140	4.56E+00	4.51E+00	3.90E+00	3.03E+00	1.03E+00	3.98E-02	1.34E-08	8.79E-26	0.00E+00	0.00E+00	0.00E+00
MO 99	4.37E+00	3.40E+00	1.24E+00	3.52E-01	2.27E-03	6.15E-10	0.00E+00	0.00E+00	0.00E+00	0.00E+00	0.00E+00
NB 95	4.68E+00	4.68E+00	4.67E+00	4.63E+00	4.34E+00	2.95E+00	1.95E-01	7.32E-05	2.69E-08	6.97E-17	4.68E-34
ND147	1.66E+00	1.56E+00	1.22E+00	8.89E-01	2.54E-01	5.91E-03	1.94E-10	2.62E-30	0.00E+00	0.00E+00	0.00E+00
PM147	6.72E-01	6.72E-01	6.74E-01	6.76E-01	6.73E-01	6.48E-01	5.31E-01	3.13E-01	1.85E-01	4.93E-02	3.52E-03
PR143	4.21E+00	4.17E+00	3.60E+00	2.82E+00	1.01E+00	4.73E-02	3.73E-08	2.35E-24	0.00E+00	0.00E+00	0.00E+00
RU103	2.30E+00	2.26E+00	2.11E+00	1.93E+00	1.35E+00	4.70E-01	3.67E-03	9.34E-09	2.38E-14	2.46E-28	0.00E+00
SR 89	3.50E+00	3.45E+00	3.27E+00	3.05E+00	2.32E+00	1.02E+00	2.34E-02	1.04E-06	4.62E-11	6.10E-22	0.00E+00

8.7 APPENDIX B4: Radioactivity in Curies of Nuclides in Peak Power Pin for HEU344 Core During Cooling Period After Discharge (Actinide)

ACTINIDES	DISCHARGE	1.0D	5.0D	10.0D	30.0D	90.0D	365.0D	1095.0D	1825.0D	3650.0D	7300.0D
U237	6.64E-02	5.99E-02	3.97E-02	2.38E-02	3.05E-03	6.43E-06	7.76E-11	7.05E-11	6.40E-11	5.03E-11	3.11E-11
NP238	5.42E-04	3.91E-04	1.05E-04	2.05E-05	2.93E-08	4.83E-14	4.80E-14	4.76E-14	4.72E-14	4.61E-14	4.41E-14
NP239	1.36E-01	1.02E-01	3.15E-02	7.22E-03	2.01E-05	5.38E-13	1.08E-13	1.08E-13	1.08E-13	1.08E-13	1.07E-13
PU238	2.92E-06	2.93E-06	2.95E-06	2.95E-06	2.95E-06	2.95E-06	2.93E-06	2.89E-06	2.84E-06	2.73E-06	2.52E-06
PU239	7.58E-06	7.59E-06	7.61E-06	7.61E-06	7.62E-06	7.62E-06	7.62E-06	7.61E-06	7.61E-06	7.61E-06	7.61E-06
PU240	4.23E-07	4.23E-07	4.23E-07	4.23E-07	4.23E-07	4.23E-07	4.23E-07	4.23E-07	4.23E-07	4.23E-07	4.23E-07
PU241	3.32E-06	3.32E-06	3.32E-06	3.31E-06	3.31E-06	3.28E-06	3.16E-06	2.87E-06	2.61E-06	2.05E-06	1.27E-06

8.8 APPENDIX C1: HEU344 PEAK PIN PHOTON SPECTRUM FOR ACTIVATION PRODUCTS (FROM CORE FUEL + AL-303 CLAD) DURING COOLING PERIOD

EMEAN	DISCHARGE	1.0D	5.0D	10.0D	30.0D	90.0D	365.0D	1095.0D	1825.0D	3650.0D	7300.0D
1.00E-02	4.14E+10	4.23E+07	4.00E+06	3.29E+06	2.50E+06	1.33E+06	3.99E+05	9.03E+04	3.67E+04	1.92E+04	1.14E+04
2.50E-02	9.00E+09	8.03E+06	1.75E+05	7.52E+04	5.93E+04	3.08E+04	2.60E+03	3.92E+02	2.31E+02	1.39E+02	1.06E+02
3.75E-02	6.02E+09	5.24E+06	1.35E+05	7.10E+04	5.98E+04	3.83E+04	1.01E+04	1.18E+03	2.01E+02	4.65E+01	2.93E+01
5.75E-02	8.94E+09	7.41E+06	1.60E+05	6.91E+04	5.56E+04	3.05E+04	3.64E+03	3.15E+02	7.78E+01	2.74E+01	1.18E+01
8.50E-02	5.67E+09	4.41E+06	9.74E+04	4.36E+04	3.59E+04	2.13E+04	3.86E+03	3.92E+02	6.44E+01	9.32E+00	2.92E+00
1.25E-01	3.86E+09	2.80E+06	5.98E+04	2.57E+04	2.12E+04	1.25E+04	2.08E+03	2.04E+02	3.80E+01	9.39E+00	3.62E+00
2.25E-01	5.61E+09	3.51E+06	7.10E+04	2.67E+04	2.09E+04	1.14E+04	8.16E+02	1.60E+01	5.16E+00	2.27E+00	8.36E-01
3.75E-01	2.77E+09	2.59E+06	1.22E+06	1.06E+06	6.46E+05	1.47E+05	4.56E+02	5.64E+00	1.39E+00	4.86E-01	1.66E-01
5.75E-01	1.62E+09	2.30E+06	1.19E+06	1.12E+06	9.20E+05	5.15E+05	3.89E+04	6.21E+02	7.65E+01	1.86E+00	6.45E-01
8.50E-01	1.84E+09	8.87E+06	8.56E+06	8.31E+06	7.42E+06	5.45E+06	2.10E+06	3.93E+05	7.77E+04	1.36E+03	3.70E+00
1.25E+00	1.03E+09	1.28E+08	1.78E+06	2.62E+05	2.43E+05	2.07E+05	1.05E+05	2.74E+04	1.44E+04	6.80E+03	1.83E+03
1.75E+00	5.63E+10	3.56E+04	2.15E+04	2.05E+04	1.68E+04	9.35E+03	6.33E+02	9.18E-01	3.58E-01	2.39E-01	1.07E-01
2.25E+00	7.40E+06	6.30E+03	2.59E-01	1.86E-01	1.54E-01	1.31E-01	1.18E-01	9.03E-02	6.94E-02	3.60E-02	9.67E-03
2.75E+00	3.57E+08	1.18E+08	1.39E+06	5.44E+03	4.11E-04	4.01E-04	3.63E-04	2.79E-04	2.15E-04	1.11E-04	2.99E-05
3.50E+00	3.16E+05	8.06E+04	9.54E+02	3.73E+00	8.68E-10	6.44E-15	6.44E-15	6.44E-15	6.44E-15	5.80E-15	4.67E-15
5.00E+00	1.37E+04	8.37E+02	9.91E+00	3.87E-02	9.02E-12	2.17E-19	2.17E-19	2.17E-19	2.17E-19	2.17E-19	2.17E-19
7.00E+00	2.45E+03	1.41E-20	1.41E-20	1.41E-20	1.41E-20	1.41E-20	1.41E-20	1.41E-20	1.41E-20	1.41E-20	1.41E-20
9.50E+00	3.97E+02	8.91E-22	8.91E-22	8.91E-22	8.91E-22	8.91E-22	8.91E-22	8.91E-22	8.91E-22	8.91E-22	8.91E-22
TOTAL	1.44E+11	3.34E+08	1.89E+07	1.44E+07	1.20E+07	7.81E+06	2.67E+06	5.13E+05	1.30E+05	2.76E+04	1.34E+04
MEV/SEC	1.08E+11	4.97E+08	1.46E+07	8.54E+06	7.45E+06	5.29E+06	1.95E+06	3.69E+05	8.45E+04	9.87E+03	2.41E+03

8.9 APPENDIX C2: GHARR-1 PEAK PIN PHOTON SPECTRUM FOR ACTINIDES + DAUGHTERS DURING COOLING PERIOD

EMEAN	DISCHARGE	1.0D	5.0D	10.0D	30.0D	90.0D	365.0D	1095.0D	1825.0D	3650.0D	7300.0D
1.00E-02	8.99E+09	5.36E+09	2.31E+09	9.83E+08	9.60E+07	1.38E+06	1.18E+06	1.18E+06	1.18E+06	1.18E+06	1.18E+06
2.50E-02	3.82E+08	1.15E+08	5.98E+07	3.06E+07	3.54E+06	4.33E+04	3.60E+04	3.60E+04	3.60E+04	3.60E+04	3.61E+04
3.75E-02	4.70E+08	4.10E+07	1.61E+07	6.08E+06	5.04E+05	2.60E+03	1.55E+03	1.56E+03	1.56E+03	1.56E+03	1.56E+03
5.75E-02	1.29E+09	9.53E+08	6.02E+08	3.51E+08	4.42E+07	1.04E+05	1.08E+04	1.10E+04	1.11E+04	1.13E+04	1.17E+04
8.50E-02	3.62E+09	1.03E+09	4.60E+08	2.04E+08	2.07E+07	8.22E+04	3.89E+04	3.89E+04	3.90E+04	3.90E+04	3.90E+04
1.25E-01	3.26E+09	2.50E+09	1.02E+09	4.06E+08	3.61E+07	1.14E+05	3.89E+04	3.89E+04	3.89E+04	3.89E+04	3.89E+04
2.25E-01	2.34E+09	1.78E+09	7.35E+08	2.98E+08	2.73E+07	1.79E+05	1.22E+05	1.22E+05	1.22E+05	1.22E+05	1.22E+05
3.75E-01	2.26E+08	1.51E+08	5.77E+07	2.09E+07	1.61E+06	4.10E+03	7.53E+02	7.56E+02	7.59E+02	7.64E+02	7.77E+02
5.75E-01	3.06E+07	5.71E+05	1.74E+05	3.94E+04	1.96E+02	9.39E+01	1.07E+02	1.28E+02	1.38E+02	1.43E+02	1.41E+02
8.50E-01	5.08E+07	4.82E+06	1.30E+06	2.53E+05	4.06E+02	4.63E+01	5.24E+01	6.22E+01	6.67E+01	6.94E+01	6.83E+01
1.25E+00	4.72E+06	3.02E+06	8.16E+05	1.59E+05	2.50E+02	2.34E+01	2.37E+01	2.44E+01	2.47E+01	2.53E+01	2.69E+01
1.75E+00	3.59E+02	6.34E+00	5.32E+00	5.33E+00	5.42E+00	5.75E+00	6.89E+00	8.75E+00	9.66E+00	1.05E+01	1.13E+01
2.25E+00	1.11E-02	1.11E-02	1.11E-02	1.11E-02	1.13E-02	1.22E-02	1.70E-02	3.66E-02	6.59E-02	1.81E-01	5.93E-01
2.75E+00	1.81E+01	1.85E+01	1.81E+01	1.83E+01	1.93E+01	2.26E+01	3.39E+01	5.20E+01	6.02E+01	6.44E+01	5.98E+01
3.50E+00	2.55E-03	2.54E-03	2.53E-03	2.51E-03	2.47E-03	2.43E-03	2.43E-03	2.49E-03	2.59E-03	2.96E-03	4.30E-03
5.00E+00	9.02E-04	9.00E-04	8.94E-04	8.87E-04	8.68E-04	8.50E-04	8.45E-04	8.43E-04	8.43E-04	8.42E-04	8.39E-04
7.00E+00	8.27E-05	8.26E-05	8.18E-05	8.10E-05	7.88E-05	7.68E-05	7.62E-05	7.60E-05	7.60E-05	7.58E-05	7.56E-05
9.50E+00	8.11E-06	8.09E-06	8.01E-06	7.92E-06	7.66E-06	7.42E-06	7.36E-06	7.34E-06	7.33E-06	7.32E-06	7.29E-06
TOTAL	2.07E+10	1.19E+10	5.26E+09	2.30E+09	2.30E+08	1.91E+06	1.43E+06	1.43E+06	1.43E+06	1.43E+06	1.43E+06
MEV/SEC	1.59E+09	9.77E+08	4.16E+08	1.75E+08	1.66E+07	8.43E+04	4.96E+04	4.97E+04	4.97E+04	4.98E+04	4.98E+04

8.10 APPENDIX C3: GHARR-1 PEAK PIN PHOTON SPECTRUM FOR FISSION PRODUCTS DURING COOLING PERIOD

EMEAN	DISCHARGE	1.0D	5.0D	10.0D	30.0D	90.0D	365.0D	1095.0D	1825.0D	3650.0D	7300.0D
1.00E-02	5.74E+12	6.48E+11	4.07E+11	3.36E+11	2.27E+11	1.34E+11	5.05E+10	1.34E+10	6.82E+09	4.73E+09	3.65E+09
2.50E-02	1.44E+12	2.27E+11	1.36E+11	9.91E+10	5.59E+10	2.94E+10	1.09E+10	2.92E+09	1.49E+09	9.96E+08	7.55E+08
3.75E-02	1.21E+12	2.97E+11	1.72E+11	1.22E+11	6.40E+10	3.33E+10	1.30E+10	3.25E+09	1.53E+09	1.03E+09	7.90E+08
5.75E-02	1.24E+12	1.34E+11	7.73E+10	6.19E+10	4.25E+10	2.62E+10	1.04E+10	2.67E+09	1.31E+09	9.00E+08	6.98E+08
8.50E-02	9.12E+11	1.49E+11	9.92E+10	6.98E+10	3.24E+10	1.82E+10	7.60E+09	1.86E+09	8.46E+08	5.50E+08	4.19E+08
1.25E-01	9.51E+11	2.78E+11	1.71E+11	1.24E+11	7.72E+10	3.50E+10	1.02E+10	2.08E+09	6.93E+08	3.56E+08	2.70E+08
2.25E-01	2.23E+12	2.90E+11	9.35E+10	5.24E+10	2.50E+10	1.49E+10	6.17E+09	1.51E+09	6.85E+08	4.50E+08	3.51E+08
3.75E-01	1.34E+12	1.43E+11	9.83E+10	7.09E+10	2.52E+10	7.44E+09	3.12E+09	7.79E+08	3.46E+08	2.05E+08	1.51E+08
5.75E-01	2.28E+12	5.40E+11	2.50E+11	1.71E+11	8.30E+10	3.15E+10	1.18E+10	8.07E+09	7.04E+09	6.05E+09	4.78E+09
8.50E-01	2.58E+12	5.81E+11	4.16E+11	3.57E+11	2.72E+11	1.57E+11	1.02E+10	2.50E+08	1.07E+08	4.28E+07	2.58E+07
1.25E+00	1.55E+12	5.50E+10	1.27E+10	5.63E+09	1.81E+09	1.25E+09	5.73E+08	1.23E+08	3.84E+07	1.42E+07	9.43E+06
1.75E+00	5.57E+11	1.53E+11	1.27E+11	9.81E+10	3.33E+10	1.42E+09	7.09E+07	1.46E+07	3.73E+06	9.34E+05	6.60E+05
2.25E+00	3.11E+11	5.04E+09	3.06E+09	2.26E+09	1.26E+09	7.77E+08	3.91E+08	6.64E+07	1.13E+07	1.41E+05	9.92E+01
2.75E+00	1.33E+11	5.59E+09	4.81E+09	3.73E+09	1.27E+09	5.11E+07	1.26E+06	2.91E+05	6.87E+04	2.01E+03	1.98E+00
3.50E+00	8.03E+10	4.85E+07	3.96E+07	3.08E+07	1.06E+07	6.03E+05	1.20E+05	3.04E+04	7.70E+03	2.48E+02	2.57E-01
5.00E+00	4.33E+10	4.88E+05	3.23E-05	1.22E-10	1.23E-10	1.24E-10	1.30E-10	1.40E-10	1.46E-10	1.53E-10	1.55E-10
7.00E+00	3.49E+08	7.93E-12	7.93E-12	7.94E-12	7.97E-12	8.06E-12	8.42E-12	9.09E-12	9.49E-12	9.90E-12	1.00E-11
9.50E+00	6.86E+04	5.01E-13	5.02E-13	5.02E-13	5.04E-13	5.10E-13	5.32E-13	5.75E-13	6.00E-13	6.26E-13	6.35E-13
TOTAL	2.26E+13	3.51E+12	2.07E+12	1.57E+12	9.41E+11	4.90E+11	1.35E+11	3.70E+10	2.09E+10	1.53E+10	1.19E+10
MEV/SEC	9.39E+12	1.37E+12	8.61E+11	6.70E+11	3.82E+11	1.75E+11	2.35E+10	6.71E+09	4.90E+09	3.97E+09	3.11E+09

8.11 Cross sectional view of cask B, C, D and E respectively